UNIVERSITÀ DEGLI STUDI DI PADOVA

UNIVERSITA' DEGLI STUDI DI PADOVA

Dipartimento di Ingegneria Industriale DII

Corso di Laurea Magistrale in Ingegneria Meccanica

Critical volume approach in multiaxial fatigue assessment of notched specimens

Supervisors:

Prof. Giovanni Meneghetti

Ing. Jan Papuga, Ph.D.

Student:

Leonardo Serri (2076571)

Academic Year 2023/2024

Dedico questo traguardo alla mia famiglia che,

inseguendo la voglia di riscatto,

oggi è arrivata fin qui.

ACKNOWLEDGEMENTS

Most of the work about this Master's thesis project was carried out during my Erasmus+ exchange experience held in Prague, Czech Republic, during the final semester of my Master's degree. A special thanks goes to Professor Giovanni Meneghetti from Department of Industrial Engineering of Università degli Studi di Padova, who put me in touch with colleagues at the Czech Technical University (CTU) and followed me during the development of this work. I would also like to thank Ing. Jan Papuga, Ph.D. and Ing. Martin Nesládek, Ph.D. from Department of Mechanics, Biomechanics and Mechatronics of the Faculty of Mechanical Engineering at CTU, who supported me during the course of this challenging experimental thesis work. This experience represented for me a great opportunity to grow both in terms of educational development, as I learned fascinating new topics about Mechanical Engineering having the opportunity to explore them in a research environment, and as a person, who was lucky to meet fantastic people in the wonderful international and multicultural environment that a city like Prague offers. Last but not least, I would like to thank my family and my friends who have always assisted me in this long journey started six years ago and now has come to the end. Without you, all this would not have been possible.

Leonardo Serri

ABSTRACT

Engineers are facing the problem of fatigue of materials since more than one century. This mechanical phenomenon is particularly challenging because it can lead to the catastrophic failure of mechanical parts without any visible warning signs. When notched components are considered, it becomes even more difficult to predict fatigue life. Presence of stress concentrators amplifies locally the stress field and makes its distribution non-uniform. As a result, the loaded component is subjected to multiaxial loading. Multiaxial fatigue loading, which can result from the application of a combination of several forces along different load channels, requires sophisticated tools to be studied. Several approaches to multiaxial fatigue have been developed over last decades, and many multiaxial fatigue strength criteria based on them were proposed. This Master's thesis project, developed at the Faculty of Mechanical Engineering at CTU in Prague, proposes a new approach to deal with multiaxial fatigue which is based on critical volume. Since the statistical size effect plays a crucial role in fatigue strength of materials, the aim of the new approach is to involve concretely such an effect into the estimation of the damage parameter, which is performed by any multiaxial fatigue strength criterion. In particular, Dang Van criterion has been considered for this study, while the experimental campaign has investigated the structural steel S355J2. The core idea of the proposed approach consists in modifying the material parameters, which are used as input in the multiaxial fatigue criterion, depending on the observed value of critical volume. This insight originates from the fact that size effect turns out to not be effectively considered in widely used methods like Theory of Critical Distances (TCD) and Relative Stress Gradient approach, which are instead more focused on the stress gradient effect. TCD has nonetheless been implemented in the current work to assess the problem using a more stable method that is validated in the literature. The main outcome obtained from this work includes the evaluated dependencies between notch fatigue strength and critical volume for both cases of axial load and torsion load. Such dependencies can be used in conjunction with Dang Van criterion, since they allow the calculation of modified material parameters that should make the chosen criterion perform more accurate multiaxial fatigue predictions. Final outputs from the method clearly indicate that further work is needed to improve how this approach is structured and to overcome some of its limitations, which represent boundary conditions fixed at the beginning to start with the study. However, the critical volume approach studied here provides valuable insights on how size effect should be properly integrated into multiaxial fatigue assessment.

The thesis structure is described hereafter. First of all, an introduction about the basics of fatigue of materials is presented. To follow, there is an overview on multiaxial fatigue problem which details various related phenomena and main solutions have been developed over the years to deal with it. This part is followed by the discussion of the theoretic and experimental fundamentals that led to the idea of developing the critical volume approach proposed here. Later, the entire experimental study is presented: fatigue tests on the examined material, finite element analyses on the specimens, and critical volume calculation are explained. Then, the data elaboration is addressed, with a particular focus on the implementation of critical volume approach that starts from a preliminary analysis based on von Mises stresses and evolves into a more complex application using the Dang Van criterion. Subsequently, the comparative application of TCD using the Point Method is presented. In the final part of the thesis, results are discussed, stressing the comparison between the outcomes from the two critical volume analyses and also confronting them with results of TCD, in order to bring to light criticalities of the approach. Conclusions resume all key points of the work, discussing issues that remain open and possible future developments of the idea. The document closes with the appendix where additional data and information useful for the understanding are collected.

Keywords: Multiaxial fatigue, notch effect, stress gradient effect, size effect, critical volume, high-cycle fatigue

ABSTRACT

Gli ingegneri affrontano il problema della fatica dei materiali da oltre un secolo. Questo fenomeno meccanico è particolarmente problematico perché può portare al cedimento di schianto di parti meccaniche senza alcun preavviso. Quando si considerano componenti intagliati, diventa ancor più difficile prevedere la loro vita a fatica. La presenza di intagli amplifica localmente il campo tensionale e rende la distribuzione delle tensioni non uniforme, facendo sì che il componente sperimenti un carico localmente multiassiale. Il carico a fatica multiassiale, che può derivare anche dalla combinazione di diverse forze applicate su più canali di carico, richiede strumenti sofisticati per poter essere studiato. Negli ultimi decenni sono stati sviluppati diversi approcci alla fatica multiassiale e sono stati proposti numerosi criteri di resistenza a fatica multiassiale basati su di essi. Questo progetto di tesi magistrale, sviluppato presso la Facoltà di Ingegneria Meccanica della CTU di Praga, propone un nuovo approccio per affrontare la fatica multiassiale basato sul volume critico. Poiché l'effetto della dimensione gioca un ruolo cruciale nella resistenza a fatica dei materiali, l'obiettivo del nuovo approccio è includere concretamente tale effetto nella stima del danno a fatica, valutato attraverso un qualsiasi criterio di resistenza a fatica multiassiale. In questo studio è stato preso in considerazione il criterio di Dang Van, mentre la campagna sperimentale ha riguardato l'acciaio strutturale S355J2. L'idea di base dell'approccio proposto consiste nel modificare i material parameters, utilizzati come input nel criterio di resistenza a fatica multiassiale, in funzione del valore di volume critico osservato. Questo concetto deriva dal fatto che l'effetto della dimensione non viene considerato efficacemente nei metodi più diffusi quali la Theory of Critical Distances (TCD) e il Relative Stress Gradient approach, i quali invece si concentrano maggiormente sull'effetto del gradiente di tensione. La TCD è stata comunque implementata in questo lavoro per valutare il problema utilizzando un metodo più stabile e ampiamente validato in letteratura. Il risultato principale ottenuto da questo lavoro include le relazioni valutate tra la resistenza a fatica dei componenti intagliati e il volume critico, sia per il caso di carico assiale che per quello torsionale. Tali relazioni possono essere utilizzate in combinazione con il criterio di Dang Van, in quanto consentono il calcolo dei nuovi material parameters che dovrebbero consentire di migliorare l'accuratezza del calcolo effettuato dal criterio selezionato. I risultati finali del metodo indicano chiaramente che è necessario ulteriore lavoro per migliorare la formulazione di questo approccio e superare alcune delle sue limitazioni, rappresentate dalle condizioni al contorno fissate all'inizio dello studio. Tuttavia, l'approccio basato sul volume critico qui studiato fornisce preziosi spunti su come l'effetto della dimensione dovrebbe essere adeguatamente integrato nel calcolo a fatica multiassiale.

La struttura della tesi è descritta qui di seguito. Innanzitutto, viene presentata un'introduzione sui concetti fondamentali della fatica dei materiali. Segue una panoramica sul problema della fatica multiassiale, che va a dettagliare i vari fenomeni ad esso correlati e le principali soluzioni sviluppate nel corso degli anni per affrontarlo. Questa parte è seguita dalla discussione dei fondamenti teorici e sperimentali che hanno portato all'idea di sviluppare l'approccio del volume critico proposto in questa tesi. Successivamente, viene presentato l'intero studio sperimentale: si riportano i test a fatica sul materiale investigato, le analisi agli elementi finiti effettuate sui provini e il calcolo del volume critico per ogni serie di provini. A seguire, vengono trattati i risultati dell'elaborazione dei dati, ponendo particolare attenzione all'implementazione dell'approccio del volume critico la quale parte da un'analisi preliminare basata sulla tensione di von Mises, per poi evolversi in un'applicazione più complessa utilizzando il criterio di Dang Van. Quindi, viene presentata la TCD applicata secondo il Point Method. Nella parte finale della tesi vengono discussi i risultati, sottolineando il confronto tra gli esiti delle due analisi riguardanti il volume critico ed evidenziando le criticità dell'approccio. Sono discussi anche con i risultati della TCD. Le conclusioni riassumono tutti i punti chiave del lavoro, discutendo le questioni ancora aperte e i possibili sviluppi futuri dell'idea. Il documento si conclude con l'appendice che raccoglie dati e informazioni aggiuntive utili alla comprensione della tesi.

Parole chiave: Fatica multiassiale, effetto di intaglio, effetto gradiente di tensione, effetto della dimensione, volume critico, fatica ad alto numero di cicli

TABLE OF CONTENTS

LIST OF SIMBOLS

a	material parameter
a_{DV}	material parameter for Dang Van multiaxial fatigue strength criterion
a_P	Peterson's material constant
a_N	Neuber's material constant
A	elongation at fracture, Kohout-Věchet regression constant
A_{net}	net cross-sectional area
β	Kohout-Věchet regression constant
b	material parameter
B	Kohout-Věchet regression constant
b_{DV}	material parameter for Dang Van multiaxial fatigue strength criterion
C_B	Basquin regression constant
C_{K-V}	Kohout-Věchet regression constant
C_1, C_2	power law constants for TCD
CV	critical volume
CV_i	critical volume of the i^{th} finite element
γ	shear strain
γ'	relative stress gradient
d	diameter
D_{PM}, D_{LM}, D_{AM}	critical distance according to Point Method, Line Method and Area Method
δ	out-of-phase angle
Δ	material plane
E	Young's modulus
ε	normal strain
f_{-1}	fully-reversed plain axial fatigue limit (or fatigue strength at a given N_f)
F	force
$\emptyset$	material plane orientation angles
θ	material plane orientation angle, angular coordinate
k	fatigue limit ratio
K_f	fatigue strength reduction factor
K_t	stress concentration factor
K_{th}	threshold stress intensity factor
$I_{1,d}$	first invariant of the stress tensor
l	length
L	El Haddad's parameter
m	total number of elements composing the critical volume
M_b	bending moment
M_t	torque
n	fatigue factor
$\hat{n}$	normal unit vector
n_i	total number of nodes in the i^{th} finite element
$n_{i,crit}$	number of nodes in the i^{th} finite element included in the critical volume
N, N_f	number of cycles to failure (or fatigue life)
q	notch sensitivity index
r	notch radius, radial coordinate
R	load ratio

R_e	yield strength
R_m	ultimate tensile strength
$RMSE$	root mean square error
R^2	coefficient of determination
s	normalized maximum principal stress
σ_0	material fatigue limit (or plain fatigue limit)
$\sigma_{0,n}$	nominal notch fatigue limit
σ_1	maximum principal stress
σ_a	normal stress amplitude
$\sigma_{a,eq}$	equivalent stress amplitude
σ_{crit}	critical stress value used to define the critical volume
σ_{eff}	effective stress according to TCD
σ_{ep}	elastic peak stress
σ_{gross}	gross nominal stress
$\sigma_{0,HS}$	hotspot notch fatigue limit (referred to as elastic peak stress amplitude)
σ_H	hydrostatic stress
σ_m	mean normal stress
σ_{max}	maximum normal stress
σ_{min}	minimum normal stress
σ_{Mises_max}	von Mises equivalent stress at the notch root
$\overrightarrow{\sigma_n}$	normal stress vector
σ_{net}	net nominal stress
σ_{nom}	nominal normal stress
σ_{PS1_max}	maximum principal stress at the notch root
σ_u	ultimate tensile strength
$\sigma_x, \sigma_y, \sigma_z$	normal stresses
$[\sigma]$	stress tensor
t	time
t_{-1}	fully-reversed plain torsion fatigue limit (or fatigue strength at a given N_f)
$\vec{t}$	total stress vector
$\vec{\tau}$	shear stress vector
τ_a	shear stress amplitude
τ_m	mean shear stress
$\tau_{xy}, \tau_{xz}, \tau_{yz}$	shear stresses
V_i	volume of the i^{th} finite element
w	Basquin regression constant
W_b	bending section modulus
W_t	torsional section modulus
ω	angular frequency
z	parameter used to define the critical stress amplitude and the critical volume

1 FATIGUE OF MATERIALS

1.1 DEFINITION OF FATIGUE

Fatigue phenomenon is the progressive structural failure that occurs through the initiation and propagation of cracks until the component failure. This happens when a material is subjected to time-variable loading: it can fail due to fatigue, even if the variation in stress is below its yield strength, and so no evident large-scale plastic deformation altering the process zone is detected. Indeed, at such a low stress level, plastic deformation is limited to a small number of grains of the material. At each solicitation the part undergoes microdamage which has no short-term consequences, but the damage accumulation leads to the part failure over time [1], [2]. The two main reasons why a component can experience variable loading are reported hereafter. First of all, operating conditions of the component, or the structure, can vary over time: thus, this determines the presence of actual work cycles. Secondly, fatigue can be also due to the presence of dynamic effects, such as vibrations [3]. Regarding this latter case, an example is represented by aircraft turbine blades which experience huge numbers of vibratory cycles during their lifetimes: in this case there is interest in fatigue at ultra-high cyclic lifetimes, such as 10^{10} cycles [4].

Since the fatigue problem still represents one of the principal causes of failures of mechanical components, its study became the focus of numerous research works [5]. This problem is much more complicated phenomenon compared to the static loading of structures, because damage features of fatigue failure are different from the static ones [6]. When static failure happens, the component usually develops a very large deflection because the stress has exceeded the material yield strength. This is especially true for ductile materials like structural alloys. For this reason, static failures give visible warning in advance, so that the damaged part can be replaced in time, despite what happens with fatigue failures. With regard to the latter case, the part can fail without any pronounced plastic deformation. As a consequence, fatigue failures are sudden and total, and hence dangerous [6], [7]. It must be pointed out that the fatigue failure arises from three stages of development called Stage I, or crack initiation, Stage II, or crack propagation, and Stage III, or final rupture [1], [6]. In Stage I fatigue is a material surface phenomenon. There is the initiation of one or more microcracks due to cyclic plastic deformation, followed by crystallographic propagation extending from grains about the origin. During this phase, cracks are not normally noticeable to the naked eye. The initiation period is supposed to be completed when microcrack growth is no longer depending on the material surface conditions. In Stage II microcracks evolve into macrocracks forming parallel plateau-like fracture surfaces separated by longitudinal ridges. These plateaus are generally smooth and normal to the direction of maximum stress. These cracked surfaces open and close continuously because of cyclic loading, rubbing together and creating wavy dark and light bands referred to as beach marks or clamshell marks. Finally, Stage III occurs when the remaining material cannot support the load anymore, resulting in a fast fracture that actually can be brittle, ductile or a combination on both [2], [6].

1.1.1 Fatigue parameters in cyclic loading

When performing the fatigue assessment, it is important to take into account some parameters: the most important ones are reported hereafter [7]. Consider a body subjected to an external system of forces as showed in Figure 1.1.

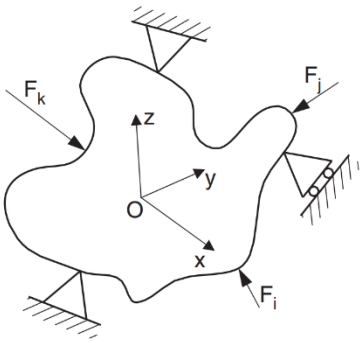

Figure 1.1: Body subjected to an external system of forces [7]

Such system of forces results, at point O, in a uniaxial stress state along the x-axis, which can be expressed as follows:

$$\sigma_x(t) = \sigma_{x,m} + \sigma_{x,a}\sin(\omega t) \tag{1.1}$$

where t is time, ω is the angular velocity, and $\sigma_{x,m}$ and $\sigma_{x,a}$ are mean stress value and stress amplitude of the stress component $\sigma_x(t)$, respectively. The maximum (1.2) and minimum value (1.3) of the stress component turn out to be:

$$\sigma_{x,max} = \sigma_{x,m} + \sigma_{x,a} \tag{1.2}$$

$$\sigma_{x,min} = \sigma_{x,m} - \sigma_{x,a} \tag{1.3}$$

thus, the range of stress variation ($\Delta\sigma_x$) is equal to:

$$\Delta\sigma_x = \sigma_{x,max} - \sigma_{x,min} = 2\sigma_{x,a} \tag{1.4}$$

In the end, the load ratio (R) can be expressed as:

$$R = \frac{\sigma_{x,max}}{\sigma_{x,min}} \tag{1.5}$$

Figure 1.2 summarizes previous definitions and reports three examples of different load ratios.

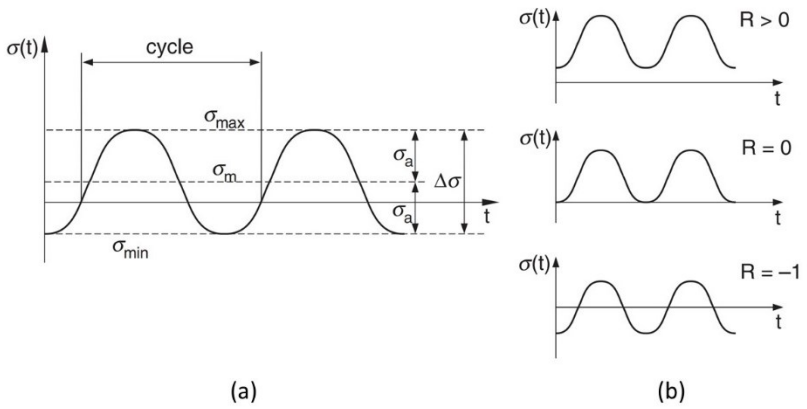

Figure 1.2: Fatigue parameters: (a) stress quantities used to assess the fatigue problem under uniaxial loading, (b) three examples of different load ratio [7].

The mean stress plays an important role in the overall fatigue strength of engineering materials. A fatigue test carried out under fully reversed loading ($R = -1$) results in no presence of mean stress effect. While it is pointed out by experimental reality that fatigue damage increases as the superimposed tensile static stress ($\sigma_{x,m}$) increases, so in case of $R > -1$ [1].

1.1.2 S-N curve

S-N curve, also called Wöhler curve, represents the dependence of fatigue strength on the number of cycles to failure. Material fatigue behaviour is studied performing several fatigue tests performed on unnotched specimens at different stress levels: reducing the stress amplitude of the applied loading, the number of cycles to failure increases. Note that strengths are obtained by experimental tests carried out until failure, or until a very high number of cycles if the failure does not occur (e.g. 10^7 cycles) [2], [8].

An example of S-N curve is reported in Figure 1.3 [2]. It refers to the CrMo steel SAE 4130 and it was obtained from unnotched specimens tested without applying any mean stress. Fatigue life (N) is usually plotted in logarithmic scale, while in literature the stress amplitude (σ_a, in figure referred to as S_a) can be presented both on a linear or on a logarithmic scale. Here the latter option is adopted, because it leads to an approximately linear relation between $\log \sigma_a$ and $\log \mathrm{N}$ in the middle region, the so-called finite life region. In the central part of the curve, it is possible to read the fatigue strengths offered by the material for given number of life cycles N. While the horizontal asymptote on the right part represents the material fatigue limit (σ_0, in figure referred to as S_f). Fatigue limit is the lowest stress amplitude which is still capable to nucleate a microcrack that can grow to failure [2]. Searching for the fatigue limit boils down to estimate a threshold stress level that must not be exceeded to avoid fatigue failure occurs at some point: for several engineering applications this represents a design criterion. The transition point to the fatigue limit is called “knee of the Wöhler curve”. Firstly, its presence depends on the type of material (e.g. steels have it, other light alloys like aluminium ones do not have it [3]), but also on the presence of a notch, the size of the notch and the surface roughness. For unnotched specimens made in low carbon steel, the Wöhler knee is assumed to occur at $\mathrm{N} = 2 \cdot 10^6$ [2]. Note that there is also another asymptote at the upper left side of the curve. It is located in correspondence with the ultimate tensile strength of the material: indeed, the specimen will fail in the first cycle as in a static tensile test.

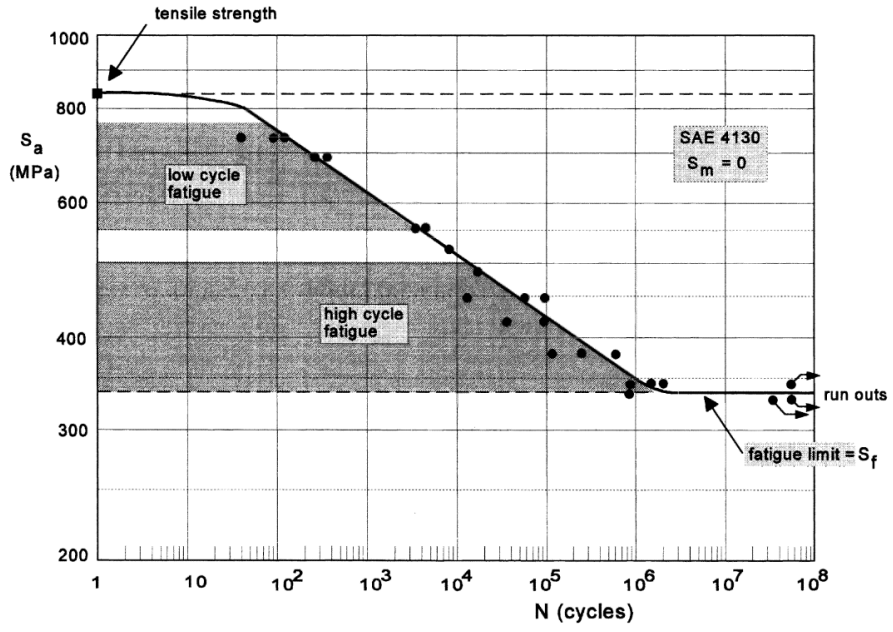

Figure 1.3: S-N curve for SAE 4130 represented in a double-logarithmic scale graph [2].

Regarding fatigue life, the two regions of low-cycle fatigue (LCF) and high-cycle fatigue (HCF) can be distinguished in the S-N diagram. There is no perfect agreement between different authors regarding the boundary condition that define these two life domains. Schijve [2] considers lives of $1 \leq N \leq 10^4$ as low-cycle fatigue, and lives of $N > 10^5$ as high-cycle fatigue lives. However, according to Shigley [6], the interval $1 \leq N \leq 10^3$ is considered to be low-cycle fatigue while lives of $N > 10^3$ are in the high-cycle fatigue region. The more relevant difference between the two regions is that low-cycle fatigue is associated with microplastic deformation at every cycle, while high-cycle fatigue is more related to an elastic behaviour on a macro scale of the material. The latter case is definitely the more common one in structural engineering [2].

In conclusion, a brief reference to the load ratio influence on fatigue damage, already discussed in the previous paragraph, is presented here. Increasing the mean stress ($\sigma_{x,m}$), which means increasing the load ratio (R), fatigue curves are seen to move downwards in S-N diagram (see Figure 1.4a). As a consequence, a decrease of R raises the material fatigue limit (see Figure 1.4b) [7].

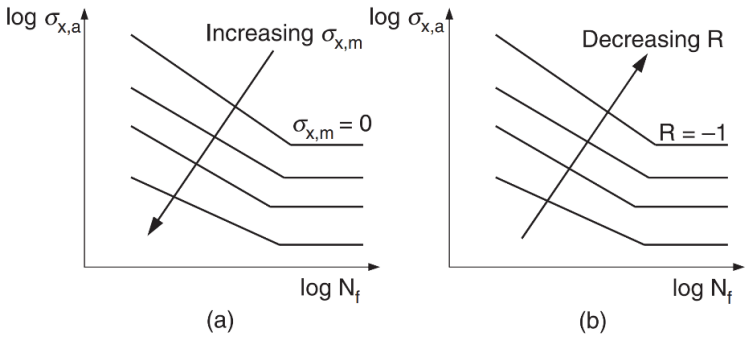

Figure 1.4: Effects of (a) mean stress and (b) and load ratio under uniaxial fatigue loading [7].

1.2 FATIGUE DATA REGRESSION MODELS

The definition of S-N curve has been already introduced in previous Paragraph 1.1.2. It must be kept in mind that a fatigue curve is built by testing different material specimens at different stress levels. During fatigue tests the stress amplitude (independent variable) is adjusted and the number of life cycles (dependent variable) is the result. Despite this, fatigue curves are usually plotted in the form $\sigma_a = f(N)$, or more often as $\sigma_a = f(logN)$ [8]. Actually, sometimes it is also preferred to adopt the logarithmic scale on both strength and life axes, because this leads to an approximately linear relation between the logarithms of the two fatigue variables [2], as also pointed out later. To build the S-N curve, experimental points must be fitted using a data regression model. It is relevant to remember that experiments carried out at the same stress level do not give in the reality the same fatigue life. There is always a scatter between results of similar tests, due to the statistical nature of the fatigue failure phenomenon [2]. One of most commonly used regression methods is the Basquin linear model, but there are also other interesting alternatives like the non-linear model of the Kohout-Věchet regression: both of them are hereafter described.

1.2.1 Basquin regression

The first function used to determine the S-N dependency was formulated by Basquin (1910), who proposed the following power law [9]:

$$\sigma = aN^b \tag{1.6}$$

where σ indicates the fatigue strength, N the number of cycles, while a and b are constants depending on the material (with b negative number). Although this model is more than 100 years old, it still represents the part of standards for steel structures (e.g. Eurocode 3) [10]. Several modifications of the Basquin function were proposed later, thereby they were called Basquin type functions. The existence of a fatigue limit, doubted by Basquin, was proved by Stromeyer (1914) who extended the formulation to the high-cycle region:

$$\sigma = aN^b + \sigma_\infty \tag{1.7}$$

where σ_∞ refers to the fatigue limit. Afterwards, Palmgren (1924) extended the function to both the low- and the high-cycle regions, introducing the additional parameter B:

$$\sigma = a(N + B)^b + \sigma_\infty \tag{1.8}$$

All Basquin type functions proposed above are summarized by Weibull [11] and Kohout-Věchet [8].

1.2.2 Kohout – Věchet regression

A new regression model comes from Czech research about fatigue. It has been proposed by Kohout – Věchet (2001) and it consists in the symmetric extension of the Basquin function to the LCF and HCF regions [8]. The new equation is based on the four parameters a, b, B and C:

$$\sigma = a \cdot \left[\frac{(N + B) \cdot C}{N + C}\right]^b \tag{1.9}$$

Thanks to the additional two parameters adopted in this model, the regression curve can follow the trend of experimental data with two bends [10]. As showed in Figure 1.5a, where both the axes are on logarithmic scale, the function bends in $N = B$ and $N = C$: these are the transition points to the

two asymptotes $\sigma = \sigma_1$ and $\sigma = \sigma_\infty$, respectively (with σ_1 referring to the ultimate tensile strength). Moreover, in the same figure the tangent line representing finite life region is also reported. This tangent is described by the logarithm of Basquin function $\log \sigma = \log a + b \log N$, which contains the mentioned parameters a and b. The tangent intersects the asymptotes in $N = B$ and $N = C$. In addition, in the mentioned points the Kohout-Věchet function (henceforth referred to as K-V) shows a slope equal to $b/2$ (see at Figure 1.5b). Meanings of all K-V parameters are now clear. As regards this current work, both Basquin and K-V regressions were implemented to fit experimental data and get the S-N curves.

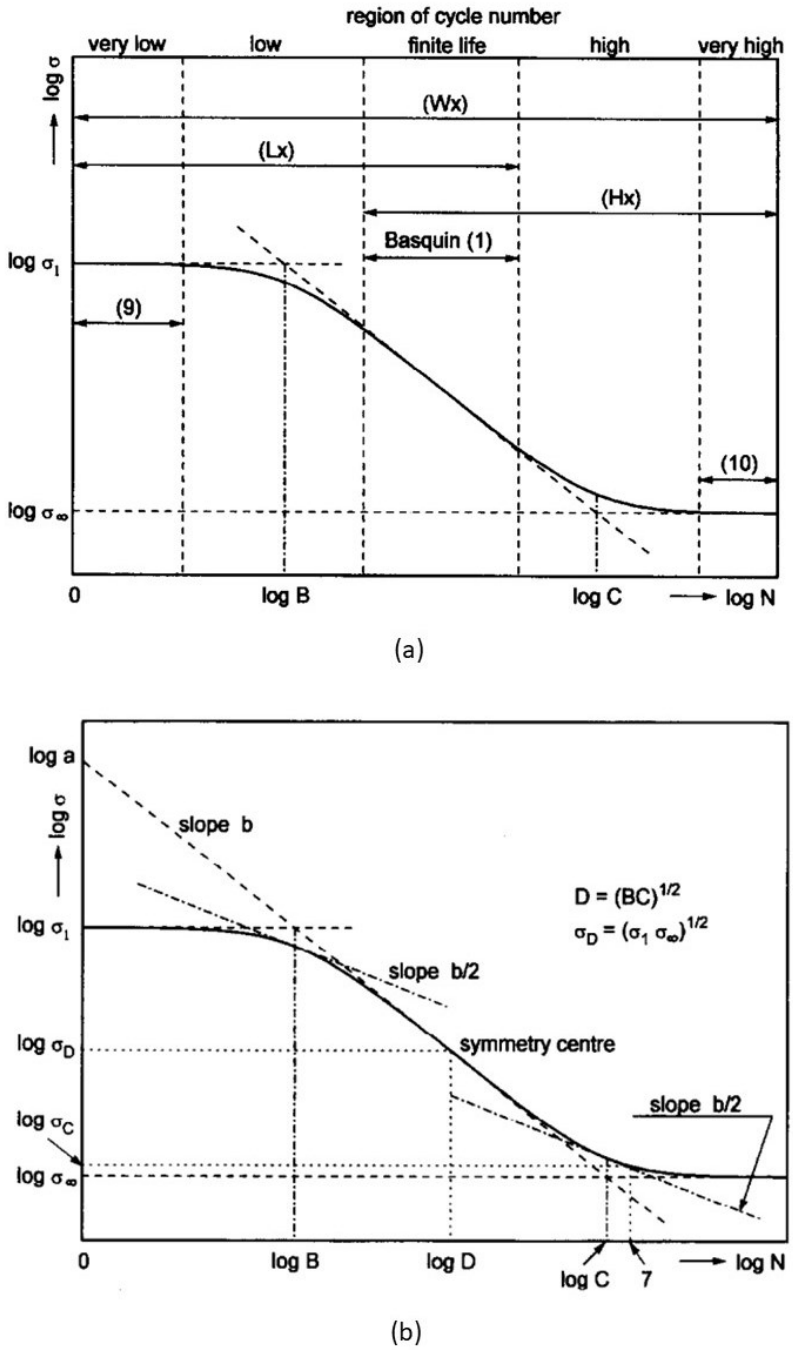

Figure 1.5: Kohout-Věchet model for S-N curve regression: (a) graph of the curve belonging to the new function, (b) geometrical meaning of all parameters [8].

The K-V regression turns out to be very interesting to use for fitting experimental data from fatigue tests. Since the Basquin function has only two parameters, it cannot include in the regression the points close to the quasi-static and the fatigue limit regions. Instead, thanks to the additional parameters, the K-V curve models a wider region, because it bends at the transition point to the asymptotes following the typical S-like shape of the S-N curve. K-V model results also to be more practical because it allows the analyst to avoid making a subjective evaluation when determining which points belong to the inclined part of the S-N curves (as it happens for the Basquin regression, where the outermost points must be excluded otherwise they would influence badly the veracity of the linear regression) [12].

1.3 NOTCH EFFECT

After fatigue was recognized as a serious threat to the integrity of a structure, it was soon understood that notches aggravate the fatigue problem considerably [2]. Real mechanical components are definitely more complicated to be studied if compared to common fatigue specimens tested in laboratory, in terms of complex geometries but also surface roughness and tolerances [13]. Complex geometries of real mechanical parts result in stress concentration phenomena, which favour the initiation of fatigue cracks. For this reason they must be properly taken into account during the design process because of their detrimental effect on the material fatigue strength [14]. Easiest stress concentrator, responsible for introducing notch effect in fatigue, to be recognised are usually related to shape variations of components, like holes, diameter narrowings, sharp edges, weld joints, etc: all kinds of notch can be held responsible for introducing notch effect in fatigue. The presence of notches reduces the fatigue strength, since the damage occurs primarily in these zones which experience the highest alternating stresses, responsible for accelerating crack initiation and propagation stages [4], [5]. The well-known general guideline is to design stress raisers having a notch root radius as large as possible, but very often this is not feasible [7].

1.3.1 Stress concentration factor

The study of fatigue on notched components can be addressed starting from the simpler scenario of uniaxial fatigue case, before delving into the multiaxial one. So, in accordance to the uniaxial loading hypothesis, some definitions derived from Peterson's studies are recalled hereafter [7]. Consider a body of homogeneous, isotropic, linear elastic material containing a stress raiser (e.g. a U-notch as showed in Figure 1.6). It is always possible to define two different reference stresses: the net nominal stress (σ_{net}) and the gross nominal stress (σ_{gross}), where the first is evaluated with respect to the net cross-sectional area and the second with respect to the gross-sectional area. As visible again in Figure 1.6, at the notch apex the first principal stress is maximum and it is identified as the elastic peak stress (σ_{ep}). Moving away from the notch root the stress gradually decreases and, if the component is large enough, it tends to the net nominal value. One interesting aspect of the linear elastic stress function is its gradient, discussed in detail in the next paragraph.

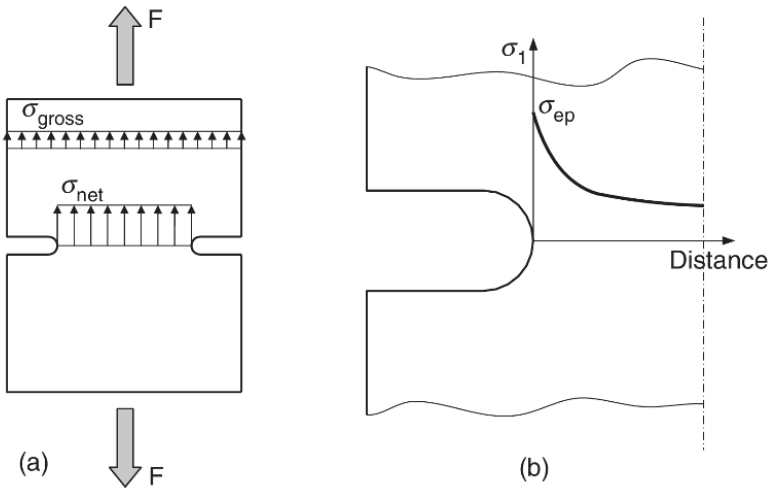

Figure 1.6: Definition of (a) net and gross nominal stress, and (b) linear elastic peak stress at the root of the root [7].

The stress raiser is described by the stress concentration factor (K_t), which can be defined referring both to the net nominal stress evaluated at the net section (1.10) and to the gross nominal stress evaluated at the gross section (1.11):

$$K_{t,net} = \frac{\sigma_{ep}}{\sigma_{net}} \tag{1.10}$$

$$K_{t,gross} = \frac{\sigma_{ep}}{\sigma_{gross}} \tag{1.11}$$

Later, when mentioning the stress concentration factor with the symbol K_t, it will refer directly to the net one ($K_{t,net}$).

1.3.2 Fatigue strength reduction factor

Assessing the notch effect in fatigue, another factor that must be taken into account is the fatigue strength reduction factor (K_f). This factor is expressed as the ratio between the plain fatigue limit of the material (σ_0) and the nominal notch fatigue limit ($\sigma_{0,n}$):

$$K_f = \frac{\sigma_0}{\sigma_{0,n}} \tag{1.12}$$

Note that such fatigue limits refer to nominal stress quantities. Because of its definition, the K_f is always bigger than 1. It must be pointed out that the fatigue strength reduction factor can be calculated not only by considering plain and notch fatigue limits, but also taking into account plain and nominal notch endurance limits for a given lifetime basis N. This latter kind of fatigue strength reduction factor, that would be correctly annotated as $K_{f,N}$, is different from the first one defined above: indeed, material and nominal S-N curves are usually not parallel in the S-N diagram, except for their fatigue limit asymptotes [15]. Factors K_t and K_f can be related together thanks to the well-known equation formulated by Peterson:

$$K_f = 1 + q(K_t - 1) \tag{1.13}$$

In this formula, q is the notch sensitivity index that describes how much sensitive the material is to the presence of the notch. Its value is between 0 and 1: $q = 0$ stands for no material notch sensitivity, which means there is not any reduction of the plain fatigue limit. While $q = 1$ stands for full material notch sensitivity, that makes the K_f to be equal to K_t with the effect of a relevant decrease of the notch fatigue limit compared to the plain fatigue limit. Several expressions to calculate the notch sensitivity index are present in literature. The most relevant expressions available in literature to calculate factor q were proposed by Peterson and Neuber, respectively [16]. Peterson formulation is the following:

$$q = \frac{1}{1 + \frac{a_P}{r}} \tag{1.14}$$

where the distance a_P is a material constant and r is the notch radius. While Neuber formulation results to be:

$$q = \frac{1}{1 + \sqrt{\frac{a_N}{r}}} \tag{1.15}$$

where a_N is again the material constant. In literature it is possible to find also graphs helpful to evaluate q. For example, notch sensitivity charts, based on Neuber equation 1.11, for bending and axial loading and for shear loading are reported in Figure 1.6 and Figure 1.7, respectively.

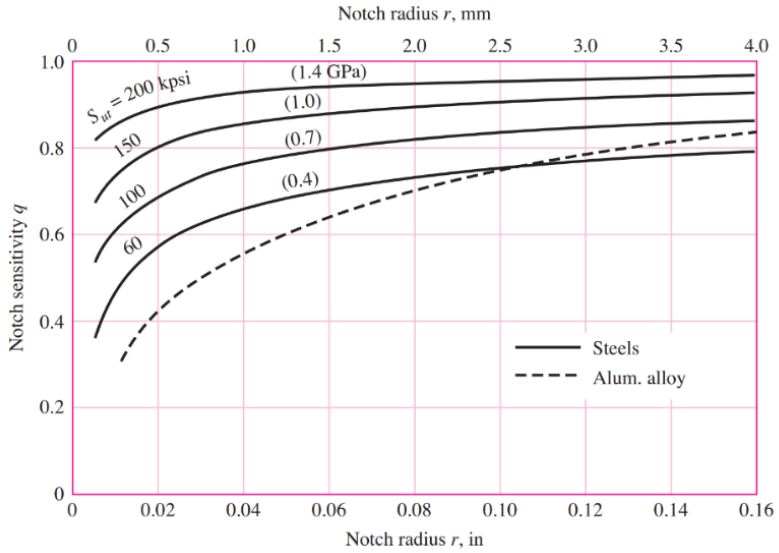

Figure 1.8: Notch-sensitivity charts for steels and UNS A92024-T wrought aluminium alloys subjected to reversed bending or reversed axial loads [6].

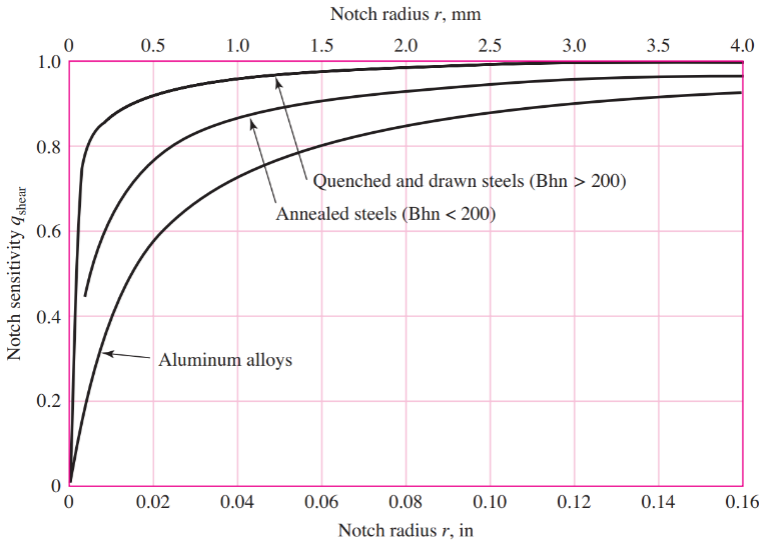

Figure 1.7: Notch sensitivity curves for materials in reversed torsion [6].

1.3.3 Stress gradient effect

Although the peak stress is of great importance in assessing fatigue of notched components, it is also interesting to know how fast the stress decreases away from the notch root [2]: the strength of the notch is related not only to the stress concentration factor, but also to the stress distribution around the notch area. The stress gradient at the notch apex gives an indication of the volume of the highly stressed material. Many research studies showed how much its effect is significant on the fatigue life of notched components [5]. It is possible to prove this aspect by taking into account a simple example reported in [2]. Consider a circular hole with radius r in an infinite sheet loaded along the y-axis in hypothesis of material linear elastic behaviour (see Figure 1.9).

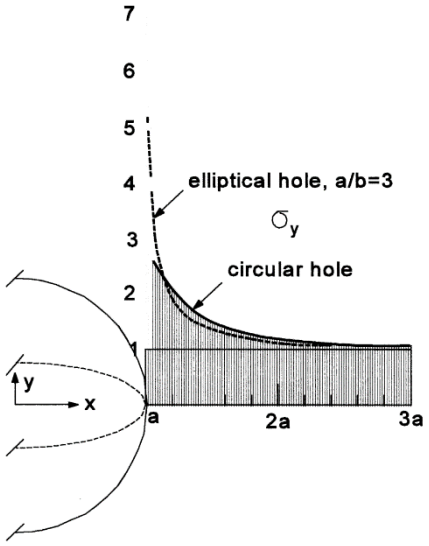

Figure 1.9: Stress gradients at the root of the notch for circular and elliptical holes [2].

The value of stress concentration factor in this case is well known from the solution provided by Kirsch (1898):

$$K_t = 3 \tag{1.16}$$

The equation of the stress gradient at the root of the circular notch, as provided in [2], results in:

$$\left(\frac{d\sigma_y}{dx}\right)_{x=\mathrm{a}} = -\left(2 + \frac{1}{K_t}\right)\frac{\sigma_{ep}}{r} = -\alpha\frac{\sigma_{ep}}{r} \tag{1.17}$$

where $\mathrm{x} = \mathrm{a}$ is the x-coordinate of the notch apex, with respect to the reference frame showed in Figure 1.9 (note that a is equal to radius r), and α is a proportionality constant. The negative stress gradient along the x-direction is proportional to the peak stress (σ_{ep}) and inversely proportional to the root radius. While the proportionality constant mentioned before can assume values inside the interval:

$$2 < \alpha < 3 \tag{1.18}$$

Apparently, the K_t factor does not have a great impact on the stress gradient coefficient α. Indeed, for notches with K_t included in the range of 2 to 5, α value would be between 2.2 and 2.5. However, the numerical example provided below helps to better understand how the stress gradient can affect the fatigue behaviour of the material. Consider the circular hole radius to be $r = 2.5\ \mathrm{mm}$ and image to want to estimate the distance d along the x-axis for a 10% drop of the y-stress component of the stress field, so from σ_{ep} to $0.9\sigma_{ep}$. Thus, distance d can be derived with equation (1.17):

$$\left(\frac{d\sigma_y}{dx}\right)_{x=a} \approx -\frac{\sigma_{ep} - 0.9\sigma_{ep}}{d} = -\left(2 + \frac{1}{3}\right)\frac{\sigma_{ep}}{2.5}$$

which gives $d \approx 0.1\ \text{mm} = 100\ \mu\text{m}$. Considering an average grain size of $50\ \mu\text{m}$, this would mean that the depth d involves just few grains. Therefore, the grains at and below the notch root surface are the most loaded ones: this has relevant consequences on the component fatigue life.

One more consideration about the stress gradient is here reported. In Figure 1.10 two specimens are presented. They have different size, but they are geometrically similar: in particular, all dimensions of specimen 2 are two times larger than the dimensions of specimen 1.

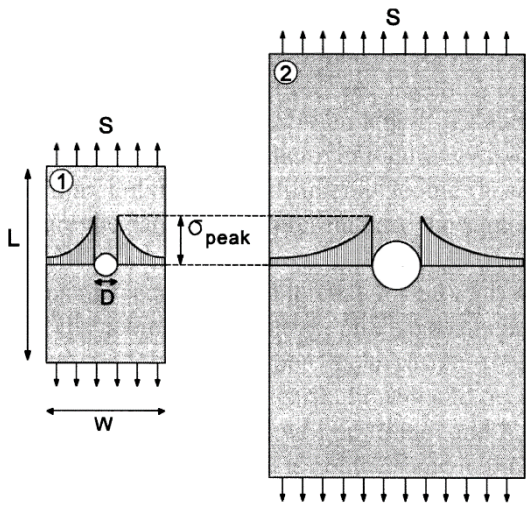

Figure 1.10: Geometrically similar specimens having the same K_t but different stress gradients. The elastic peak stress (σ_{ep}) is referred to as σ_{peak} in the figure [2].

This means that all dimensional ratios are equal between the two cases. It is worth noting that because K_t is a dimensionless ratio, it can depend on dimensionless ratios only. As a result of the geometric similarity, all displacements in the specimen 2 are two times bigger than the ones in specimen 1, but the strains are the same. As a consequence, a geometrically similar stress distribution should occur in both specimens. The same elastic peak stress will be found, and K_t is the same. However, the stress gradient is not the same because it is not a dimensionless quantity. Therefore, the larger the notched specimen, the larger the volumes and the notch surface areas of highly stressed material, which is significant for the size effect on fatigue (discussed later in the next paragraph) [2].

The stress gradient of σ_y along the x-axis has been considered so far (Figures 1.9 and 1.10). But it is also interesting to study what concerns the stress gradient along the other orthogonal direction. From Figure 1.11 it is possible to see that the tangential stress to the edge of the hole decreases along such an edge relatively slowly in comparison to what happens in the x-direction which is perpendicular to the notch root. Apparently the highly stressed layer of material is the one under the notch edge surface, thus the stress gradient along the edge is of greater importance than the stress gradient perpendicular to it [2].

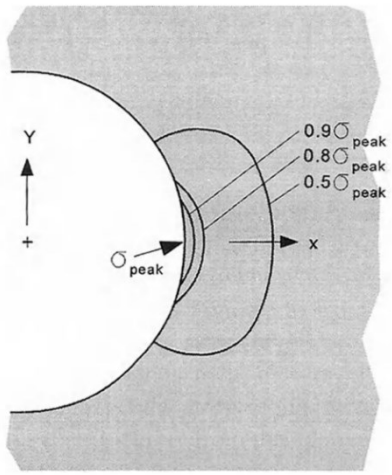

Figure 1.11: Constant principal stress lines show how the stress decreases along perpendicular and tangential directions to the notch edge [2].

1.3.4 Size effect

Size effect implies that larger specimens may have a lower fatigue strength. For instance, a size effect can be observed on the fatigue limit of unnotched specimens. It must be remembered that fatigue limit is primarily a matter of some specific weak spots that favour crack nucleation (at the material surface or just below it) [2]. Figure 1.12 reports the fatigue limits (indicated with S_f) for unnotched specimens realised in different steel alloys for different testing scenarios. In particular, in Figure 1.12a values of fatigue limit referred to rotating bending are reported, while in Figure 1.12b both tension-compression and rotating bending cases are presented for a Cr-steel. There are two very important aspects showed in the graphs to be pointed out. Firstly, specimens with a smaller diameter show higher fatigue limits, as indicated in Figure 1.12a. Secondly, the type of load, which is evidently also co-invoked in the size effect, has an influence on the fatigue limit. The idea is that the probability of having such weak spots where crack can start is higher in components that have a larger material surface area experiencing the maximum stress cycle. This holds true for specimens with larger dimensions, but it is clear that such a portion of highly stressed material depends also on the imposed loading mode and the related stress distribution. The critical material surface area of an unnotched specimen loaded in cyclic push-pull is relatively large if compared to the case of the same specimen loaded in cyclic bending: therefore, the fatigue limit in the first case may be expected to be

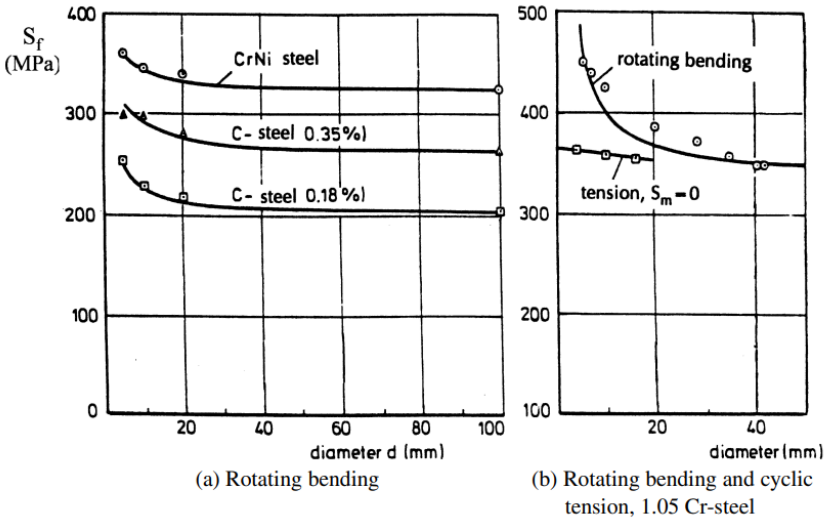

Figure 1.12: Size effect on the fatigue limit of different types of steel tested (a) under rotating bending and (b) under tension-compression [2].

lower than in the second case, as showed in Figure 1.12b. The discussion can be extended to notched specimens. It was already noted in the 1930s that, for a fixed value of K_t, specimens with a larger notch root radius could have a lower fatigue limit. This holds true because the size effect depends on stress gradient at the root of the notch, which is indeed influenced by the notch geometry itself. Therefore, the larger the notch root radius, the bigger the highly stressed volume: Figure 1.10 can help to understand that [2].

In the end, size effect is a matter of how much volume of material carries out the high cyclic stress, and this is something indissolubly related to the stress gradient effect. It is no surprising that stress gradient and size effects are often superposed [17]: this evidence, as explained later, will represent a crucial reason of the development of the new approach presented in this research work.

2 MULTIAXIAL FATIGUE

2.1 INTRODUCTION

When the purpose is designing mechanical components and structures against fatigue, it is quite common to face with multiaxial loading and, thus, with the multiaxial fatigue problem. This holds true for many industries as automotive, aerospace, power generation among others. The earliest studies on multiaxial stress states, although under monotonic loading, refers to classical theories of Lame and Tresca in the late 19th century and then of von Mises in the early 20th century. Besides, the first bending-torsion combination is attributed to Lanza (1886) and the first systematic study of multiaxial fatigue was conducted by Gough and Pollard (1930s). Their works laid the foundation for the next fatigue models developed in the 1950s like Gough, Sines and Findley ones, and many other came. The advent of more accurate multiaxial fatigue testing equipment during last five decades allowed to go deeper in the topic with much additional work carried out. However, the problem still remains elusive and, due to its practical application significance, further research is needed to develop accurate and reliable solutions for multiaxial fatigue design, life estimation and failure assessment [18].

It is important to point out that, in real problems, the multiaxiality of the stress field in a mechanical part can be induced in two ways. One possibility is to load the component by a combination of different external forces, such as concentrate or distributed forces, torques, bending moments, etc. The second possible reason of multiaxiality is the presence of stress concentrators from which the distortion of the stress field originates. It is proved that if a notched component is uniaxially loaded, the presence of the notch results in a more complex stress-strain response and different stress-strain distributions [5]. In the field of research, multiaxial fatigue experiments can be carried out in several ways. It is evident that the design selected for the experimental specimen affects the applicable load combinations. Just to report some examples, one way to study multiaxiality is to test cruciform specimens loaded by two axial loads (either bending or push-pull) and torque. Another possibility is to use hollow bar specimens which can be also internally pressurized. Note that, pressurizing the inner surface of this kind of samples, it is possible to induce circumferential and radial stresses [12].

2.1.1 Stress tensor projection onto a generic material plane

Before delving into the complexities of the multiaxial fatigue problem, it is worth studying the equations suitable for determining the stresses relative to a generic material plane within a mechanical component, which is subjected to a cyclic load history.

Consider a body, like the one in Figure 1.1, and focus on a material point O belonging to it. The absolute reference frame $Oxyz$ is centred in such a point. A material plane Δ passing through point O and having a normal unit vector $\hat{n} = (n_x, n_y, n_z)$ can be located by using the spherical coordinates $\emptyset$ and θ, as illustrated in Figure 2.1. Angle $\emptyset$ is the angle between the projection of the normal $\hat{n}$ on plane x-y and the x-axis, while angle θ is the angle between the normal $\hat{n}$ and the z-axis. According to this schematization, all the possible material planes passing through point O can be investigated by varying angles $\emptyset$ and θ between 0 and 2π and between 0 and π, respectively [7], [19].

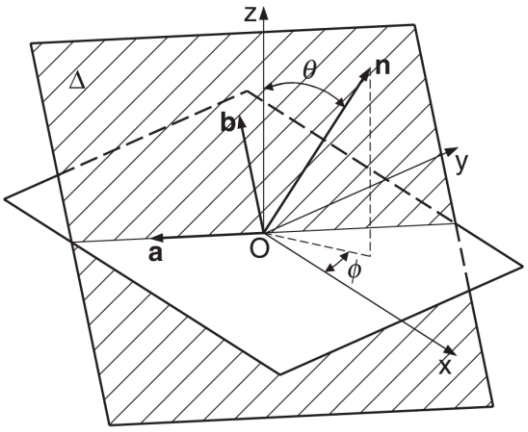

Figure 2.1: Definition of the material plane Δ passing through point O and normal to the unit vector $\hat{n}$ [7].

Components of the normal unit vector $\hat{n}$ can be expressed as functions of the angles $\emptyset$ and θ:

$$\begin{aligned} n_x &= \sin\theta \cdot \cos\emptyset \\ n_y &= \sin\theta \cdot \sin\emptyset \\ n_z &= \cos\theta \end{aligned} \tag{2.1}$$

Two additional arbitrary directions, $\hat{a}$ and $\hat{b}$, can be defined to establish another reference frame $Oabn$. These unit vectors $\hat{a}$ and $\hat{b}$ lie on plane Δ and are orthogonal to each other:

$$\begin{aligned} \hat{a} &= (a_x, a_y, a_z) \\ \hat{b} &= (b_x, b_y, b_z) \end{aligned} \tag{2.2}$$

The components of $\hat{a}$ and $\hat{b}$ can be expressed in terms of the angles $\emptyset$ and θ:

$$\begin{aligned} a_x &= -\sin\emptyset \\ a_y &= \cos\emptyset \\ a_z &= 0 \end{aligned} \tag{2.3}$$

$$\begin{aligned} b_x &= -\cos\theta \cdot \cos\emptyset \\ b_y &= -\cos\theta \cdot \sin\emptyset \\ b_z &= \sin\theta \end{aligned} \tag{2.4}$$

In the most general case, the stress state damaging the material in point O is triaxial. Consequently, at any time instant (t) of the applied cyclic load history, the stress tensor ($[\sigma(t)]$) at O can be expressed as follows:

$$[\sigma(t)] = \begin{bmatrix} \sigma_x(t) & \tau_{xy}(t) & \tau_{xz}(t) \\ \tau_{xy}(t) & \sigma_y(t) & \tau_{yz}(t) \\ \tau_{xz}(t) & \tau_{yz}(t) & \sigma_z(t) \end{bmatrix} \tag{2.5}$$

Accordingly, the total stress vector ($\vec{t}$) results in:

$$\vec{t}(t) = \left[t_x(t), t_y(t), t_z(t)\right] \tag{2.6}$$

Components of $\vec{t}$ are derived from the stress tensor in 2.5:

$$\begin{aligned} t_x(t) &= \sigma_x(t) \cdot n_x + \tau_{xy}(t) \cdot n_y + \tau_{xz}(t) \cdot n_z \\ t_y(t) &= \tau_{xy}(t) \cdot n_x + \sigma_y(t) \cdot n_y + \tau_{yz}(t) \cdot n_z \\ t_z(t) &= \tau_{xz}(t) \cdot n_x + \tau_{yz}(t) \cdot n_y + \sigma_z(t) \cdot n_z \end{aligned} \tag{2.7}$$

Finally, normal and tangential stresses relative to the investigated plane can be obtained as follows:

$$\sigma_n(t) = t_x(t) \cdot n_x + t_y(t) \cdot n_y + t_z(t) \cdot n_z \tag{2.8}$$

$$\begin{aligned} \tau_{na}(t) &= t_x(t) \cdot a_x + t_y(t) \cdot a_y + t_z(t) \cdot a_z \\ t_{nb}(t) &= t_x(t) \cdot b_x + t_y(t) \cdot b_y + t_z(t) \cdot b_z \end{aligned} \tag{2.9}$$

$$\tau_n(t) = \sqrt{\tau_{na}^2(t) + \tau_{nb}^2(t)} \tag{2.10}$$

These equations represent the basic tools for those multiaxial fatigue strength criteria, further elaborated later, that apply the concept of a critical plane in which the stress state must be evaluated [7], [19].

2.1.2 Proportional and non-proportional loading

When multiple load channels are activated, it is interesting to study their phasing [12]. To do that, it is necessary to first define the concepts of proportional loading and non-proportional loading. Consider the cylindrical specimen in Figure 2.2, which is loaded by both cycling tension-compression ($F(t)$) and torsion ($M_t(t)$) loads.

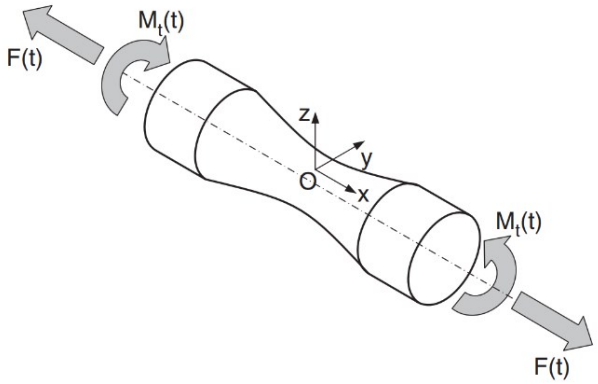

Figure 2.2: Cylindrical specimen subjected to combined tension and torsion, with the absolute reference frame $Oxyz$ centred in O [7].

In correspondence with the absolute reference frame fixed in point O, the two stress components can be written as follows (according to what already seen with equation 1.1):

$$\sigma_x(t) = \sigma_{x,m} + \sigma_{x,a} \sin(\omega t) \tag{2.11}$$

$$\tau_{xy}(t) = \tau_{xy,m} + \tau_{xy,a} \sin(\omega t - \delta) \tag{2.12}$$

where δ is the phase angle representing the phase shift between the two stress components [19]. Looking at the figure below, examples of in-phase (Figure 2.3a) and out-of-phase (Figure 2.3b) load histories characterized by $R = -1$ are reported.

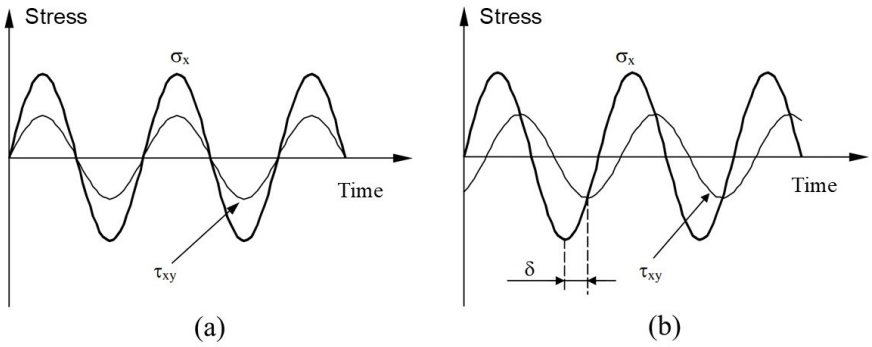

Figure 2.3: Examples of superposed push-pull and torsion load histories with R=-1: (a) in phase loading, (b) out-of-phase loading. Adapted from [19].

Proportional loading, also called in-phase loading, occurs when the stress tensor at one instant is multiple of a stress tensor at any other instant of the evaluated load history (similarly for the strain tensor). In this case, principal stress/strain directions remain fixed and do not change during the time. Referring to the previous example in Figure 2.3a, it is immediately clear that maximum load is reached at the same time both for axial and shear stresses (it is the same for the minimum load). Proportional loading paths are represented by cases 0 and 5 in Figure 2.4: the load path in the $\varepsilon - \gamma$ diagram (equivalent to the $\sigma - \tau$ one) goes through the origin $(0, 0)$ as a straight line. As already said, even a component is under uniaxial loading it often experiences multiaxial stresses, although typically in-phase, due to geometric constraints at notches [13], [18].

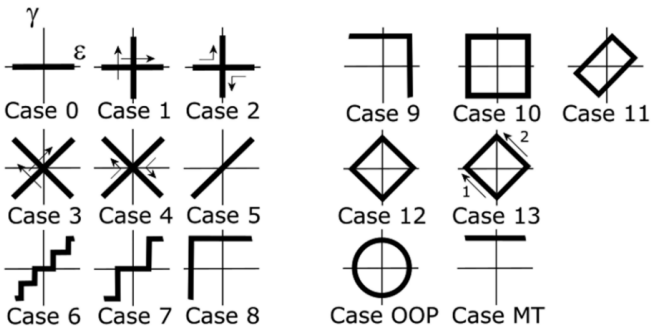

Figure 2.4: Different examples of proportional and non-proportional load paths. Note that only Case 0 and Case 5 represent cases of in-phase loading [13].

Whereas, if the previous hypothesis about proportionality of stress tensors evaluated at different time instants is not satisfied, and so normal and shear stress components change independently, the non-proportional loading, also referred to as out-of-phase loading, occurs (see Figure 2.3b). In this case the phase-shift angle will not be zero: this is a very important aspect because it is experimentally proved that, for equal stress amplitudes and mean values, the fatigue damage increases with the phase angle and reaches the maximum for $\delta = 90°$ [19]. In particular, among all out-of-phase loadings, the worst case comes with such a value of δ and a stress ratio between shear stress and normal stress amplitudes equal to [20]:

$$\frac{\tau_a}{\sigma_a} = 0.5 \tag{2.13}$$

With respect to the loading path diagram represented in the $\varepsilon - \gamma$ graph, note that any straight line shifted away from the zero results in a rotation of principal directions during the loading, so it must be classified as non-proportional loading (e.g. look at the case MT in Figure 2.4). Load non-proportionality is expected to be induced when the in-service component is loaded by several load channels [13]. There are different ways to do that, for example it is possible to induce out-of-phase

loading by providing two load channels where one is static and the other one is cyclic (again, it is possible to take as an example case MT in Figure 2.4). Alternatively, non-proportional loading can be obtained by providing a load ratio (R) which assumes different values over the different co-acting load channels [12], [21]. A shorter fatigue life is usually observed for specimens tested under out-of-phase loading. This evidence is often attributed to the additional non-proportional hardening, a material phenomenon caused by the rotations of principal directions during the loading cycle, which holds particularly true for metals [19]. However, there are materials that, although they are not characterized by this hardening, they also last for a shorter life under such a kind of loading [12], [18]. But there is more. According to Susmel [7], different isotropic materials are characterized by different sensitivities to out-of-phase loading, which could have a detrimental effect, or even a beneficial effect or no effect at all on their fatigue strengths. The presence of non-zero out-of-phase angles do not always result in an increase of fatigue damage as commonly presumed. Also Verreman [20] agrees with him and, with referring to previous researches (e.g. Nishihara and Kawamoto (1945) or Sonsino (1995)), both of them remember that HCF strength of ductile materials is apparently higher for some out-of-phase loading configurations. The accurate way to quantify such a sensitivity mentioned by Susmel definitely consists in running appropriate experiments on the considered materials. In the end, for sure the topic needs to be investigated more. There are a lot of issues still not solved, especially for what concerns HCF. A better understanding of HCF damage mechanisms is desirable to make better life estimations [20].

One more peculiarity about load phasing, that deserves to be pointed out, is reported hereafter. Consider a material plane Δ, whose orientation is defined by the normal $\hat{n}$, and consider also a point belonging to this plane. Stress vector ($\vec{t}$) consists of two components: the normal stress vector ($\overrightarrow{\sigma_n}$) and the shear stress vector ($\vec{\tau}$), the latter tangent to Δ. In case of proportional loading all these vectors ($\overrightarrow{\sigma_n}$, $\vec{\tau}$ and so $\vec{t}$) maintain their own directions during the cycle (see Figure 2.5a). Instead, when the material undergoes non-proportional loading only $\overrightarrow{\sigma_n}$ conserves its direction, while $\vec{\tau}$ component and thus also the resultant $\vec{\sigma}$ rotate (see Figure 2.5b) [22]. Consequently, the path created by the terminal point of the stress vector gets multidimensional, and it is not a straight line anymore [23].

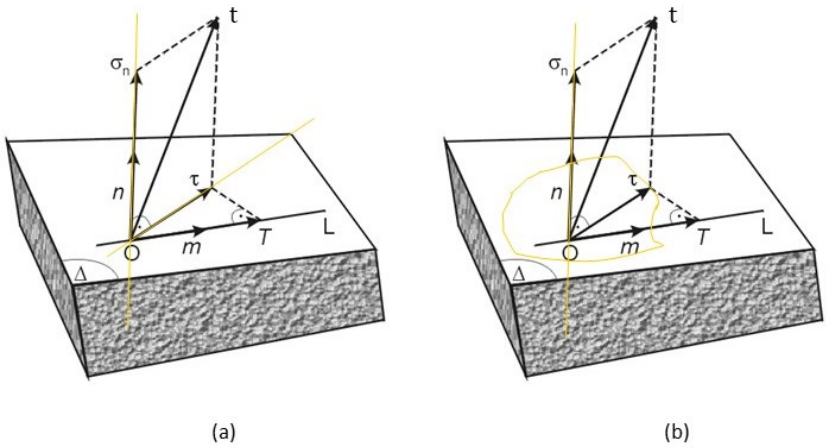

Figure 2.5: Stress vector components varying under (a) proportional loading and (b) non-proportional loading (stress components' paths are highlighted in yellow) [22].

Dealing with non-proportional loading, the problem of how to describe the effect of the changing shear stress on the evaluated plane arises [13]. In literature there are various methods available to deduce shear stress amplitude and mean value from the shear stress path. Papuga [23] emphasizes the key role of the selected procedure to process the stress path in non-proportional multiaxial contexts, because it directly affects the equivalent stress evaluation. Methods to assess the shear stress path available in literature are reported below [13]:

A. maximum projection method (MPM);
B. longest chord method (LCM);

C. minimum circumscribed circle method (MCCM);
D. minimum circumscribed ellipse method (MCEM);
E. maximum prismatic hull (MPH);
F. maximum convex hull (MCH).

These methods are summarized in Figure 2.6: ψ is the generic curve laying on the considered plane Δ which describes the shear stress path, while C_a, C_m and $C(t)$ are shear stress amplitude, shear stress mean value and resulting shear stress vector, respectively.

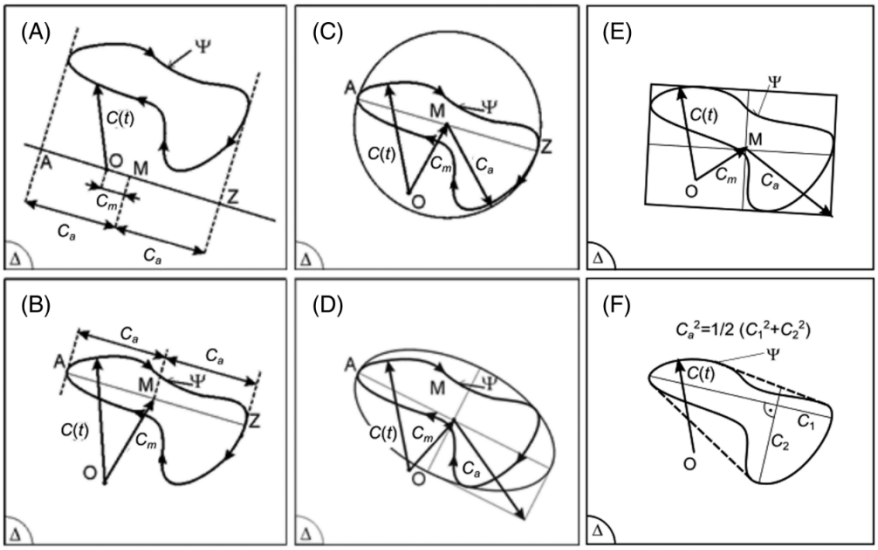

Figure 2.6: Methods of shear stress analysis on the evaluated material plane: (A) MPM, (B) LCM, (C) MCCM, (D) MCEM, (E) MPH and (F) MCH [13].

2.2 ADOPTED COMPUTATIONAL APPROACHES

Before analysing several types of multiaxial fatigue criteria have been developed over the years, it is important to point out one aspect. Regardless of the approach adopted to perform fatigue assessment, the starting point of any technique is the location of the components' weakest points. Here the stress/strain states must be determined, typically using the Finite Element (FE) method. After that, such stress/strain states have to be recalculated in terms of quantities which are suitable for be used with the adopted fatigue criterion [7].

Literature is populated by a rather large variety of multiaxial fatigue strength criteria that can be used to evaluate the fatigue damage parameter over the loaded component. It is interesting to note that one of the main reasons why all these criteria have been developed is to deal in some way with the problem of non-proportional loading. Indeed, researchers have found that traditional uniaxial strength criteria (e.g. von Mises or Tresca-Guest) cannot consider the complexity of the stress state in presence of non-proportional fatigue loading. As already explained, out-of-phase loading makes the principal directions to rotate during the cycle, so the positions of the maximum loaded planes clearly change as well. Because the non-proportional loading scenario is far from rare in engineering practice, and since basic uniaxial criteria often fail to result in acceptable fatigue life estimates (even for the simplest configurations), it is very important to address the problem adopting multiaxial fatigue strength criteria [12], [21]. The discussion about how to deal with multiaxial fatigue problem remains anyway of vital interest even for proportional loading case, which is the one treated in detail in this experimental work.

Putting all available criteria in a clear order is far from straightforward. As already mentioned, multiaxial fatigue problem is a "hot topic" in mechanical engineering and the number of existing multiaxial fatigue solutions is unpleasantly high [13]. An explanation of some of the currently most common approaches to the problem is reported below. Taking inspiration from classifications made by some authors like Papuga et al. [21], Fojtík et al. [10] and Susmel [7], multiaxial fatigue criteria are presented divided into the following main groups:

1. Critical plane-based criteria;
2. Integral criteria;
3. Criteria based on 5D Ilyushin deviatoric space.

To complete the overview, Liu et al. [5] point out that also other two families should be mentioned:

4. Equivalent strain-based criteria;
5. Energy based-criteria.

2.2.1 Critical plane-based criteria

The critical plane approach represents one of the most common solutions adopted in this field, because of the way how it perceives the physical mechanism of crack initiation and propagation [5]: for this reason, it is here explored. This kind of criteria assesses the fatigue failure on a specific plane, the so-called critical plane, which is located within the component. Representation of the stress components on a material plane has been already addressed in Paragraph 2.1.1 (see Figure 2.1). Although the common aspect of all criteria based on this approach is that they look at a critical plane where some stress/strain components (or a combination of them) exhibit a maximum value, they are characterized by different methods to define the critical plane orientation [24]. Some examples about this type of approach are reported hereafter:

- one idea is to define the critical plane as the one in which stress parameters should result in the highest equivalent stress amplitude. This is how, for instance, Findley (1959) and Dang Van (1973, 1989, 1993) criteria work [7], [10];

- another approach, implemented in criteria by Matake (1977) and McDiarmid (1991, 1994), considers critical plane the one experiencing the maximum shear stress range. Moreover, it states that multiaxial fatigue damage depends also on the maximum stress normal to such a plane [7], [10];

- one more alternative is represented by considering to be critical the plane where maximum shear strain amplitude is found. This proposal has been pursued by Fatemi et al. (1988) and more recently by Li et al. (2014) [24].

Regardless of the specific applied method, it is evident that the critical plane manifests the fatigue response of the whole specimen [10].

Reviewing the state of art about this approach (which is, as said, widely spread), it must be pointed out that there are different points of view from one author to another. In particular, the debate is rather open for what concerns the response of such methods in case of non-proportional loading. According to Fatemi [18], critical plane damage models, with both stress and strain terms, are the most appropriate ones to assess the multiaxial fatigue problem. He states their strong point is that they fully capture the physical nature of the damage process, reflecting the material constitutive response under both proportional and non-proportional loading. Also Susmel [7] remarks that criteria based on critical plane approach result to be highly accurate in estimating multiaxial fatigue limits also in presence of non-proportional loading. As already discussed in the early introduction Section 1.1, the fatigue life of a mechanical component consists of three stages. In particular, it is interesting to focus on stage I and stage II which correspond to crack nucleation and crack growth phases, respectively. In ductile-behaving materials cracks typically nucleate along slip systems which are aligned with the maximum shear stress planes, unlike brittle-behaving materials which often show crack nucleation directly at discontinuities like defects, inclusions or voids (even if nucleation in shear is possible also for the latter category of materials). Once the crack nucleation occurred (so stage I is finished and stage II has begun), the growth phase is made up by two substages that can be named substage 1 and substage 2, to not be confused with the previously mentioned stages. Substage 1 is a shear-controlled process associated with micro-crack growth along maximum shear planes, while the substage 2 is a tensile-controlled process associated with crack growth along maximum tensile stress planes. The relative life spent in each substage depends on material, loading type and stress level. It has been found out that micro-crack growth life of ductile materials is typically dominated by substage 1 growth (along maximum shear stress planes) which represents an important part of total life, meanwhile crack growth life in brittle-behaving materials is substage 2 growth dominated (along maximum tensile stress planes). As a result, research works made possible to state that crack nucleates and grows on preferred planes rather than with random orientation. Such experimental observations provided the physical basis for developing the critical plane approach. Moreover, the presence of a preferred orientation for crack nucleation and propagation has also been observed for non-metallic systems, such as elastomers. Indeed, applicability of critical plane based-methods has demonstrated valid also for this family of materials [18], [20]. In contrast with the general positive response on critical plane approach stated by Fatemi and Susmel that has been detailed above, there is also another different and contrasting viewpoint regarding the application of such a family of criteria in case of non-proportional loading, especially for what concerns the Dang Van criterion. Papuga [25] warns that out-of-phase loading cannot be analysed correctly by the Dang Van criterion because it has been noted that its predictions are inclined to be non-conservative compared with experimental data. It is also important to point out that the general non-conservativeness of Dang Van method in out-of-phase cases found by author comes from evaluating the criterion in conjunction with the minimum circumscribed circle method (MCCM) used to determine the shear stress path

(look at case C in Figure 2.6). Adopting other methods for the same purpose could provide other results.

Critical plane-based criteria evaluate the history of the stress tensor components on a specific critical plane. Projecting the load history onto a plane Δ, these criteria simplify the calculation to some extent. Referring to what already explained in Paragraph 2.1.2 (and thus illustrated in Figure 2.5), it must be remembered that the shear stress component, tangential to such a plane Δ, never changes its orientation when the component is loaded under proportional loading. Instead, under non-proportional loading the description of the shear stress history results to be more problematic since the load path projection onto the critical plane is not a linear object. Opening a parenthesis on integral multiaxial fatigue criteria that are explored in the next paragraph, it can be anticipated that the same issue exists also for this latter mentioned group. Indeed, these criteria integrate over all planes the output of the equivalent stress obtained from the calculation on each plane. It must be kept in mind that the way in how integral criteria deal with the load path projection onto each of the evaluated planes is identical to the one adopted by critical plane criteria [23].

2.2.2 Integral criteria

This is another important group of approaches adopted by some multiaxial fatigue criteria. In this case, instead of looking for a critical plane which experiences a maximum of a given variable, the damage parameter is computed over all planes at the examined point [25]. Basically, the composition of stress parameters, which are evaluated on all the planes defined by two Euler angles φ and θ (see Figure 2.1), results in its integral mean value to be input into the final formulation of the equivalent stress amplitude. For example, Liu and Zenner criterion (2000) and also Papadopoulos one (1994, 1997) belong to this family [10], [13]. This integral solution should better conform to non-proportional loading, where the definition of a specific critical plane orientation is doubtful since the principal stress directions rotate. Larger studies would be needed anyway to valid such an assumption. However, the integral approach seems to be more computationally demanding because of the potential requirement for a small integration step, which could be needed to reduce the integration error [13].

2.2.3 Criteria based on 5D Ilyushin deviatoric space

One more class that deserves to be mentioned is the one about criteria based on the Ilyushin deviatoric space. The main point here is that the load path is analysed in a five-dimensional space: stress tensor components can be reduced from six to five, with any loss of information and with the advantage of reducing computational costs, thanks to the dependency of stress deviator components on its trace [10], [25]. Comparing this approach with the previous two, where many analyses must be carried out on the various candidate critical planes, it is possible to state that the circumscribed hyperball or hyperellipsoid is computed only once, with a substantial reduction of computation time. Some examples of this type of solution are represented by Crossland (1956) and Sines (1959) criteria [13], [21]. It is worth noting that such two methods assume that fatigue damage depends both on the square root of the second invariant of the stress deviator and on the hydrostatic stress. But, nevertheless, such criteria result to provide inaccurate fatigue damage predictions when applied in case of non-proportional loading [7]. In the end, a further consideration can be stated in order to emphasize why to be interested in this kind of criteria that work in a five-dimensional space. As said before, critical plane-based and integral criteria analyse the stress state on many various planes, and, in order to get the shear stress value on each of the considered planes, they must run one of the methods presented above (refer to Figure 2.6) in a 2D space. Criteria built on the Ilyushin deviatoric space must run the chosen method in a 5D space, but only once and not many times as for critical plane criteria and integral criteria: this aspect makes criteria based on 5D Ilyushin deviatoric space resulting in a quicker solution [22].

2.2.4 Equivalent strain- and energy-based criteria

A brief description of the last two groups mentioned above is presented. The approach based on evaluating the equivalent strain is implemented in fatigue life prediction due to its simple form. Previous research showed that it works well in case of uniaxial and multiaxial proportional loading, while for multiaxial non-proportional loading the fatigue life predictions are inclined to danger, because the additional non-proportional hardening effect is not considered [5]. While, according to the energy based-approach the fatigue failure of material, which is an irreversible process, occurs when the fatigue damage reaches a critical level. Criteria like these ones can estimate fatigue life properly, but they cannot predict the crack initiation direction because the energy parameter is a scalar quantity [5].

In the end, concluding this summary, it can be pointed out that the quality of the multiaxial fatigue strength criterion chosen for a specific application plays an important role in the computation procedure. Moreover, it is worth remembering that all the approaches briefly reviewed above were specifically devised to be used in assessing the multiaxial fatigue problem in mechanical components made of homogeneous and isotropic materials. Thus, they cannot be used in case of anisotropic materials (for instance, composites) [7].

2.3 UNIAXIAL AND MULTIAXIAL FATIGUE STRENGTH CRITERIA

Research literature offers plenty of multiaxial fatigue strength criteria that have been developed in the last decades, but in engineering practise the application of such criteria is still not widely used. Adopting simple uniaxial criteria even for multiaxial load cases comes out to be easier, faster and more convenient for engineers working in the industry. Reasons behind this fact are several. First of all, dealing with multiaxial solutions requires a good understanding of the problem and the access to a multiaxial fatigue software. Without that, the engineer must program such methods himself/herself. In addition, calculations are usually time consuming, meanwhile traditional uniaxial solutions are simple to implement even in an Excel spreadsheet. Conscious about this problem, Papuga et al. [21] presented a comparison between several uniaxial and multiaxial fatigue strength criteria referring to a fatigue database related to unnotched specimens, mostly tested under multiaxial loading, in order to validate or discard the use of uniaxial solutions in multiaxial loading scenarios. One of the major important warnings, that the authors report, is that criteria based on a single load parameter (e.g. von Mises stress on the octahedral plane, or Tresca stress on the maximum shear stress plane) cannot take into account the real complexity of the stress state when there is non-proportional loading, since the principal directions change during the loading and thus the position of the maximum loaded planes change as well. In conclusion the use of a second parameter, affected by the potential phase shift of normal and shear stress components, is the only practicable and correct solution. The applicability of uniaxial solutions should be limited at most to in-phase loading cases.

In the next paragraphs of this section, two fatigue criteria are introduced. The first is the Manson-McKnight criterion, originally developed to predict fatigue life under uniaxial cycling loading and later tested for its applicability to more complex multiaxial loading scenarios. The second is the Dang Van criterion, which provides a more specific solution for multiaxial fatigue analysis. Both criteria turned out to be interesting for implementation in current study to assess fatigue of notched specimens and to support the development of the new critical volume approach. At the end of Paragraph 2.3.2 a short comparison between the two criteria is presented.

2.3.1 Manson-McKnight criterion

The von Mises criterion is certainly one of the most famous and widely used strength criteria concerning the design and the verification of metallic structures. However, there is a solution that took inspiration directly from von Mises, and it is represented by the Manson-McKnight criterion (MMK). Assuming $i,j = x,y,z$, stress amplitude and mean stress related to each single component of the stress tensor (2.5) are calculated as follows:

$$\sigma_{i,a} = \frac{\max\limits_{t}(\sigma_i) - \min\limits_{t}(\sigma_i)}{2} \tag{2.14}$$

$$\tau_{ij,a} = \frac{\max\limits_{t}(\tau_{ij}) - \min\limits_{t}(\tau_{ij})}{2} \tag{2.15}$$

$$\sigma_{i,m} = \frac{\max\limits_{t}(\sigma_i) + \min\limits_{t}(\sigma_i)}{2} \tag{2.16}$$

$$\tau_{ij,m} = \frac{\max\limits_{t}(\tau_{ij}) + \min\limits_{t}(\tau_{ij})}{2} \tag{2.17}$$

So, the equivalent stress amplitude (2.18) and the equivalent mean stress (2.19) result in:

$$\sigma_a = \sqrt{\frac{1}{2}\left[\left(\sigma_{x,a} - \sigma_{y,a}\right)^2 + \left(\sigma_{y,a} - \sigma_{z,a}\right)^2 + \left(\sigma_{z,a} - \sigma_{x,a}\right)^2 + 6\left(\tau_{xy,a}^2 + \tau_{yz,a}^2 + \tau_{zx,a}^2\right)\right]} \tag{2.18}$$

$$\sigma_m^* = \sqrt{\frac{1}{2}\left[\left(\sigma_{x,m} - \sigma_{y,m}\right)^2 + \left(\sigma_{y,m} - \sigma_{z,m}\right)^2 + \left(\sigma_{z,m} - \sigma_{x,m}\right)^2 + 6\left(\tau_{xy,m}^2 + \tau_{yz,m}^2 + \tau_{zx,m}^2\right)\right]} \tag{2.19}$$

The reason why the mean stress is marked with * is because the several variants of MMK criterion differ mainly in how the final equivalent mean stress σ_m is defined. In particular, the original MMK formulation involves the sign of the first stress invariant to determine such a component:

$$\sigma_m = \sigma_m^* \cdot sgn\left(I_{1,d}\right) \tag{2.20}$$

where $I_{1,d}$ is the maximum value of the first stress tensor invariant during the loading cycle [21].

To obtain only one fatigue parameter from the criterion, which would be the equivalent stress amplitude capable to include the effect of the mean stress (if such an effect is present), it is possible to use some correction expressions available in literature like Goodman's relation, Gerber's one, Walker's one and so on. For example, the Goodman's relation incorporates the mean stress into the equivalent stress amplitude as follows [26]:

$$\sigma_{a,eq} = \frac{\sigma_a}{1 - \frac{\sigma_m}{\sigma_u}} \tag{2.21}$$

where σ_u is the ultimate tensile strength of the material.

2.3.2 Dang Van criterion

The Dang Van criterion is for sure one of the most popular multiaxial fatigue solutions not only in research literature but also for what concerns commercial implementations [21], [25]. As mentioned before, it belongs to the family of criteria that adopt the critical plane approach. Two versions of Dang Van exist: they define the damage parameter on the critical plane with two equations that slightly differ each other.

The original Dang Van formulation expresses the equivalent stress amplitude as a linear combination of the maximum shear stress amplitude (τ_a) and the maximum value of the hydrostatic stress ($\sigma_{H,max}$) [27]:

$$\sigma_{a,eq} = a_{DV} \cdot \tau_a + b_{DV} \cdot \sigma_{H,max} \tag{2.22}$$

where a_{DV} and b_{DV} are the Dang Van material parameters which are defined as:

$$a_{DV} = k = \frac{f_{-1}}{t_{-1}} \tag{2.23}$$

$$b_{DV} = 3 - \frac{3}{2}k \tag{2.24}$$

Equivalent stress amplitude expressed in 2.22 has to be compared with f_{-1}, which is the plain fatigue limit (or alternatively the plain fatigue strength at a given lifetime N_f) that can be obtained, for

example, from fully reversed push-pull tests. For instance, in case where f_{-1} represents the plain fatigue limit, if:

$$\sigma_{a,eq} \leq f_{-1} \tag{2.25}$$

no fatigue failure should occur. In addition, it is worth noting that parameter a_{DV} (2.23) is equal to parameter k which is known as fatigue limit ratio: indeed, it is calculated as the ratio between fully reversed push-pull fatigue limit (f_{-1}) and fully reversed torsion fatigue limit (t_{-1}) [21], [25].

Starting from late 1980's, another version of Dang Van criterion was proposed. The damage parameter is defined as the maximum value (over the time) of the linear combination of instantaneous shear stress $\tau(t)$, which is computed from the stress deviators, and hydrostatic stress $\sigma_H(t)$ occurring at the same moment [12], [26]:

$$\max_t [a_{DV} \cdot \tau(t) + b_{DV} \cdot \sigma_H(t)] \leq f_{-1} \tag{2.26}$$

Material parameters a_{DV} and b_{DV} are again calculated as shown in 2.23 and 2.24, respectively. Although such parameters remain the same, the two versions of Dang Van criterion explained above do not coincide. First of all, there are differences in terms of how the equivalent stress amplitude is computed:

- the original version (2.22) uses maxima of both shear and hydrostatic stresses inside the linear combination;

- while the newer formulation (2.26) looks instead for the maximum value of the combination of such two stresses.

Furthermore, even if no differences are found concerning the case of proportional loading, the two Dang Van versions differ in terms of how they behave in case of non-proportional loading:

- the newer version of Dang Van formulation (2.26) leads to higher fatigue strength predictions if compared to the original version (2.22), which means the latter results in a more conservative method than the former [12];

- but it is important to remember what already stated in the section 2.2 while describing the critical plane approach, whereby it is suspected that Dang Van is unable to assess properly the out-of-phase loading. This opinion, supported by Papuga [25], was validated by implementing the original version of the criterion (2.22) in conjunction with the minimum circumscribed circle method (MCCM, illustrated in figure 2.6).

To conclude this section dedicated to uniaxial and multiaxial fatigue strength criteria, a brief comparison between MMK and Dang Van methods is presented here. The previously mentioned study by Papuga [21] is again taken as a reference: in that study the original version of Dang Vang criterion (2.22) was taken into account, and moreover, the same fatigue database used in [25] was involved. The comparison considered several groups of experiments, for a total of 407 tests on different materials. Each group represented a specific load scenario: for instance, proportional and non-proportional loading were considered, combining axial and torsion loading in several ways. Mean stress was included in some of the analysed cases. Here, a brief summary of some of the main outcomes from the review work are presented [21]:

1. in case of loading on the axial load channel only with mean stress, MMK and Dang Van methods result in a similar prediction quality;

2. in case of loading on the torsion load channel only with mean stress, Dang Van appears to make non-conservative predictions, despite of MMK which appears to be more conservative.

As a consequence, the easier and apparently safer MMK solution could be adopted in such scenarios;

3. in case of proportional bi-axial tensile loading with mean stress, MMK can decently work even if Dang Van results in better fatigue predictions;

4. in case of non-proportional bi-axial tensile loading with mean stress, MMK (and its modified versions) should be avoided because it comes out to be totally inaccurate.

In conclusion, if the analysis is focused on proportional loading without any presence of mean stress (as the case examined in the experimental part of the current work), the uniaxial solution of MMK seems to provide adequate and safe predictions because its results would not be significantly worse than a multiaxial solution like Dang Van (except in the case of brittle materials). Meanwhile it is generally true that in case of non-proportional loading, multiaxial fatigue strength criteria achieve better results than uniaxial ones (i.e. MMK), even if the reader is alerted about the issue that Dang Van can badly respond in case of out-of-phase loading.

2.4 FATIGUE LIFE ESTIMATION INCLUDING THE NOTCH EFFECT

Assessing the notch effect in fatigue life estimation regarding the HCF domain, several approaches can be adopted [15], [28]. Three of them are reported hereafter, paying particular attention to the Theory of Critical Distances that will be applied later.

2.4.1 Nominal stress approach

The nominal stress approach (NOM) represents the traditional and straightforward way to deal with fatigue of notched components. Nominal notch fatigue limit ($\sigma_{0,n}$) is decreased compared with the plain fatigue limit (σ_0) by calculating the fatigue limit reduction factor (K_f) using equations 1.12 or 1.13 [28]. Similarly to the fatigue limit asymptote, the whole nominal S-N curve must shift downwards with respect to the material one. Thus, it is possible to calculate also the fatigue strength reduction factor at a given lifetime N ($K_{f,N}$). The value of such a factor changes with life N, indeed also the problem of how to define the new slope of nominal S-N curve of the notched specimen must be addressed [15], [28].

This approach looks unsuitable for nowadays mechanical design. A component characterized by a complex geometry does not facilitate a proper definition of a nominal cross-section, thus the application of the NOM solution results in a very cumbersome approach that cannot fit properly with the automated processing of stress data from Finite Element (FE) analyses, which provides immediately to the user the elastic peak stress at the notch apex [28], [29]. Hence, a simple way to proceed would be the direct use of the maximum stress at the root of the notch with the material S-N curve: it is easy to understand that the problem would consist in a too much conservative fatigue life estimation (as it is possible to state looking at Figure 2.7). This is something not anymore acceptable in the engineering, since the goal of a wise engineer should be design the lightest possible component in order to save costs related to material, to manufacturing process and maybe also to its functioning (if it is a part of a moving assembly that requires energy to move) [17], [28]. Here come the two modern approaches presented in the next two paragraphs, which can better deal with the effect of non-constant stress distribution caused by the presence of the notch. They are the approach based on the Theory of Critical Distances and the one based on Relative Stress Gradient.

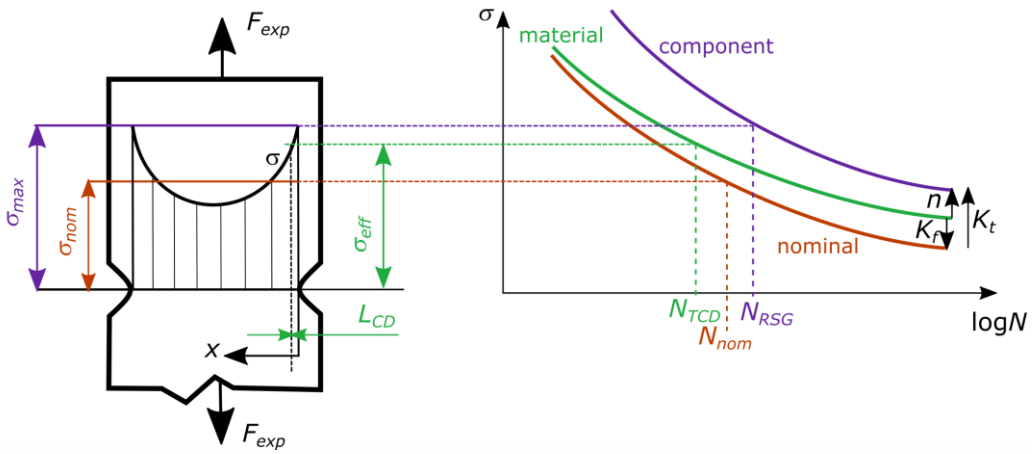

Figure 2.7: Comparison of different approaches to mastering the notch effect in fatigue: NOM solution (red), TCD solution (in green) and RSG solution (in violet) [17].

2.4.2 Theory of Critical Distances

The Theory of Critical Distances (TCD) allows to estimate high cycle fatigue strength of mechanical components experiencing stress concentration phenomena. Thanks to its features, this theory can accurately estimate fatigue damage in components containing not only cracks but also any kind of notch. The capability of TCD to successfully predict fatigue behaviour in both short- and long-crack cases was proved by Taylor (1999) [7]. Such a theory was born for predicting the effects of notches in both cases of static fracture and fatigue failure [30]: of course, its application to the fatigue case is the one explored in the present context. The idea behind TCD was presented at first by Neuber (1958). His starting hypothesis was that the elastic stress due to the stress concentration effect does not reach values as high as those predicted by the continuum mechanics theory. Thus, he proposed to find an effective stress representative of the real stress damaging the fatigue process zone, by averaging the linear elastic stress below the notch root over some material units (e.g. crystals or structural particles). Later, Peterson (1959) argued that this idea could be simplified by determining the effective stress, to be used to design notches against fatigue, at a given distance from the notch apex. Both of the two mentioned illustrious authors theorised in advance the Line Method and the Point Method respectively, which are two of the different variants of TCD (as described in detail later) [7], [14]. In recent times, TCD has been object of interest of many research studies, taking advantage of both the Linear Elastic Fracture Mechanics (LEFM) and the accuracy of the FE method in calculating the linear elastic stress fields around any kind of stress concentrator. It is worth remembering that at the time of Neuber and Peterson, the ideas behind TCD were not easy implementable due to the lack of analytical tools and the related computational power [7]. On the contrary, starting from the end of the 1990's the application of TCD has been rediscovered especially thanks to the increased use and availability of FE analyses, since this approach is particularly easy to use in conjunction with them [30]. Latest works about TCD have been carried out by Taylor (2007) and then again by him in collaboration with Susmel (2007): together, they checked the accuracy of the theory when applied to estimate notch fatigue strength under different loading configurations, and they also reformulated the theory in order to make it suitable for fatigue predictions in the medium-cycle fatigue regime [7], [14].

The TCD starts from the assumption that the fatigue damage in the presence of stress concentration phenomena has to be evaluated by using a stress quantity which is representative of the entire linear elastic stress field damaging the fatigue process zone [7]. Therefore, TCD solution keeps using the material S-N curve (obtained from tests on unnotched specimens) but referring to a suitable effective stress (σ_{eff}) acting at the notch, which is obtained depending on the so-called critical distance under the notch apex. As a consequence, the effective stress is smaller than the elastic peak: this leads to a longer lifetime estimation than if the maximum stress at the notch is given as input directly to the material S-N curve or, even worse, to the nominal one [17], [28]. Such a consideration can be visualized in Figure 2.7. As anticipated, the theory can be formalised according to the different ways how the critical distance, and thus the effective stress, are computed to be used for fatigue predictions. One parameter that comes out to be crucial is the material characteristic length L, also known as El-Haddad parameter. This quantity comes from the LEFM theory and is defined as follows:

$$L = \frac{1}{\pi}\left(\frac{K_{th}}{\sigma_0}\right)^2 \tag{2.27}$$

where K_{th} is the threshold value of the stress intensity factor and σ_0 is the plain fatigue limit. It is evident that L is a material property since it depends on two material properties [14]. Parameter L is involved in the expression used for calculating the critical distance, thus also the critical distance is a material property. TCD can be used to predict notch fatigue limits. Indeed, a notched component experiences its fatigue limit if the effective stress is equal to the plain fatigue limit [7]:

$$\sigma_{eff} = \sigma_0 \tag{2.28}$$

There are different variants of the TCD, illustrated in Figure 2.8: the difference between a method and the other is just a matter of how the integration domain used to calculate the effective stress is defined [7], [14]. Consider a notched specimen which is axially loaded by a gross nominal stress (σ_{gross}). Fix a reference frame at the notch apex, whose x-axis points in the direction of the surface normal, and define a polar coordinate system (r, θ), as evidenced in Figure 2.8a. The linear elastic stress field expressed in terms of maximum principal stress (σ_1) is observed.

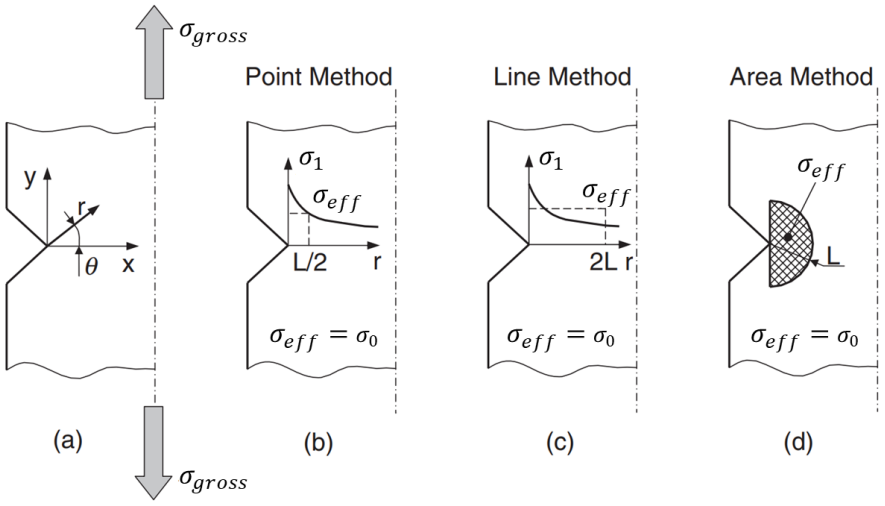

Figure 2.8: Different formalisations of the Theory of Critical Distances. Adapted from [7].

1. Point Method (PM). As already mentioned, such a method reflects Peterson's idea (Figure 2.8b). The effective stress is calculated at the given critical distance D_{PM} referring to the maximum principal stress:

$$\sigma_{eff} = \sigma_1(r = D_{PM}, \theta = 0) \tag{2.29}$$

where:

$$D_{PM} = \frac{L}{2} \tag{2.30}$$

2. Line Method (LM). This method was the very first concept of TCD to be invented [30] (Figure 2.8c), since it recalls Neuber's insight which states that the effective stress is calculated by averaging the linear elastic maximum principal stress along the notch bisector over the distance D_{LM}:

$$\sigma_{eff} = \frac{1}{D_{LM}} \int_0^{D_{LM}} \sigma_1(r, \theta = 0)\, dr \tag{2.31}$$

where:

$$D_{LM} = 2L \tag{2.32}$$

1. Area Method (AM). This third method comes from the idea of Sheppard (1991) to average the stress field over a finite volume. Thus, Taylor (1999) reproposed it but considering an area instead of volume [31]. In particular, the area method (Figure 2.8d) consists in

calculating the effective stress by averaging the linear elastic maximum principal stress over a semicircular area centred at the notch apex and characterized by a radius equal to D_{AM}:

$$\sigma_{eff} = \frac{4}{\pi {D_{AM}}^2} \int_{-\pi/2}^{\pi/2} \int_{0}^{D_{AM}} \sigma_1(r,\theta)\, dr\, d\theta \tag{2.33}$$

where:

$$D_{AM} = L \tag{2.34}$$

Going back to the idea of applying the TCD considering a volume, that will not be detailed here, it is worth mentioning that Bellet et al. (2005) supported such an idea and suggested to average the linear elastic maximum principal stress over a hemisphere centred at the notch tip and having a radius equal to $1.54\mathrm{L}$ [7]. About PM and LM, both were revisited by Tanaka (1983), Lazzarin and co-workers (1992-1997) and Taylor (1999). They reviewed the methods linking them to the LEFM independently, and what is interesting to observe is that all of them came to similar conclusions [31], [32]. Anyway, Fojtík and Papuga [17] consider the presence of such many methods to evaluate the critical distance as a weak point of the theory, especially because they can lead to very different results.

TCD was born for estimating HCF strength of notched mechanical parts and found a solid application for predicting notch fatigue limits. However, the authors of latest improvements of the theory, thus Taylor and Susmel, worked also on its extension to the medium-cycle fatigue domain, in order to estimate fatigue lifetime of notched components failing in the medium-cycle fatigue regime [7], [14]. They assumed that the material characteristic length (L) changes as the number of cycles to failure (henceforth referred to as N_f). In particular, it decreases with N_f according to a relationship that can be expressed as a power law (similarly to what happens between fatigue strength and fatigue life according to S-N curves):

$$L(N_f) = A \cdot N_f^B \tag{2.35}$$

where A and B are material constants, especially $A > 0$ and $B < 0$. These constants, and thus equation 2.35, depend on the material and the load ratio. It is worth noting that, since the critical distance (D_{PM}, D_{LM} or D_{AM}) is a function of L, it will change as well with the fatigue life. Susmel and Taylor attempted two strategies to define such a power law relationship existing between L and N_f. The first one determines the power law considering the material properties defined at the two extremes of the S-N curve: the static failure on the top left side of the fatigue curve, and the fatigue limit in correspondence of the Wöhler knee on the bottom right side of the curve. This approach, though it is correct and it does not present any theoretical inconsistency, contained some problems in its practical application. The second strategy follows a calibration procedure referring to two fatigue curves, where the first curve is generated by testing unnotched specimens and the second one is obtained testing notched specimens. According to the authors, this approach results to be simpler and capable to reach a higher accuracy. For instance, considering the PM the critical distance can be determined for any given fatigue life N_f as follows. For a fixed value of N_f, the critical distance from the notch tip (2.30), at which the local amplitude of the linear elastic maximum principal stress (σ_1) equals the nominal stress applied to the smooth specimen to generate a failure at N_f, can be calculated by using either a FE analysis or other analytical methods [7], [14].

2.4.3 Relative Stress Gradient approach

The Relative Stress Gradient approach (RSG) originates from the German research, as evidenced by its implementation in the in FKM-Guideline. The RSG solution uses the value of the relative stress gradient calculated at the root of the notch to modify the material S-N curve into a new component

S-N curve that refers to local stress amplitudes at the notch. The relative stress gradient (γ') is calculated as follows [15], [28]:

$$\gamma' = \frac{1}{\sigma_{ep}} \frac{d\sigma}{dx} \tag{2.36}$$

where x represents the direction perpendicular to the notch tip and σ_{ep} always refers to the elastic peak computed at the notch tip. Depending on the value of the stress gradient, the FKM proposes several ways to shift the S-N curve upwards along the direction of the stress axis, as regards the change of its slope and, eventually, the horizontal shift of the fatigue limit knee point along the life axis [15]. As it is possible to see in Figure 2.7, entering with the elastic peak stress (read at the root of the notch) in the new component S-N curve allows to obtain a more optimistic fatigue life estimation which is less conservative than the other options already mentioned above [17]. Focusing on this problem of shifting the fatigue curve upwards, the so-called fatigue factor n (also known as fatigue support number from other authors like Leitner [29]) must be taken into account. It describes the multiple by which the plain fatigue limit (σ_0) should be increased to derive the hotspot notch fatigue limit ($\sigma_{0,HS}$) [29]:

$$n = \frac{\sigma_{0,HS}}{\sigma_0} \tag{2.37}$$

It is extremely important to not confuse $\sigma_{0,HS}$ with $\sigma_{0,n}$: both refer to the notch S-N curve, but the former is expressed in terms of local stress and it relates to hotspot fatigue limit (and so to the component S-N curve), the latter refers to the nominal notch fatigue limit (thus to the nominal S-N curve). Alternatively, it is easy to demonstrate that the fatigue factor can be also expressed as the ratio between the stress concentration factor and the fatigue strength reduction factor [28]:

$$n = \frac{K_t}{K_f} \tag{2.38}$$

Once the physical meaning of the factor n is clear, it is opportune to see what formulation the FKM-Guideline proposes to calculate such a factor. Stieler method is reported in the 6th edition of the guideline as one of the “traditional” ways to calculate the fatigue factor using the relative stress gradient value. Such a formulation is proposed here:

$$n = 1 + \gamma'^{c} \cdot 10^{-0.5+e^{\frac{R_m}{2700}}} \tag{2.39}$$

where R_m is the ultimate tensile strength of the material and c is a coefficient [15]. However, a new definition of fatigue factor has been introduced in the newest versions of FKM-Guideline, especially starting from the 6th edition. This new formulation, described by the manual as material mechanical support factor [15] or as fatigue support number [29], is given by the product of three different factors:

$$n = n_{st} \cdot n_{def} \cdot n_{fm} \tag{2.40}$$

which are:

- statistical support factor (n_{st});
- material response support factor (n_{def})
- fracture mechanics support factor (n_{fm}).

The statistical support factor (n_{st}) is defined through the Weibull distribution model, which evaluates the ratio between the highly stressed surface areas of a reference specimen ($A_{HSS,ref}$) and of the evaluated specimen respectively, raising them up to the Weibull exponent (k_w) [15]:

$$n_{st} = \left(\frac{A_{HSS,ref}}{A_{HSS}}\right)^{\frac{1}{k_w}} \tag{2.41}$$

Such highly stressed surface areas are defined as the ones stressed at least at the 90% of the maximum value reached in the loaded component. They can be computed analytically or numerically, e.g. through the FE method which is usually used for complex notch geometries [15], [29]. Several research works proposed to decline the RSG approach in another method, i.e. using volumes instead of areas. Leitner [29] affirms that this kind of approach acts as an enhancement of the stress gradient concept. The highly stressed volume ($V_{HSS,ref}$ and V_{HSS}, defined similarly to what already seen in equation 2.41) represents the relevant parameter to assess such a statistical support number:

$$n_{st} = \left(\frac{V_{HSS,ref}}{V_{HSS}}\right)^{a} \tag{2.42}$$

where the exponent a is different from the one used in 2.41.

The material response support factor (n_{def}) refers to the material behaviour above the yielding point. The FKM-Guideline propose to compute it through the following equation, valid for steels and for wrought aluminium alloys [15]:

$$n_{def} = \sqrt{1 + \frac{E \cdot \varepsilon_{pl,th}}{\sigma_0}(n_{st})^{\frac{1}{n'}-1}} \tag{2.43}$$

where E is the Young's modulus, $\varepsilon_{pl,th}$ is the non-damaging plastic strain, σ_0 is the plain fatigue limit and n' is a parameter depending on the type of material.

Finally, the fracture mechanics support factor (n_{fm}) describes the difference in terms of crack growth properties between a homogeneous stress state and a non-homogeneous stress state, in the case of tension-compression of the unnotched specimen and the notched specimen respectively. It is formulated as follows:

$$n_{fm} = \frac{5 + \sqrt{\gamma'}}{5 \cdot n_{st} \cdot n_{def} + \frac{R_m}{R_{m,FM}}\sqrt{\frac{7.5 + \sqrt{\gamma'}}{1 + 0.2\sqrt{\gamma'}}}} \tag{2.44}$$

where R_m is the ultimate tensile strength and $R_{m,FM}$ is the same but intended as a reference value given by the guideline [15].

In the real application of the RSG approach, a linear elastic finite element analysis is required in order to obtain the stress distribution at the notch. In particular, the stress gradient can be calculated, with respect to the stress profile along the path below the notch and normal to it, taking the elastic peak stress and the stress value below the notch apex, specifically at the neighbouring node belonging to the first row of finite elements. Nesládek et al. [15] observe something interesting about the role of mesh density. A fine mesh leads to higher stress gradients, thus to better predictions of the component S-N curve. But making a very fine mesh is not usually a common practice in industry, due to the resulting high computational costs. However, the use of a less computational demanding rougher mesh brings with it two conflicting effects. In one hand, the lower relative stress gradient leads to a more conservative fatigue estimation (since the component S-N curve is less shifted upwards). On the other hand, rougher mesh causes the elastic peak stress at the notch tip to be underestimated, having a negative impact on the conservativeness of the fatigue life estimation. Again, Nesládek et. al [15] affirm that relative stress gradient-based solutions, especially the ones

implemented in the FKM-Guideline, are promising because they provide better fatigue life estimates than the ones obtained via TCD.

In conclusion, going back to Figure 2.7 it is possible to compare all the previous three approaches. It is worth noting the order of fatigue curves in the S-N diagram, starting from the component one on top to the nominal one on the bottom. Factors n, K_t and K_f highlight the relations they express between the three different proposed curves.

2.5 CRITICAL VOLUME APPROACH

The approaches to fatigue life estimations in multiaxial fatigue load contexts that have been described in previous Section 2.4 are widely debated in literature. In this section it is pointed out that the statistical size effect, which plays a crucial role in both static and fatigue failures of structures, seems to not be properly taken into account by the mentioned solutions. Indeed, both TCD and RSG approaches are mainly focused and based on the stress gradient effect resulting in not be able to include an adequate description of such a size effect [17]. For instance, TCD takes into consideration the stress gradient effect (since the computed critical distance is strictly related to the stress profile under the notch tip) but it does not consider the size effect. Moreover, also the RSG approach cannot consider at the same time stress gradient and size effects, at least till the 5th edition of the FKM-Guideline [33]. Consider two notched specimens with different sizes that show same (or similar) stress gradients below the notch root: a method like the one based on RSG does not make any distinction between the big sample and the small one because the size effect is not involved at all. It is interesting in this regard to point out one effect known from the past knowledge. An increase in specimen size has a larger impact on the fatigue strength of notched specimens than of smooth ones: this is a clear evidence of the interaction that exists between size and notch effects [34]. Something new in the direction of considering the size effect in the RSG approach is presented in newest editions of the FKM-Guideline, especially the 6th (2012) and the 7th (2020). Here, as already reported in the dedicated Paragraph 2.4.3, the fatigue factor is not just a function of γ' but it is calculated as the product of the three sub-factors n_{st}, n_{def} and n_{fm}. The first one, n_{st}, represents a statistical factor related to the size effect. However, Fojtík and Papuga [17] argue that the FKM-Guideline does not state a definite answer to the joint problem of load multiaxiality and notch effect. Moreover, they point out another weak point of both RSG and TCD solutions that is related to the fact that such methods usually cover the stress distribution only in one direction. Always Papuga [35] underlines that TCD and RSG concepts are rarely compared in the same data sets, while being quite widely used and even implemented in commercial fatigue solvers [35].

The insight, which represents the core idea of this research work, holds that if size effect were involved, fatigue predictions in multiaxial loading scenarios could be improved. The goal is to develop a method, to be applied in conjunction with multiaxial fatigue strength criteria, that takes into account another physical quantity: the critical volume. Before going on with the review of previous literature works about the topic, it is necessary to give the definition of such a critical volume.

2.5.1 Definition of the critical volume

The critical volume is the region of material where crack originates from [34]. Suppose σ_{ep} to be the elastic peak stress at the root of the notch, and consider the parameter z to assume values included in the interval:

$$0 < z < 1 \tag{2.45}$$

It is possible to define the critical stress, which basically represents a threshold value, as follows:

$$\sigma_{crit} = z \cdot \sigma_{ep} \tag{2.46}$$

Consequently, the critical volume can be determined by the condition:

$$\sigma \geq \sigma_{crit} \tag{2.47}$$

In other words, the critical volume is the portion of material that experiences a high cyclic stress equal to at least the threshold value (σ_{crit}) has been set [17], [34]. Note that the elastic peak stress to be

referred to may be different from case to case, depending on the type of stress chosen for evaluating expressions 2.46 and 2.47. For example, referring to a couple of papers that are better explored in the next paragraph, in [34] authors chose to evaluate the critical volume considering the σ_y that is the stress state component along the y-axis, corresponding to the specimens' symmetry axis. While in [17] authors preferred to use the equivalent von Mises stress to evaluate the critical volume. One more consideration deserves to be reported: once the value of z has been fixed and the load configuration has been chosen, the value of critical volume is totally defined and constant for the evaluated notched specimen, since it is a specific feature of the considered geometry and material of the specimen.

2.5.2 Previous works on this topic

The idea of dealing with the critical volume is not new. The current thesis work takes inspiration from some previous studies about the topic, already cited introducing the current section and reviewed more in detail hereafter. The key reason behind pursuing the idea of involving the critical volume in multiaxial fatigue assessment is the following. Nowadays there is not any approach capable to consider simultaneously the stress gradient effect and the size effect, which are concurrent effects that superpose each other (as anticipated at the end of Paragraph 1.3.4). The introduction of a volumetric quantity in dealing with multiaxial fatigue could allow to take into account both effects, resulting in a kind of unified approach which could be better than trying to evaluate stress gradient and size effects separately, or not at all. The size effect is related to the size of critical volume in which the crack can initiate from. Mžourek et al. [34] pointed out that in the HCF domain it is observed that the larger the critical volume, the more likely the crack initiation. Indeed, larger volumes have a higher probability of containing a bigger defect or an inhomogeneity, in the close vicinity of which a crack will more easily initiate. Things may be different in LCF domain, where an increased size of the specimen can have beneficial effect on fatigue strength because the bigger dimension allows to protract the crack propagation phase. Focusing on the first case (HCF), the stress gradient effect becomes clearly visible when, for example, similarly sized specimens are loaded under push-pull and bending modes: stress distributions come out to be different in the two cases, and so they affect differently the fatigue lives. Such an observation can be also interpreted as an evidence of size effect. Thus, the smaller the part of the cross section that is maximally loaded according to both size effect and stress gradient effect, the smaller probability of crack initiation. In the previous example, this highly stressed part under bending load is smaller than under push-pull load. It is clearly impossible to treat such effects separately. Opening a bracket about material fatigue behaviour under these different load modes considered in the example, it is curious to note that the growth of an initiated crack is slowed down under bending load mode, unlike in push-pull case, because the stress level decreases in the same direction [17].

For instance, Fojtík and Papuga (2021) [17] studied a critical volume-based solution clearly influenced by the RSG approach because of the way it operates. Indeed, it must be remembered that the RSG method uses the relative stress gradient (γ') to modify the material S-N curve (obtained from smooth specimens) into the component S-N curve. This is done according to specific equations reported in the FKM-Guideline or in manuals of commercial fatigue solvers, like Femfat [15]. Therefore, the derived curve refers to elastic peak stress amplitudes at the notch root and not to nominal stress amplitudes anymore. It must be remembered that multiaxial fatigue strength criteria take as input the material parameters (a, b) which usually depend on plain fully reversed fatigue limits, or strengths at given lifetime N_f, in push-pull and torsion loadings (f_{-1}, t_{-1}): from now, "fatigue strength" will refer always to the broad sense without specifying every time "limit" or "strength at N_f cycles", in order to streamline the discussion. So, the new solution developed by Fojtík and Papuga proposes to modify such material fatigue strengths depending on the evaluated critical volume rather than the γ'. Material parameters a and b are transformed into "component parameters" related to the observed magnitude of critical volume, before being used as inputs in the multiaxial fatigue strength

criterion chosen for further analyses. Regarding this latter aspect, multiaxial fatigue strength criteria considered in [17] for validating the new approach remained unchanged, even if both size and stress gradient effects were involved in the analysis. To implement such an idea, it is evident that the life N_f must be kept constant. As a result, four section cuts of specimens' S-N curves have been considered, which are 0.2, 0.5, 1.0 and 2.0 million cycles. Authors' expectation was that critical volume and fatigue strength, in both axial loading and torsion loading cases, are linked together by a power law similar to the one used for obtaining S-N curves. To keep the analysis simpler, they calculated critical volumes referring to the von Mises equivalent stress considering two values of parameter z: 0.95 and 0.99. The power law conjecture seems to be verified as showed in Figures 2.9a and 2.9b, where dependencies between critical volume and fully reversed fatigue strengths under axial and torsion loading modes, respectively, are presented considering a constant value of life equal to $2 \cdot 10^6$ (note that only the orange and the grey series are of interest for the current discussion). To sum up, the use of such dependencies can be summarised as follows:

1. the engineer has to perform preliminary linear elastic FE analysis on the evaluated component in order to calculate von Mises equivalent stresses. In this way, he/she can compute a rough value of critical volume of such a component under fatigue load (for a fixed value of z);

2. the engineer provides the computed critical volume as input to the dependencies that have been found for the considered material (which come from the fittings of experimental points in Figures 2.9a and 2.9b). In this way, component fatigue strengths in both fully reversed push pull and torsion loadings (f_{-1}, t_{-1}) can be found in their "updated" version;

3. at this point new material parameters a, b can be calculated using the new component fatigue strengths (f_{-1}, t_{-1}) found at the previous point, according to equation of the chosen fatigue strength criterion (e.g. considering Dang Van criterion, a and b must be calculated as showed in 2.23 and 2.24);

4. in the end, the engineer can apply the multiaxial fatigue strength criterion to the case to be evaluated using the new material parameters (a, b). As a result, the criterion works in its updated version, which should provide accurate fatigue strengths for the considered fatigue life.

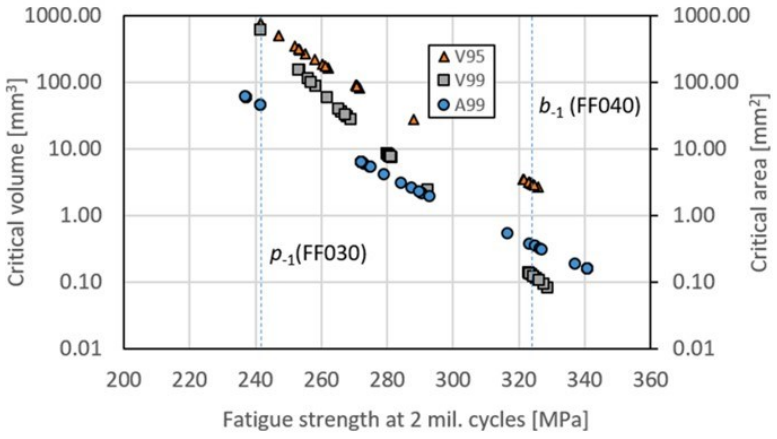

(a)

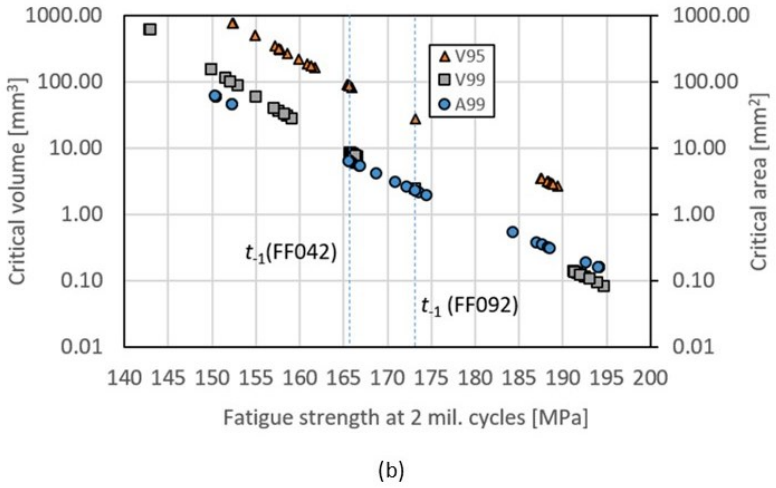

Figure 2.9: Critical volume vs. fatigue strength dependencies found in [17] referring to (a) axial loading and (b) torsion loading at $N_f = 2 \cdot 10^6$. Right vertical axis reports the critical area, but the area-based variant of the approach was discarded because it produced lower-quality output.

Fojtík and Papuga also tried a similar structured approach with the only difference that critical areas were considered instead of volumes: the outcome was that this critical area solution produced a lower-quality output, especially in the case of repeated bending ($R = 0$). Further words should be spent about the value assumed by the parameter z. Typical values adopted for this purpose are {0.8, 0.9, 0.95, 0.99}. In the reviewed work [17] authors evaluated the values {0.9, 0.95, 0.99} for parameter z, but they discarded 0.9 because, according to their experimental results, it gave a weak output. About this fact, in [34] Mžourek et al., who studied smooth and notched specimens made in 42CrMo4+QT, found 0.971 to be the optimum z value via some regression analysis. However, they state that such a parameter is strongly dependent on the geometry of the analysed specimens. Going back to [17], the final point to examine concerns how the experimental campaign has been set. Authors analysed unnotched and hourglass specimens made by structural steel ČSN 41 1523. They induced multiaxial stress states by providing several load combinations, including internal pressurization of hollow specimens (there was only one full bar specimen geometry). Non-proportional loading was also involved. However, that study did not solve the multiaxiality problem at all for several reasons. For example, critical volumes were defined using von Mises equivalent stresses, with the awareness that von Mises criterion cannot completely capture the multiaxial fatigue phenomenon: thus, the dependencies derived from such critical volumes could be negatively affected by this aspect. Moreover, although several load cases were involved, only unnotched geometries were tested: thus, the notch effect was not effectively taken into account. In the end, authors recommended to perform a larger experimental campaign to validate those results.

To support the statements and considerations above, referred to the new concept of critical volume, the example illustrated in Figure 2.10 can be analysed. Consider two specimens subjected to tension loading, characterized by different notch geometries: one presents a blunt notch (Figure 2.10a), the other one a sharp notch (Figure 2.10b). The linear elastic maximum principal stress field can be plotted in each case with respect to the reference frame fixed at the notch root, together with the critical volume evaluated for a fixed value of z (highlighted in red). The stress gradients under the notches and the critical volumes are inherently connected. Specifically, it is evident that:

- blunt notches result in mild stress gradients and large critical volumes;
- sharp notches result in high stress gradients and small critical volumes.

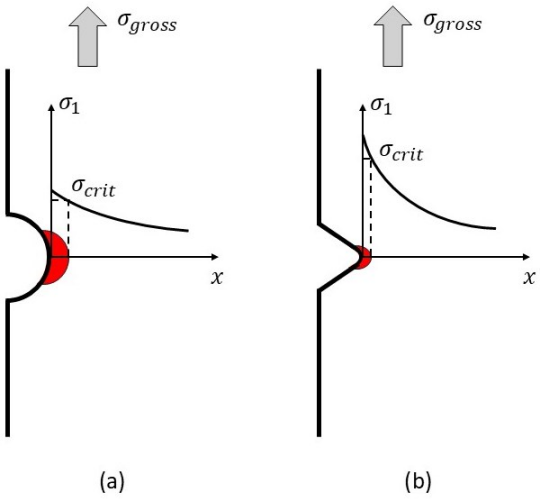

Figure 2.10: Schematic representation of the relationship between the stress gradient effect and the size effect which results in the concept of critical volume, referring to (a) blunt notch case and (b) sharp notch case.

In conclusion, the new critical volume-based approach would state that the larger the critical volume, the more likely the crack initiation. So, referring to the example showed above, for fixed values of life N_f and parameter z, and referring to hotspot fatigue strengths at the notch tip, it would be expected that:

- blunt notches show lower fatigue strengths;
- sharp notches withstand higher fatigue strengths.

The development of the critical volume approach has been pursued, encouraged by the positive results got by Fojtik and Papuga, who stated that their proposed critical volume method is a promising solution that responds better to both stress gradient and size effects, integrating them into a single “critical volume effect”. Authors said explicitly that the aim is to achieve the maximum simplification that would allow anyone to continue using existing multiaxial solutions but taking into account these improvements based on the critical volume evaluation [17].

3 EXPERIMENTAL STUDY

3.1 FATIGUE TESTS

3.1.1 Description of material and specimens

The material was investigated is the low carbon structural steel named ČSN 41 1523 according to the Czech designation, which is equivalent to the S355J2 in conformity with the European Standard EN 10025. It is one of the most commonly used structural steels in mechanical and civil engineering applications, like construction of bridges, halls, railways, vehicle parts, etc. It is characterized by good weldability and a minimum yield strength of 355 MPa [15], [36]. Mechanical and chemical properties of such a material used to manufacture the specimens are given in Tables 3.1 and 3.2, respectively.

$\mathbf{R_m}$ [MPa]	$\mathbf{R_e}$ [MPa]	**A** [%]
555	401	29.4

Table 3.1: Mechanical properties of ČSN 41 1523 used in the experimental campaign. R_m is the ultimate tensile strength, R_e is yield strength and A is the elongation at fracture.

C [wt %]	**Mn** [wt %]	**Si** [wt %]	**P** [wt %]	**S** [wt %]	**Cu** [wt %]
0.18	1.08	0.22	0.013	0.011	0.2

Table 3.2: Chemical composition of ČSN 41 1523 used in the experimental campaign.

A set of different specimens tested under various loading conditions was prepared to carry out this experimental study. Some of them were already involved in a previous research work conducted by Nesládek et al. (2024) [15]. In that paper, the authors studied only four specimen geometries of the total of six reported below, and they only considered push-pull and torsion loads. Thus, some information about these mentioned cases, that are also involved in the current work, are available in [15]. As anticipated, in the present project, two more geometries were adopted for the specimens made in ČSN 41 1523. Each geometry is identified by the denomination scheme FF20XY, where:

- X digit stands for the geometry of the specimen;
- Y digit stands for the type of load applied to the specimen.

Table 3.3 summarizes the coding of specimens' series, while technical drawings of specimens are available in Appendix 9.1. It is possible to note that all specimens are full bar samples, except for the unnotched one that is characterized by a hollow geometry. One consideration should be stated regarding the unnotched specimen. Smooth samples are usually involved into fatigue experimental studies because they reflect the pure material response to the imposed cyclic loading, since any notch effect is present. Testing the unnotched geometry in push-pull, torsion and plane bending, it is possible to obtain the S-N curves for all the considered load cases: this allows to read plain fatigue limits or plain fatigue strengths at different values of life N_f for each loading configuration. However, the real problem is more complex. An unnotched specimen with a unit stress concentration factor ($K_t = 1$) can theoretically be obtained adopting a prismatic geometry (like the cylindric one used here). But it is worth noting that the specimen must me clamped at both ends to be solidly linked to the testing machine, as a result a stress concentration at the two ends cannot be avoided. The role

of the large fillet radius present between the clamping part and the gauge section of the specimen is to reduce as much as possible this effect and keep the K_t close to 1 [2]. In the end, it is important to point out that for the current experimental work the fatigue data coming from tests performed on unnotched specimens (FF2030, FF2032, FF2035) are treated as data which describe the material response to the fatigue loading.

Unnotched	FF2030	Push-pull
	FF2032	Torsion
	FF2035	Plane bending
V-notch R1.3	FF2040	Push-pull
	FF2042	Torsion
	FF2045	Plane bending
U-notch R1.5	FF2050	Push-pull
	FF2052	Torsion
	FF2055	Plane bending
Fillet R0.7	FF2060	Push-pull
	FF2062	Torsion
	FF2065	Plane bending
U-notch R5	FF2070	Push-pull
	FF2072	Torsion
	FF2075	Plane bending
Fillet R0.2	FF2080	Push-pull
	FF2082	Torsion
	FF2085	Plane bending

Table 3.3: Denomination of tested specimen series.

3.1.2 Experimental setup

All 20X0, 20X2 and 20X5 series were tested respectively under fully-reversed tension, fully-reversed torsion and fully-reversed plane bending: this means that everywhere the load ratio is $R = -1$ and there is no effect of the mean stress. Experiments were carried out at ambient temperature.

Uniaxial tension-compression tests were performed using a high-frequency INOVA FU-63-930-V1 hydraulic pulsator with load control at a frequency of $25\ \mathrm{Hz}$, showed in Figure 3.1. Meanwhile torsion tests were conducted on an upgraded and modified electromechanical Schenck PWXN machine, equipped by control of torque, at a frequency of 25 Hz. Figure 3.2 reports a specimen mounted on board before being tested. Such a torsion machine was used also for plane bending fatigue tests, adopting the special fixture illustrated in the CAD render in Figure 3.3a, which enables bending of the specimen to be induced. Such a fixture was developed by researchers of Technical University of Ostrava, where experimental tests were carried out, and its use is documented in previous works [17] and [12]. Figures 3.4 and 3.5 show a specimen mounted on such a fixture used for plane bending tests, while Figure 3.3b comes from another experimental campaign treated in [10] and it is reported just to help the reader to understand how the specimen is clamped in bending tests.

Figure 3.1: INOVA FU-63-930-V1 machine used for push-pull tests.

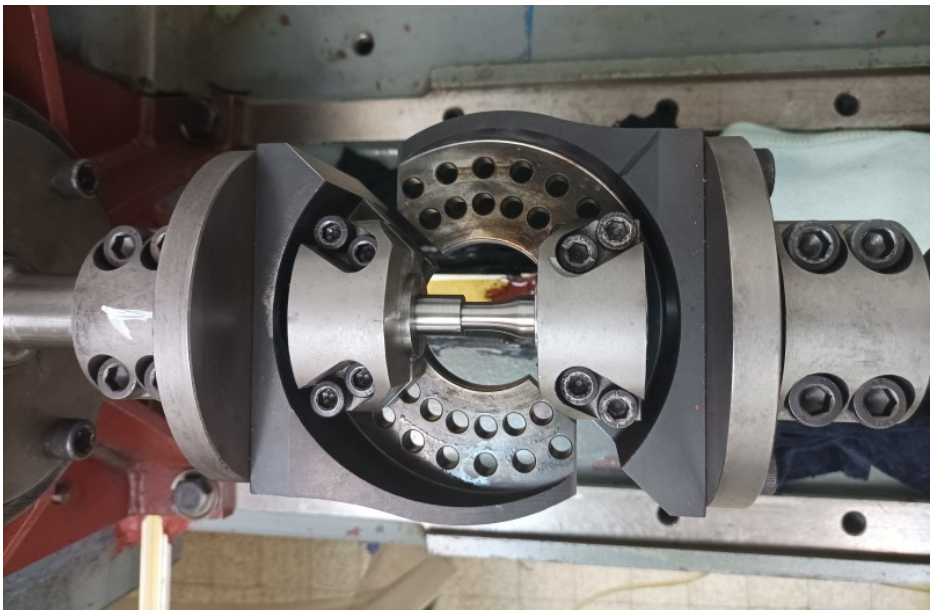

Figure 3.2: Picture of a specimen mounted on Schenck PWXN machine for torsion tests.

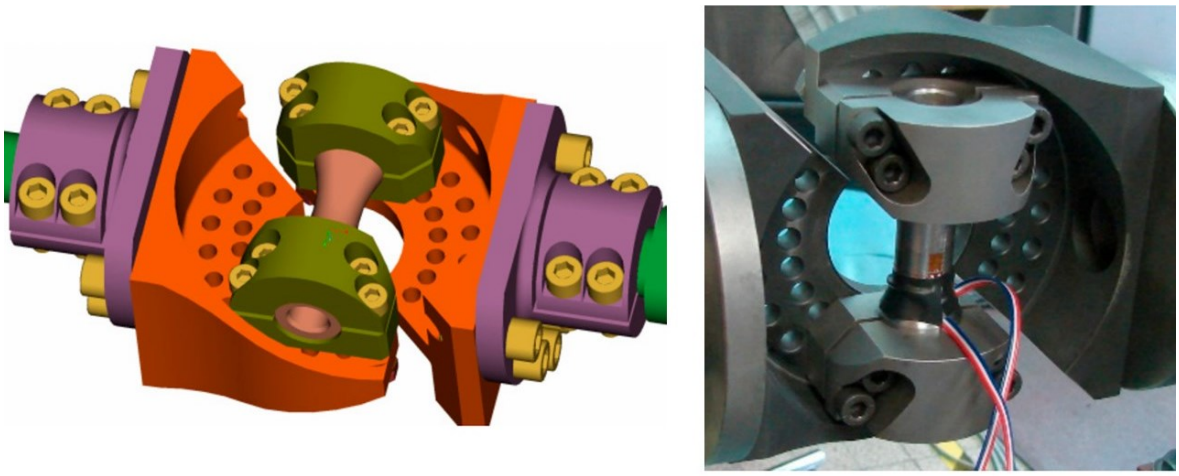

(a) (b)

Figure 3.3: Pictures from [10] about the special fixture adopted to perform plane bending tests using the Schenck PWXN torsion machine: (a) CAD render of the fixture, (b) specimen mounted on it.

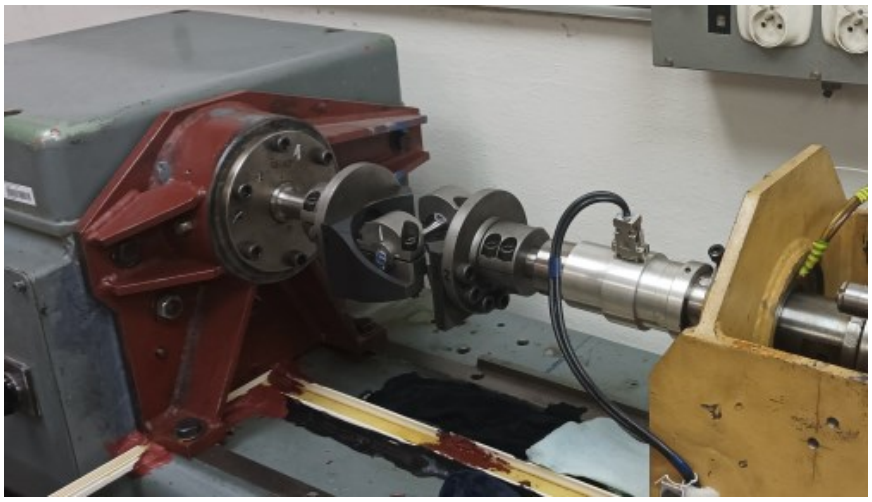

Figure 3.4: Specimen mounted on the Schenck PWXN machine for plane bending tests.

Figure 3.5: Another of the same specimen ready to be tested under plane bending load.

An important aspect about bending tests that must be considered concerns how the bending load is transmitted to the specimen. The component is loaded by a shear force rather than a pure bending moment, thus the stress distribution in the specimen will be the result of the combination of shear stresses and normal stresses (the latter according to Navier's formula). As results, the bended specimen is similar to the cantilever beam scheme presented in Figure 3.6.

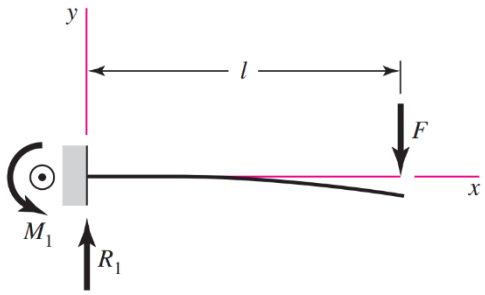

Figure 3.6: Schematic representation of a cantilever beam of length l. F is the shear force transmitted from the machine to the specimen, while R_1 and M_1 are the reaction force and the reaction moment, respectively, on the other clamped end of the specimen which is fixed [6].

The test termination condition was established as reaching the threshold of 10^7 cycles: this means that specimens went over this fatigue life value were labelled as runouts. Otherwise, the test was stopped when the specimen developed a visible macrocrack approximately 5 mm in length. However, this condition practically meant the end of the test by fracture for hollow specimens [15]. All experimental data obtained from fatigue tests are collected in the Appendix 9.2 (Paragraph 9.2.1).

3.1.3 Considerations about specimens' surface roughness

A further aspect to be examined concerns the surface roughness. Regarding the gauge section of hollow Unnotched specimen (refer to Appendix 9.1), the roughness on its outer surface defined in the technical documentation is in the state before surface polishing which was carried out by the laboratory staff. While the inner surface remained in as-reamed condition, quite similar to the finish condition of notched outer surfaces in the other specimens. In [15] the authors have wondered if fatigue experimental data could be affected by different roughness on the outer surfaces of unnotched and notched specimens. About the unnotched specimens, they noted that in the case of push-pull loading the crack initiated from the inner surface. As already said, such a surface should have comparable roughness with the one of outer notched surfaces: thus, authors assumed a negligible difference in surface roughness between material S-N curve and notched specimens' S-N curves. In Figure 3.7a and 3.7b, pictures of fracture surfaces of hollow unnotched specimens tested under fully reversed tension are reported. Instead, regarding the torsion tests it is a general understanding that, under pure torsion loading, crack initiation is less sensitive to surface roughness than in case of push-pull loading [15]. Figures 3.7c and 3.7d show photographs of fracture surfaces of the same type of specimens but tested under fully-reversed torsion. The red arrows indicate the most probable sites of primary crack initiation from the outer surface in torsion cases.

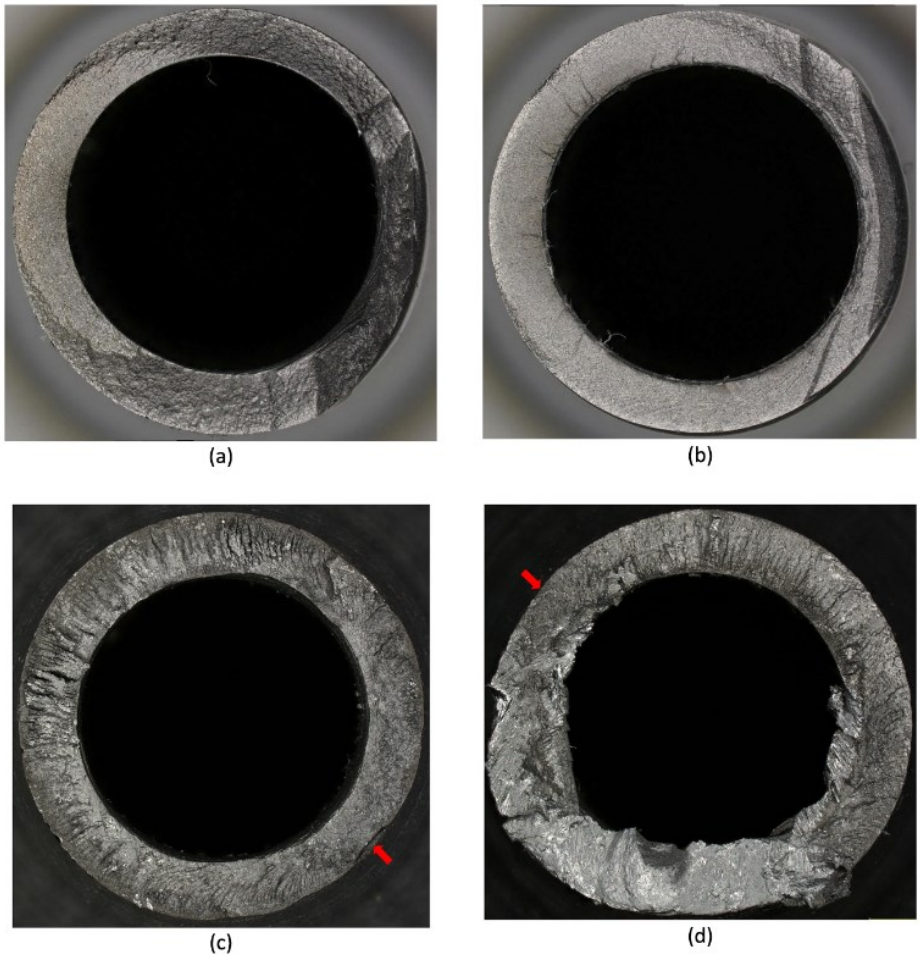

Figure 3.7: Fracture surfaces of unnotched specimens involved in this experimental work [11]. Push-pull tests: (a) $N_f = 772\,578$, (b) $N_f = 194\,250$. Torsion tests: (c) $N_f = 1\,056\,430$, (d) $N_f = 2\,703\,030$.

3.2 FINITE ELEMENT ANALYSIS

Besides the experimental tests campaign there is a significant work done concerning linear elastic analyses using the Finite Element Method. The goal has been to evaluate the stress condition at the notch root and the highly-stressed volume under it for what concerns all the various loading modes and specimen geometries taken into account. Analyses were carried out using Simulia Abaqus CAE 2019, a finite element solver developed by Dassault Systèmes. Even if all specimens have axisymmetric geometry, two different types of finite element models were prepared in Abaqus for each of them, depending on the load case. Indeed, axisymmetric models were suitable to analyse push-pull and torsion cases for all the six axisymmetric geometries. Quadratic planar finite elements were adopted for this purpose. But the situation is different for the bending case, where the stress distribution within the material is more complex. Shear force applied at one of the two specimen's ends induces both shear and normal stresses in the material, the latter deriving from the bending moment and described by the Navier stress distribution. Thus, a three-dimensional model with quadratic solid finite elements was required.

3.2.1 Mesh quality

Some simplifications in specimens modelling were adopted where possible, to save computational burden of the analyses. Regarding the axisymmetric models, such as the ones with unnotched, U-notch and V-notch geometries, only one half was modelled by reason of the plane symmetry present in correspondence of the midsection. Of course, this was not possible to do with fillet-shaped specimens, which required the entire geometry to be considered because of the notch features. Several meshing iterations were performed in order to reach a detailed converged mesh in each case. Figures 3.8, 3.9 and 3.10 show specimens' mesh details, with particular focus on the regions around the notch.

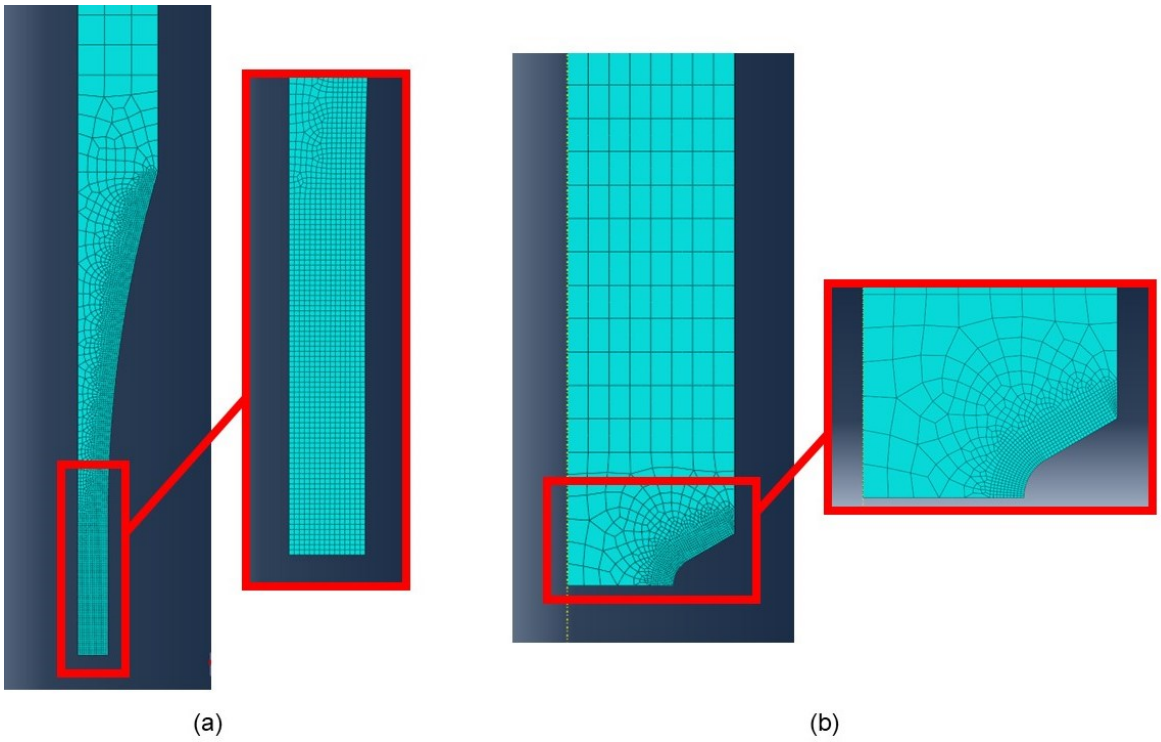

Figure 3.8: Mesh details of axisymmetric models: (a) Unnotched specimen, (b) V-notch R1.3 specimen.

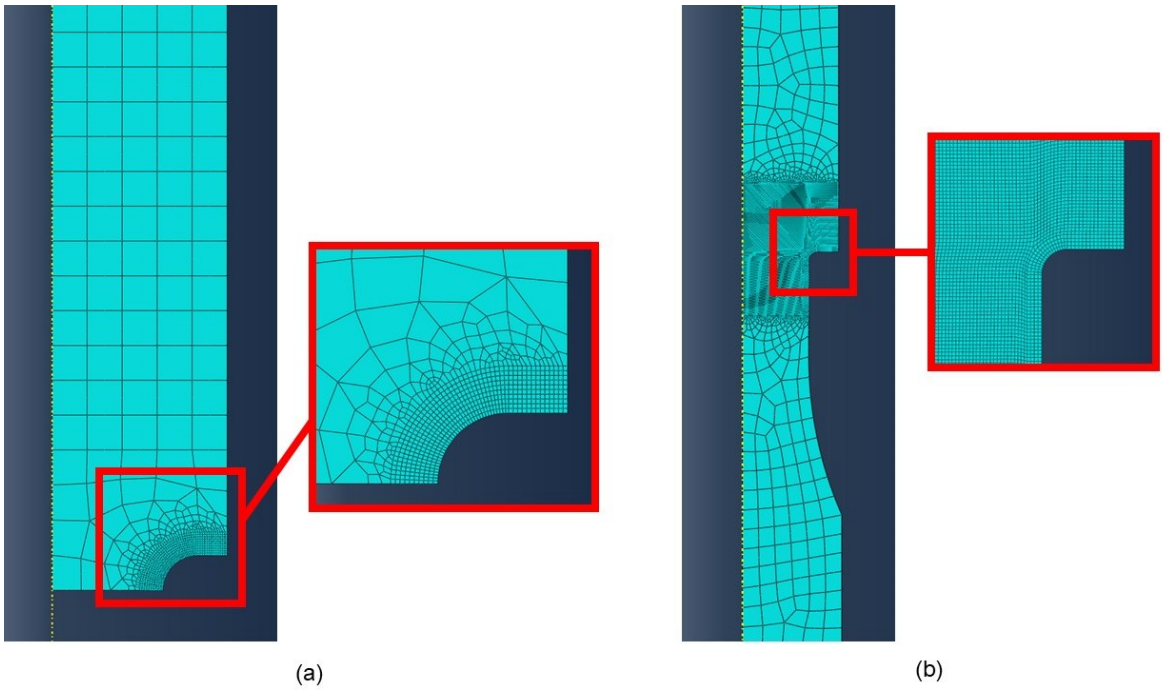

Figure 3.9: Mesh details of axisymmetric models: (a) U-notch R1.5 specimen, (b) Fillet R0.7 specimen.

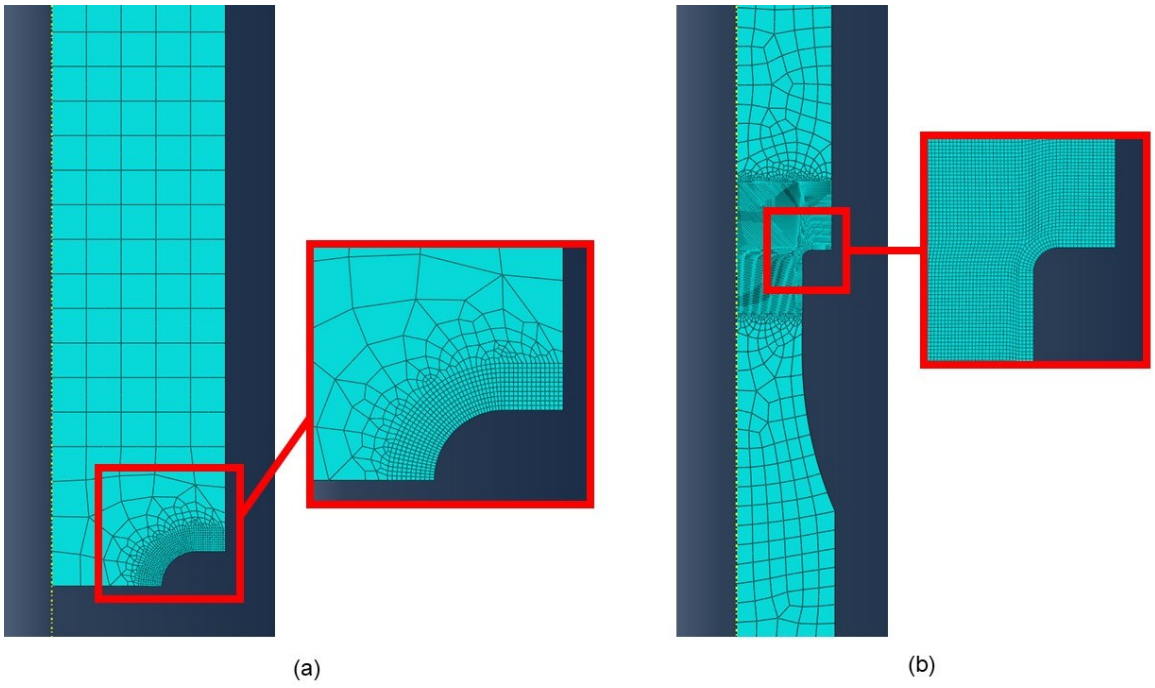

Figure 3.10: Mesh details of axisymmetric models: (a) U-notch R5 specimen, (b) Fillet R0.2 specimen.

Unfortunately, it was not possible to use the same previous trick also for the three-dimensional models used for the plane bending case. Note that the specimen midsection is completely included in the critical volume, object of the current research. Finding the suitable boundary conditions in correspondence of that critical section surface was quite tricky and led to issues over the several iterations performed, such as non-correct stress distributions and numerical errors. Therefore, a better solution to be adopted was to model the specimens over their entire length, but still only modelling one half of them, taking advantage of the plane symmetry with respect to the plane containing the axis of the specimen. But there was also another issue which turned out to be challenging as well, related to the complexity of the mesh. If reduced integration is enabled, each quadratic brick element has 20 nodes: dealing with a three-dimensional mesh means that a high number of nodes is reached quite fast over very few meshing iterations. The direct consequence of this problem is that the FE method computation becomes too much demanding, even for a computer equipped with a good hardware. To overcome this problem, submodelling strategy was adopted. At first, the global model of each specimen was created and analysed with coarse mesh. Later, the submodel was generated isolating the portion of the original model which includes the critical part close to the notch. At this point the FE model was split in half again, exploiting the stress distribution symmetry around the neutral axis (symmetry intended in terms of stress absolute values). In this way, the submodel refers to one quarter of the original specimen notch region. Finally, mesh density was increased in the submodel through several meshing iterations which were repeated till reaching the convergence. In Figures 3.11, 3.12 and 3.13 snapshots of global models and related submodels of specimens are reported.

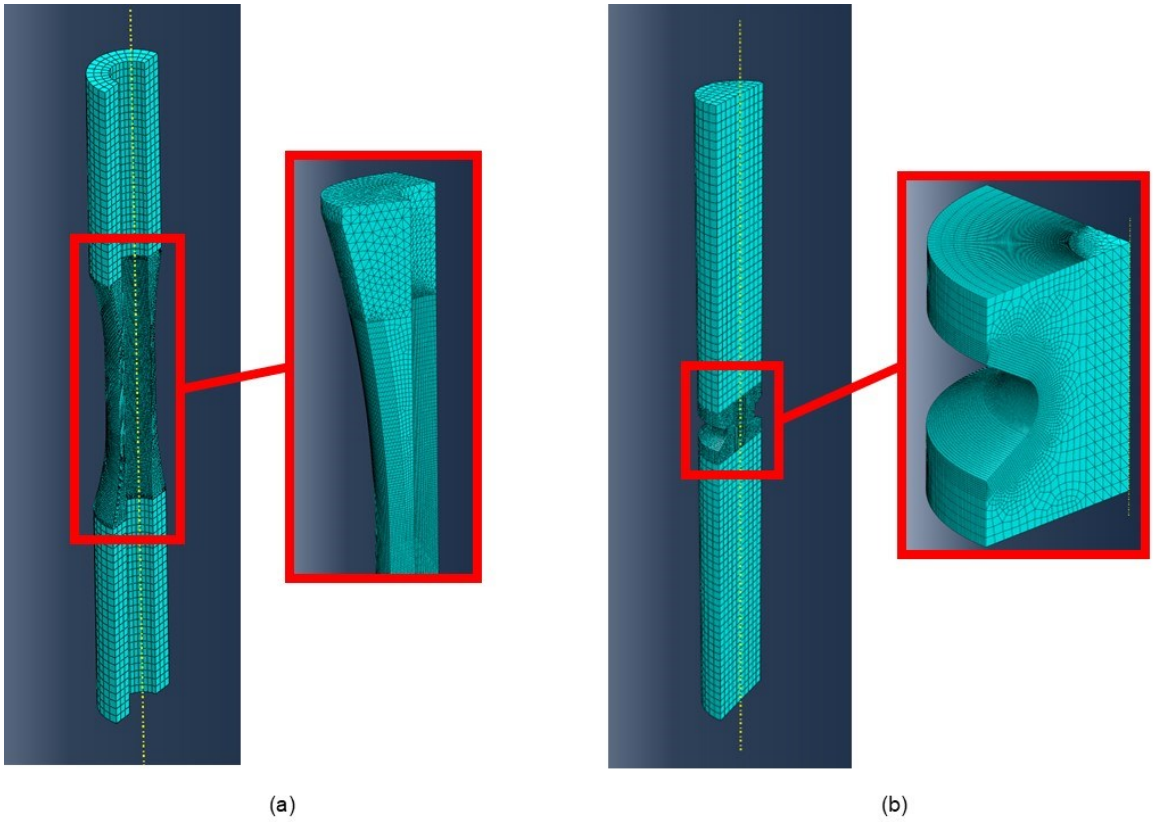

Figure 3.11: Mesh details of 3D models: (a) Unnotched specimen, (b) V-notch R1.3 specimen.

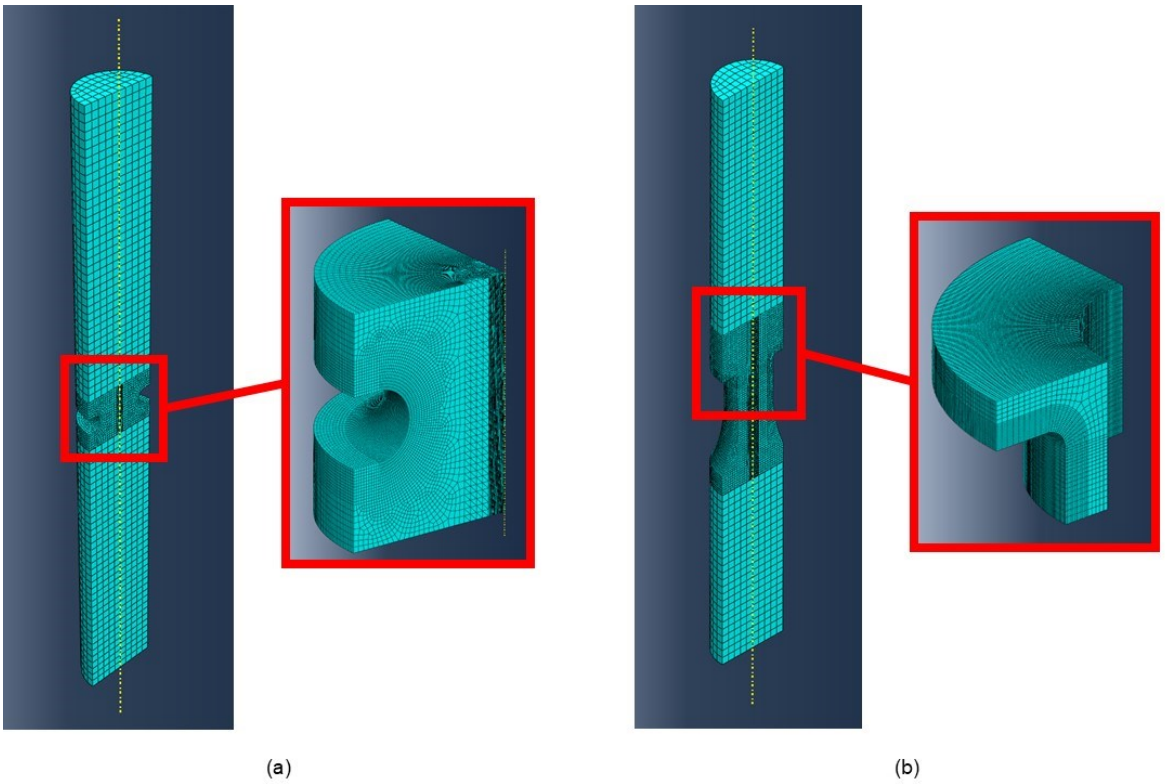

Figure 3.12: Mesh details of 3D models: (a) U-notch R1.5, (b) Fillet R0.7.

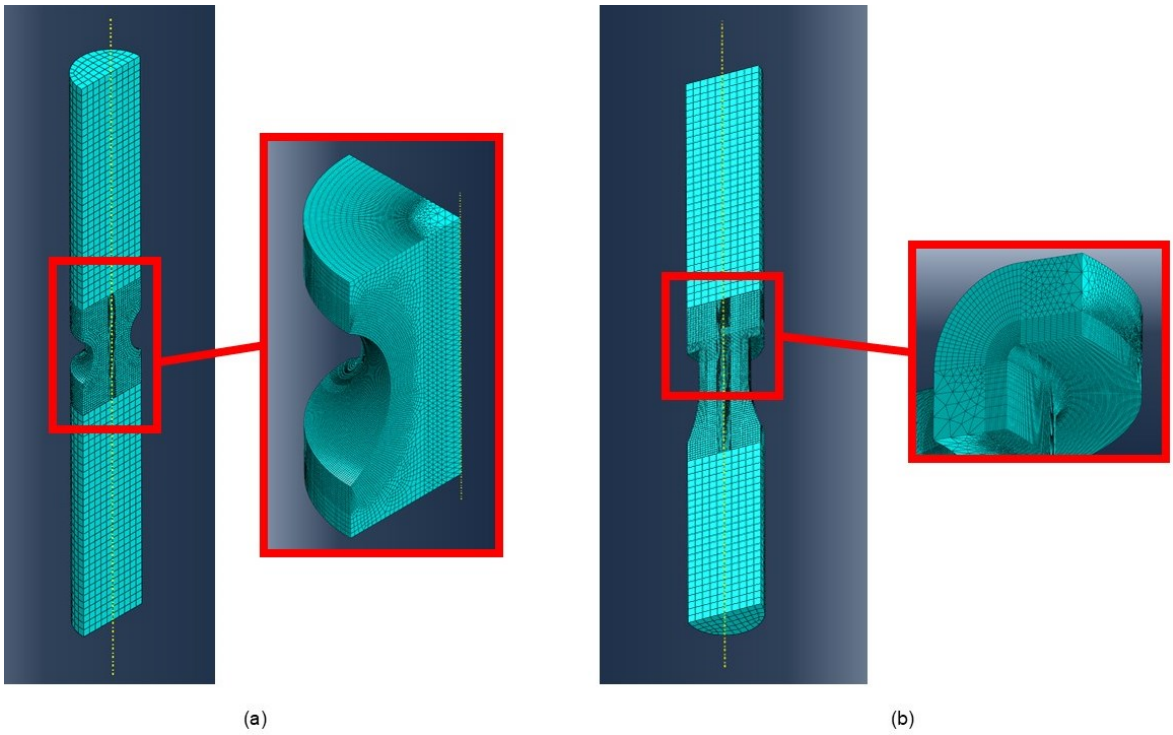

Figure 3.13: Mesh details of 3D models: (a) U-notch R5 specimen, (b) Fillet R0.2 specimen.

Table 3.4 reports the main features concerning mesh around the notch for each specimen, since this is the most critical part from the point of view of FE method computation. The mesh around the notch is structured mesh made up by quadratic elements, with reduced integration enabled in the solver. As said above, final elements size was obtained through several meshing iterations: the error calculated on the maximum von Mises stress between one iteration and the previous one was monitored. Mesh convergence was assumed to be reached when this error fell under 1.5% in all cases, except the 3% obtained in the case of the 3D model of the fillet R0.2 specimen (that was nevertheless considered acceptable).

Model type	Specimen	Notch radius [mm]	Mesh element type	Element size [mm]
axisymmetric	Unnotched	∞	8 nodes, planar	0.1
	V-notch R1.3	1.3	8 nodes, planar	0.06÷0.1
	U-notch R1.5	1.5	8 nodes, planar	0.06÷0.1
	Fillet R0.7	0.7	8 nodes, planar	0.065÷0.1
	U-notch R5	5	8 nodes, planar	0.09÷0.125
	Fillet R0.2	0.2	8 nodes, planar	0.005÷0.01
3D	Unnotched	∞	20 nodes, brick	0.125 ÷ 0.2
	V-notch R1.3	1.3	20 nodes, brick	0.065 ÷ 0.1
	U-notch R1.5	1.5	20 nodes, brick	0.062 ÷ 0.125
	Fillet R0.7	0.7	20 nodes, brick	0.044 ÷ 0.078
	U-notch R5	5	20 nodes, brick	0.077 ÷ 0.12
	Fillet R0.2	0.2	20 nodes, brick	0.01 ÷ 0.025

Table 3.4: Notch radii, types of element and related ranges of element size for FE models of every specimen.

It is worth to point out that, when performing a linear elastic analysis using the FE method, it does not matter what value of the load applied to the part is given as input. Indeed, results (e.g. stresses or strains) can be scaled with a proper scale factor in order to lead back the analysis to the real experimental case. Moreover, it is important to remember that the critical volume is a “component feature” of the specimen, that depends on the material elastic properties and on the notch geometry, according to the its definition given in Section 2.5. Thus, the input value of the force in the FE analysis is again not relevant for evaluating the critical volume dimension.

3.2.2 Derived stress concentration factors

FE analyses allowed to calculate stress concentration factors for all specimens in the various loading configurations. Factors K_t were calculated referring to the net cross-sectional area (the subscript *net* is again omitted in the symbols) and referring to both von Mises equivalent stress and maximum principal stress. These stresses evaluated at the root of the notch are referred to as σ_{Mises_max} and σ_{PS1_max}, respectively.

Concerning tension case, the net nominal stress is calculated as the ratio between the pull force (F) and the net cross-sectional area (A_{net}):

$$\sigma_{nom} = \frac{F}{A_{net}} \tag{3.1}$$

So, the net stress concentration factor can be calculated according to von Mises equivalent stress and maximum principal stress as follows:

$$K_{t,ten\_Mises} = \frac{\sigma_{Mises\_max}}{\sigma_{nom}} \tag{3.2}$$

$$K_{t,ten\_PS1} = \frac{\sigma_{PS1\_max}}{\sigma_{nom}} \tag{3.3}$$

Regarding the torsion case, if d is the specimen diameter referred to the net cross-section, the torsional section modulus (W_t) results to be [2]:

$$W_t = \pi \frac{d^3}{16} \tag{3.4}$$

Thus, the nominal shear stress is calculated as the ratio between the torque M_t and the torsional section modulus [2]:

$$\tau_{nom} = \frac{M_t}{W_t} \tag{3.5}$$

According to von Mises, in pure torsion the normal stress is equal to $\sqrt{3}$ times the shear stress [3]. So, the net stress concentration factor referred to von Mises criterion can be calculated as follows:

$$K_{t,tor\_Mises} = \frac{\sigma_{Mises\_max}}{\sigma_{nom}} = \frac{\tau_{max}\sqrt{3}}{\tau_{nom}\sqrt{3}} = \frac{\tau_{max}}{\frac{M_t}{W_t}} \tag{3.6}$$

Meanwhile, remembering that the maximum principal stress in pure torsion is equal to the maximum shear stress, the stress concentration factor can be expressed as [2]:

$$K_{t,tor\_PS1} = \frac{\sigma_{PS1\_max}}{\tau_{nom}} = \frac{\tau_{max}}{\tau_{nom}} = \frac{\tau_{max}}{\frac{M_t}{W_t}} \tag{3.7}$$

As a result, stress concentration factors referred to both von Mises and maximum principal stresses turn out to be the same.

In the end, plane bending case is analysed. The nominal stress is calculated as the ratio between the bending moment (M_b) and the bending section modulus (W_b) referred to the net cross-sectional area. As said previously, the load cannot be considered as pure bending, because it is induced by a shear force: so, the specimen bends under the application of a shear load, whether a bending load. One clarification on this case is needed. Specimen under bending load has been modelled in Abaqus as schematized in Figure 3.14 and as described hereafter. The shear force F has been applied in the reference point called RP-2, which is located in the middle of the gripping length situated on the right end of the specimen. The mentioned length corresponds to $l_{grip} = 36$ mm and it is the same for all bended specimens. Another reference point RP-1 is positioned on the opposite specimen's end and it has all degrees of freedom fixed to the ground. The distance between these two reference points, which is smaller than the entire length of the specimen (l_{spec}), has been considered the effective arm to be used in the computation of the bending moment. Its length can be calculated as:

$$l = l_{spec} - 2 \cdot l_{grip} \tag{3.8}$$

Considering the reference frame fixed in RP-1, it is possible to write the linear bending moment function by imposing the equilibrium on rotations to the elastic beam:

$$M_b = F \cdot (l - x) \tag{3.9}$$

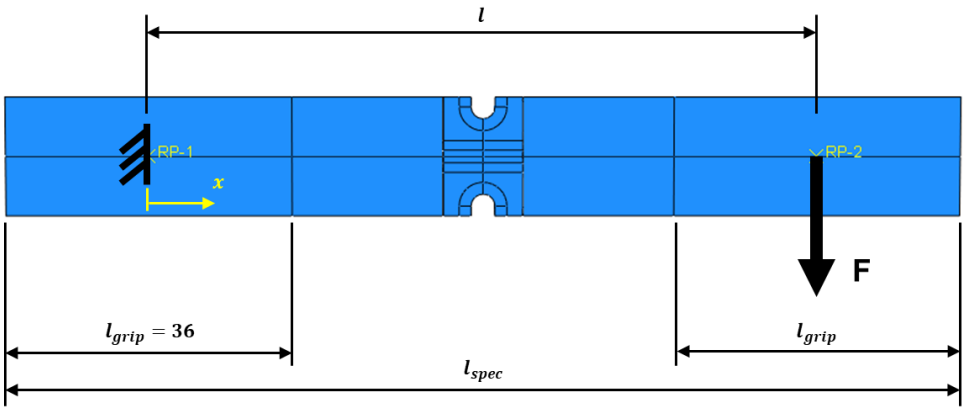

Figure 3.14: Scheme illustrating how the bending load case has been modelled in the FE solver.

For notched specimens, the hotspot corresponds to the notch apex that stands in the middle section, thus at $x = {}^{l}/_{2}$. For the smooth sample the hotspot position is shifted closer to the fixed end (RP-1), so the correct value of x has been evaluated directly from the plots of FE results.

If d represents again the diameter of net cross-section, the bending section modulus can be calculated as:

$$W_b = \pi \frac{d^3}{32} \tag{3.10}$$

Therefore, the net nominal stress results in:

$$\sigma_{nom} = \frac{M_b}{W_b} \tag{3.11}$$

Finally, net stress concentration factor for plane bending case can be calculated in the two versions as follows:

$$K_{t,ben\_Mises} = \frac{\sigma_{Mises\_max}}{\sigma_{nom}} \tag{3.12}$$

$$K_{t,ben\_PS1} = \frac{\sigma_{PS1\_max}}{\sigma_{nom}} \tag{3.13}$$

To sum up, Table 3.5 reports all the stress concentration factors, referred to both von Mises equivalent stress and maximum principal stress.

K_t	Tension		Torsion		Plane bending	
Specimen	Mises	Max Principal	Mises	Max Principal	Mises	Max Principal
V-notch R1.3	1.990	2.224	1.434	1.434	1.636	1.823
U-notch R1.5	1.885	2.102	1.390	1.390	1.558	1.733
Fillet R0.7	2.095	2.328	1.480	1.480	1.806	1.997
U-notch R5	1.303	1.408	1.141	1.141	1.176	1.264
Fillet R0.2	3.338	3.731	2.055	2.055	2.764	3.044

Table 3.5: Stress concentration factors calculated through FE analyses referring to both von Mises and maximum (or first) principal stress.

3.3 CRITICAL VOLUME EVALUATION

One of the most important steps of the current experimental work consists in evaluating the critical volume. Theoretical fundamentals have been already given in Section 2.5, while the effective calculation of this critical quantity is described here. Values of critical volume obtained for each specimen in each loading scenario are later used to implement the new approach.

3.3.1 Python scripts and PyLife package

Calculation of critical volume using only the FE software was not totally possible. All commercial solvers have a post-processing environment where the results of the structural analysis can be displayed graphically. Focusing only on stress analysis, a typical feature that most common FE software have is to let the user to query and visualize the exposed volume: it consists in the portion of the model made up of all finite elements which stresses at nodes (e.g. equivalent von Mises stresses) are included in the range set by him/her. Unfortunately, for the aim of this project, this feature was not so useful as expected for many reasons reported hereafter.

As recommended in literature [17], [34], critical volume should be evaluated for different values of parameter z, like in a range from 0.8 to 0.99. As previously suggested, such a factor should be optimized, becoming to all intents and purposes a fitting parameter of the dependencies between fatigue strength and critical volume (which will be evaluated later). According to that, it means that some iterations should be performed. It is easy to image how much tough and time consuming the iterations for plotting the critical volume at different z values in the post-processing environment would be, doing it all manually or, at least, using some macro scripts to be run in the FE software. Feasibility of this latter option concerning macros was not checked because it would still be limiting for this application, since the user should know well the macro's programming language which can differ from one solver to another one. Furthermore, in some cases it is also not possible to query the volume of elements. This is the case, for example, of axisymmetric models analysed in Abaqus: the user is not allowed to query manually, from the results visualization environment, any element volume since the mesh is made up by planar (2D) and not brick (3D) elements. Note that this happens even if the element volume is computed during the analysis and stored in the output file. It is clear that this would have represented an insurmountable obstacle for the current work, since the fact that the models for tension and torsion loading cases are axisymmetric. Just to remark what reported above, it is interesting to refer to the already mentioned Fojtík and Papuga's paper [17] and analyse the work they carried out to quantify the critical volume. The investigated specimens were modelled in the FE software Ansys APDL. After the linear elastic analyses were completed, the critical volumes were calculated but without first having spent a very long time to perform manually the entire procedure reported hereafter, which was applied for each specimen twice since the authors considered two values of z (0.95 and 0.99). The FEM results were plotted for a specific value of z, thus the map of von Mises equivalent stresses was cut along two perpendicular sections. Thanks to the use of a CAD software, it was possible to measure the critical volume from the sections' images. It is worth noting a further issue, that would be related to the implementation of this cumbersome method in conjunction to a multiaxial fatigue strength criterion. A manual graphic procedure, like the one reported in [17], can work with von Mises equivalent stresses which computation is already implemented in all FE solvers. But the state of art in terms of multiaxial fatigue criteria could not be implemented in a scenario like this, because the common commercial solver would be probably not equipped with such criteria.

The idea of elaborating output results from FE analysis by running a script developed in some programming language seemed to be more reasonable in terms of feasibility, reusability of the code, reduced risk of human error and thus quality of results. The choice fell on Python, one of the most used and versatile open-source programming languages nowadays. Besides, it must be pointed out

that fatigue researchers of Czech Technical University embraced a project supported by Bosh Research called PyLife, as documented by the related workshop hosted in their Faculty of Mechanical Engineering in Prague last 14th and 15th December 2023 [37]. PyLife is an open-source Python library used in lifetime assessment of mechanical components subject to fatigue load [38]. As declared by one of the engineers involved in its development, Johannes Mueller, the aim of this project is "*to make specialistic knowledge available to others through open-source software*" [39]. This aspect represents one of the strongest points of PyLife and of its use in scientific research. Indeed, it goes in the completely opposite direction of commercial FEM and fatigue software, which ones often appear like "black boxes" that are not accessible by the user in case of issues while pre-processing, running or post-processing the analyses. Definitively, there is also another appealing advantage of Python language compared to other famous languages like MATLAB, and it is represented by costs: coding in Python is free since it is an open-source language, therefore everyone can use it without being forced to pay an expensive licence. For sure this last aspect would represent attractive towards the research world, either in the universities and in the companies. Last but not least, another PyLife's useful feature concerns the possibility to read directly Abaqus output files (characterized by the *.odb* extension). This came out to be interesting since the FE analyses for this project work were carried out using such a software. Unfortunately, Abaqus still comes with the old Python 2.7 engine, while the latest Python 3.x version can be downloaded at present. So, thanks to the use of a special client called *odbserver* (which run inside a Python 2.7 environment) the output database file is accessible from within Python 3.x code. It is reasonable to imagine that this Abaqus – Python compatibility, enhanced by PyLife, encouraged the code implementation based on Python language [38].

3.3.2 Algorithm for critical volume calculation

Since evaluating the critical volume in the "manual way" through the FE software was not feasible for the explained reasons, a Python script was developed to calculate this physical quantity. Abaqus was asked to calculate and store in the output database file the volumes of all finite elements composing the mesh. The critical volume is expected to be around the specimen notch. It could happen that elements located at the border of the critical volume are only partially included in such a volume. Indeed, it is extremely likely that some mesh elements, located at such a border region, have some nodal stresses above the threshold (defined by the critical stress σ_{crit}), and other nodal stresses belove it. This means that not the entire element volume can be considered critical or non-critical.

So, at this point the question about how to deal with the mentioned situations came out, and two possible ways to proceed were individuated. The first one is the overestimating approach, while the second one results to be the underestimating approach. For now, the following approaches are referred to computations that involve von Mises equivalent stresses.

1. According to the overestimating approach, elements with at least one node inside the threshold defined by σ_{crit} should be completely included in the critical volume evaluation: the direct and obvious effect would be an overestimation of the real critical volume. It must be pointed out that this way of operating is the same as that adopted by Abaqus when the user asks for the graphical display of critical volume in the results visualization environment. This incorrect critical volume estimation can be immediately visualised in cases of acute notches, where the high stress gradient makes the stress profile descending quite vertically under the notch root and thus the critical volume results to be very small and strongly located at the notch tip. This aspect is even more enhanced by considering the bending load mode and high values of parameter z. In Figure 3.15, von Mises equivalent stress map is presented concerning the Fillet R0.7 specimen under plane bending (test FF2065), with a particular focus on the critical volume evaluated at $z = 0.85$. Referring to the second picture, the red

spots are the nodes which have an equivalent nodal stress value equal to or higher than the threshold value (σ_{crit}). Such nodes are the ones that really belong to the critical volume, which does not involve all the other nodes that are not highlighted. Thanks to this visualization, it is possible to notice that critical volume by Abaqus is for sure larger than the "real" one.

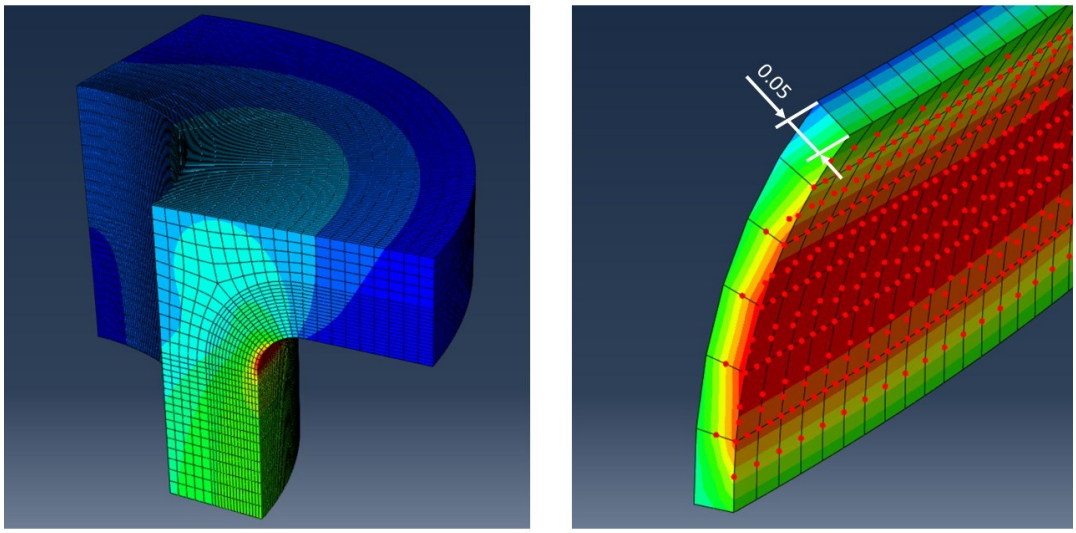

Figure 3.15: In (a), equivalent von Mises stress results for Fillet R0.7 specimen loaded under plane bending. In (b), critical volume referred to $z = 0.85$ is illustrated. Note the mismatch between the plotted critical volume and the nodes which stress is above the threshold value. Radial element size is equal to 0.05 mm.

2. The underestimating approach would instead consider in the calculation only the elements that have all the nodes included in the stress threshold. But, according for example to what already seen in Figure 3.15, it is totally clear that this way to proceed would lead to serious estimation problems: there would be some cases (like the one presented above) where the evaluation of such a volume would not consider any element, resulting in a critical volume equal to zero.

Another way, that would represent a cross between the two discussed options, could consist in considering part of the critical volume only border elements that have a determined number of nodes (assumed according to some criterion) that are included in the critical volume condition. A random example of a criterion for critical volume evaluation is proposed here: such a volume could include only those border elements with at least 50% of nodes above the σ_{crit} and thus included in the volume. When the problem of studying a solution about the critical volume calculation was addressed, this last option was not taken into account, but it is anyway not interesting considering the work done subsequently.

A more functional approach was designed, and its development is now described. Consider the generic finite element i, present somewhere in the mesh. In the generality, such an element could stand across the border line of the volume that must be investigated. The idea is to calculate the critical volume by evaluating a proportion between the number of element nodes and the magnitude of element volume. The number of nodes included in the threshold (that means their equivalent nodal stress is greater than or equal to the σ_{crit}) is counted by $n_{i,crit}$. Instead, the total number of nodes is equal to n_i: it must be kept in mind that $n_i = 8$ for quadratic planar elements used in axisymmetric model, while $n_i = 20$ for quadratic brick elements used in 3D models (the reduced integration is always active). The ratio $n_{i,crit}/n_i$ must be equal to the ratio between the critical volume object of the calculation (CV_i) and the total volume of the considered element (V_i). Thus, the proportion would be:

$$n_{i,crit} : n_i = CV_i : V_i \tag{3.14}$$

from which it is possible to obtain the fraction of critical volume belonging to the i^{th} finite element:

$$CV_i = V_i \cdot \frac{n_{i,crit}}{n_i} \tag{3.15}$$

In the end, if m is the total number of finite elements involved in the critical volume, so it means they have at least one node included in the threshold, the overall critical volume value of the specimens is the sum of all the CV_i contributes:

$$CV = \sum_{i=1}^{m} CV_i \tag{3.16}$$

Equations 3.15 and 3.16 summarise the most important steps of the critical volume calculation, for all specimens in all loading scenarios. The aim of this paragraph was to illustrate the trace of the algorithm that has been implemented in Python code. The script is reported in the Appendix 9.3. There are two important aspects to point out:

1. such an algorithm works considering the average nodal stresses. It means that, considering a single node, the script is able to: read all the stress components on that node ($\sigma_x, \sigma_y, \sigma_z, \tau_{xy}, \tau_{xz}, \tau_{yz}$), average the values of such components derived from all finite elements sharing that same node (arithmetic mean), and finally apply the equivalent stress formulation;

2. equivalent stresses of the considered static linear elastic analyses represent the equivalent stress amplitudes of the fatigue problem. Such equivalent stress amplitudes were evaluated in the calculations performed by Python script, in particular they have been obtained using the Manson-McKnight criterion at first, and the Dang Van criterion later.

3.3.3 Validation of the proposed algorithm

As already said, the algorithm explained above has been implemented in Python code. It is worth examining how such a code for critical volume evaluation was validated. Validation process was applied to ensure that any bugs were encountered through the several calculation steps. This validation check was fulfilled in the early stages of development of the critical volume method, considering von Mises equivalent stresses computed by Abaqus.

The basic idea of the check procedure is to compare the outcomes of the analysis run in Python and the critical volumes plotted by Abaqus in the results visualization environment. As already said, Abaqus does not allow the user to query the critical volume of axisymmetric models. So, the check procedure was implemented only considering the 3D models, where this manual operation is allowed by the software. It has already been pointed out that Abaqus follows the “overestimating approach” when it plots the critical volume. Thus, making a direct comparison between the value of critical volume plotted by Abaqus and the one estimated via the proposed algorithm did not make any sense. To demonstrate this, such a comparison has been performed anyway and the results are presented few lines below. While the idea that was actually considered consists in having modified temporally the script, downgrading it to the Abaqus “way of thinking”. Basically, instead of calculating the CV_i for each element with at least one node included in critical volume using the equation 3.15, such a term has been considered equal to the entire V_i of each element:

$$CV_i = V_i\,, \qquad \forall i \in [1, 2, \dots, m] \tag{3.17}$$

Putting Abaqus and the Python code on the same level, it has been possible to calculate the percentage error of the critical volume estimation performed by the script with respect to the Abaqus result. This check procedure, carried out for all 3D cases, resulted in a positive response. Tables below report, for instance, the Fillet R0.7 sample referring to its 3D model used to analyse the plane bending case (FF2065): interval of z values from 0.55 to 0.99 is observed. The relative error between the value of critical volume computed by Python script and the one computed by Abaqus is defined as:

$$error[\%] = \frac{CV_{Python} - CV_{Abaqus}}{CV_{Abaqus}} \cdot 100 \tag{3.18}$$

Table 3.6 compares values of critical volume computed via the developed code with the ones read from FEA results visualization environment, confirming that Abaqus is affected by the overestimation issue: in some cases, this overestimation error is quite huge. Meanwhile Table 3.7 illustrates the wiser comparison conducted involving the modified version of Python code. The 0% error demonstrate the robustness of the developed script. Similar good results have been obtained also for other 3D models (not reported here), even if it must be mentioned that such an error reached the outermost value of -8.80% for the unnotched model (FF2035). This outcome could be related both to the fact that definition of the critical volume edge in the unnotched specimen can be more erratic (since such a volume turns out to be much larger than other cases) and to any possible rounding error of decimal digits. In the end, this was absolutely considered acceptable and it has been assumed not compromising the validity of the developed idea.

z	**Critical volume (plane bending) [mm^3]**		**error [%]**
	Abaqus computation	Python computation	
0.55	5.9318	4.7425	-20.05
0.60	2.1621	1.5087	-30.22
0.65	1.2976	0.8279	-36.20
0.70	0.8133	0.4699	-42.23
0.75	0.5884	0.3004	-48.94
0.80	0.3910	0.1700	-56.53
0.85	0.2461	0.0984	-60.04
0.90	0.1741	0.0565	-67.53
0.95	0.1038	0.0290	-72.09
0.99	0.0352	0.0074	-78.91

Table 3.6: Comparison between critical volumes computed by Abaqus and the ones computed by the proposed Python algorithm, referring to the example of Fillet R0.7 loaded in bending (FF2065).

z	Critical volume (plane bending) [mm^3]		error [%]
	Abaqus computation	Python computation*	
0.55	5.9318	5.9318	0
0.6	2.1621	2.1621	0
0.65	1.2976	1.2976	0
0.7	0.8133	0.8133	0
0.75	0.5884	0.5884	0
0.8	0.3910	0.3910	0
0.85	0.2461	0.2461	0
0.9	0.1741	0.1741	0
0.95	0.1038	0.1038	0
0.99	0.0352	0.0352	0

Table 3.7: Comparison between critical volumes computed by Abaqus and the ones computed by the modified version of the Python proposed algorithm, referring to the example of Fillet R0.7 loaded in bending (FF2065).*

4 S-N CURVES

4.1 DATA REGRESSIONS

4.1.1 Considerations about the regression models adopted

Data collected from the experimental campaign allowed to calculate the S-N curves related to each specimen series. Eight specimens were tested for each series, except for cases FF2030 and FF2040 which involved one extra test for the S-N curve construction. This additional record refers to a finished runout sample which was retested at highest possible load level, in order that the previous damage (accumulated during the runout test) had a negligible impact on the fatigue lifetime at this new level.

The regression models that have been adopted are the ones detailed in Section 1.2: the least-square fit by Basquin formula and the non-linear fit by the Kohout-Věchet model. For this purpose, an alternative to the Basquin formulation already seen in equation 1.15 is proposed here:

$$\sigma_a{}^w N = C_B \tag{4.1}$$

Equation 4.1 is totally equivalent to the equation 1.6 already explained, indeed they merely represent two slightly different ways to express the power law. In addition, the non-linear K-V regression model (proposed in 1.9) has been arranged as follows:

$$\sigma_a = A \cdot \left[\frac{(N+B)\cdot C_{K-V}}{N + C_{K-V}}\right]^{\beta} \tag{4.2}$$

Subscripts “B” and “K-V” allow to distinguish the two types of regressions [15]. Another noteworthy aspect concerns the statistical parameters. Coefficients of determination (R^2), standard deviations of logarithmic of cycles (s_{logN}) and standard deviations of stress amplitude (s_σ) of both regression models are not directly comparable. Basquin coefficients are obtained by minimizing the sum of squared errors in terms of life cycles: this corresponds to the nature of the fatigue experimental setup, where the applied load is the known input and the number of cycles (that the specimen is able to sustain) corresponds to the unknown output. Instead, since K-V function is used for fitting data in the quasistatic and in the infinite life regions (low N and high N, respectively) thanks to its two horizontal asymptotes, the fitting optimization cannot consider errors in terms of cycles to failure: the minimized objective function is expressed via squares of errors in terms of fatigue strength. In the end, it is possible to state that the Basquin fitting optimizes along the horizontal $\log N$ axis, while the K-V fitting optimizes along the vertical strength axis [35].

4.1.2 Fatigue test results

Basquin and K-V fits are presented in Figures 4.1 to 4.6: all these graphs report the net nominal stress amplitude vs. the number of cycles to failure, with the latter expressed on a log scale. Regression parameters obtained for these S-N curves are collected in Tables 9.1 and 9.2 in Appendix 9.2. Fitting quality of these regressions was evaluated checking the statistical coefficients mentioned above, thus R^2, s_{logN} and s_σ.

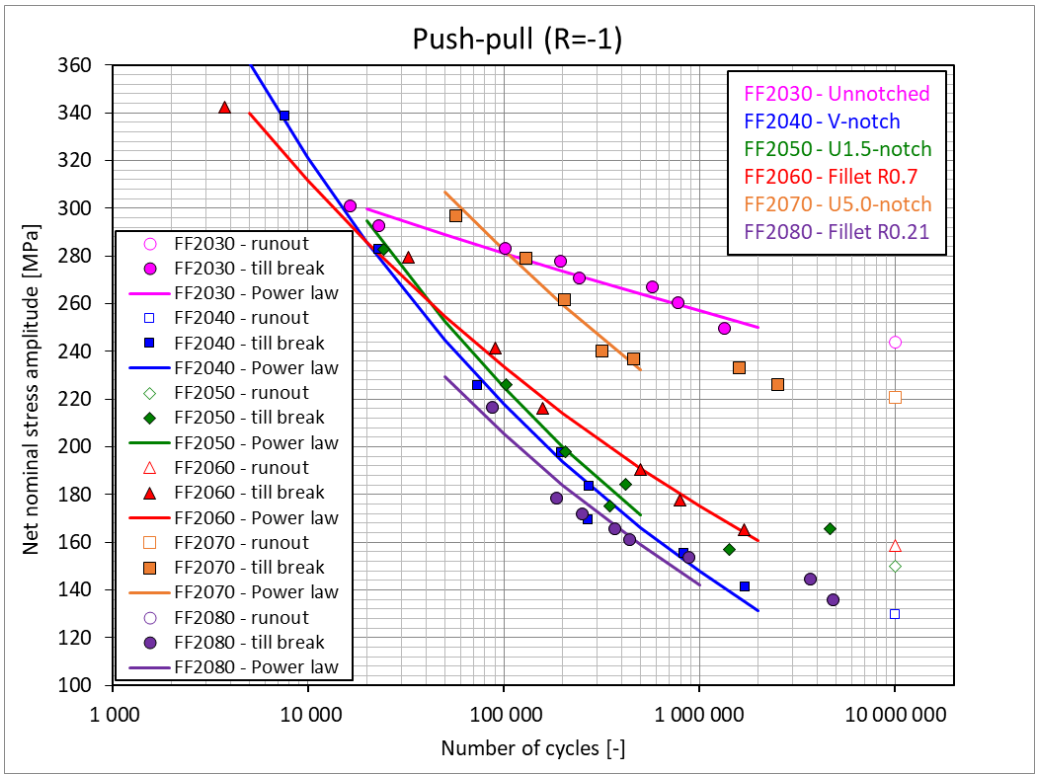

Figure 4.1: S-N curves of fully reversed push-pull tests fitted with Basquin regression model.

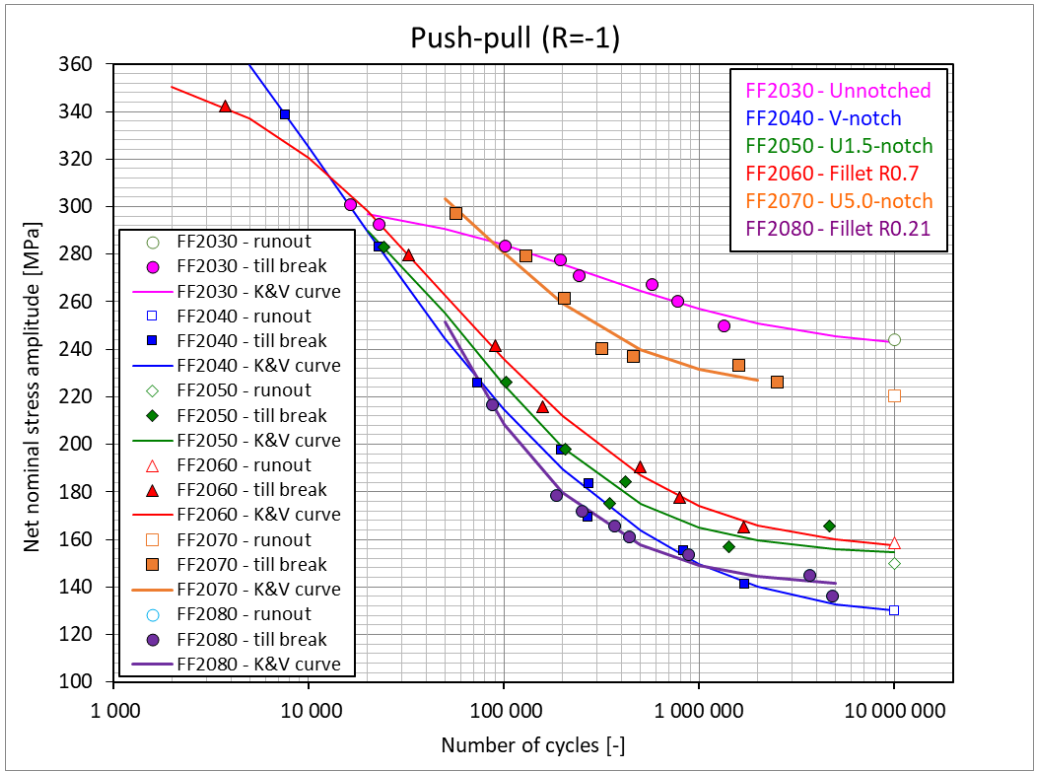

Figure 4.2: S-N curves of fully reversed push-pull tests fitted with K-V regression model.

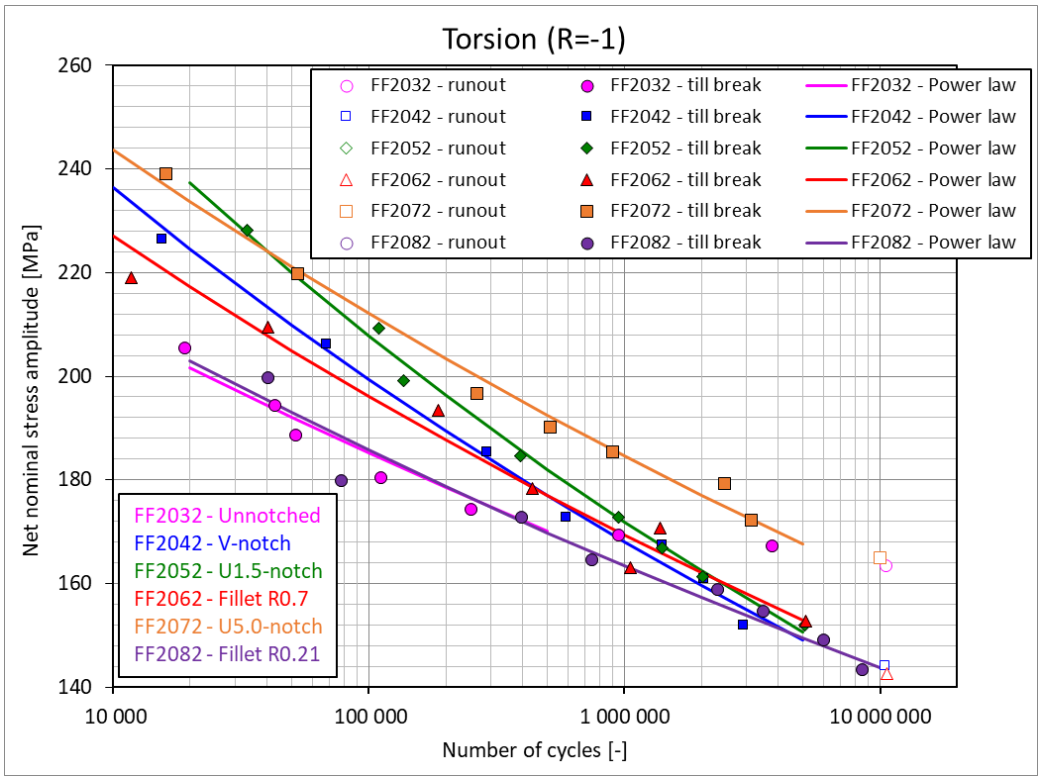

Figure 4.4: S-N curves of fully reversed torsion tests fitted with Basquin regression model.

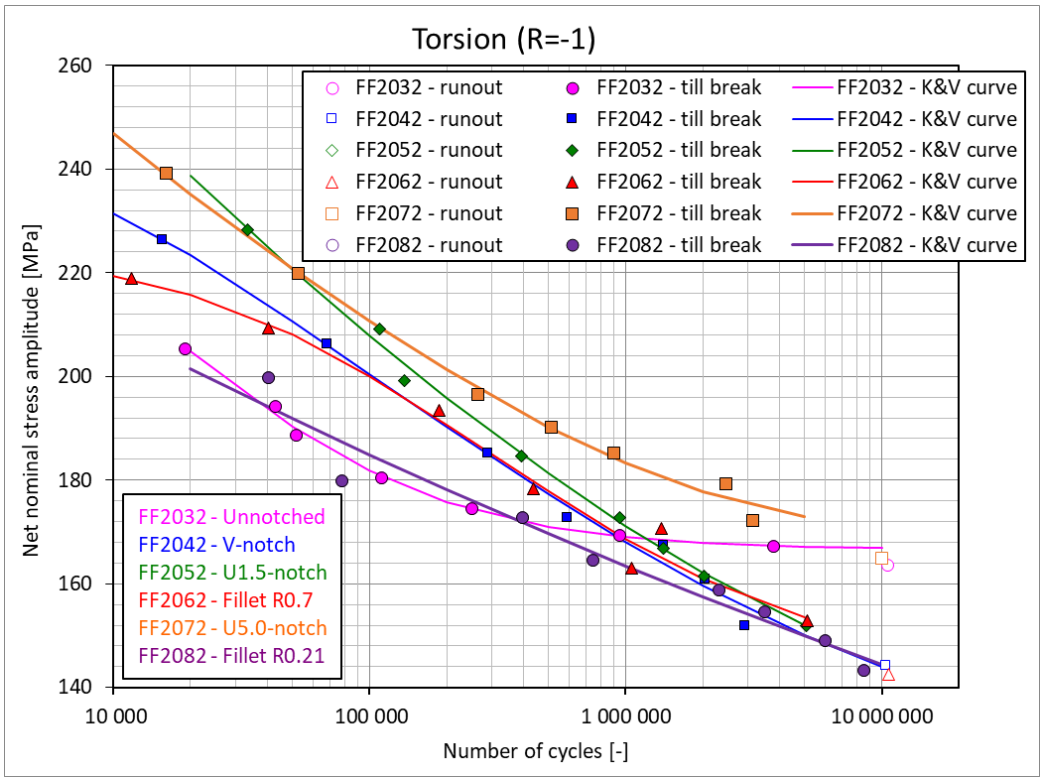

Figure 4.3: S-N curves of fully reversed torsion tests fitted with K-V regression model.

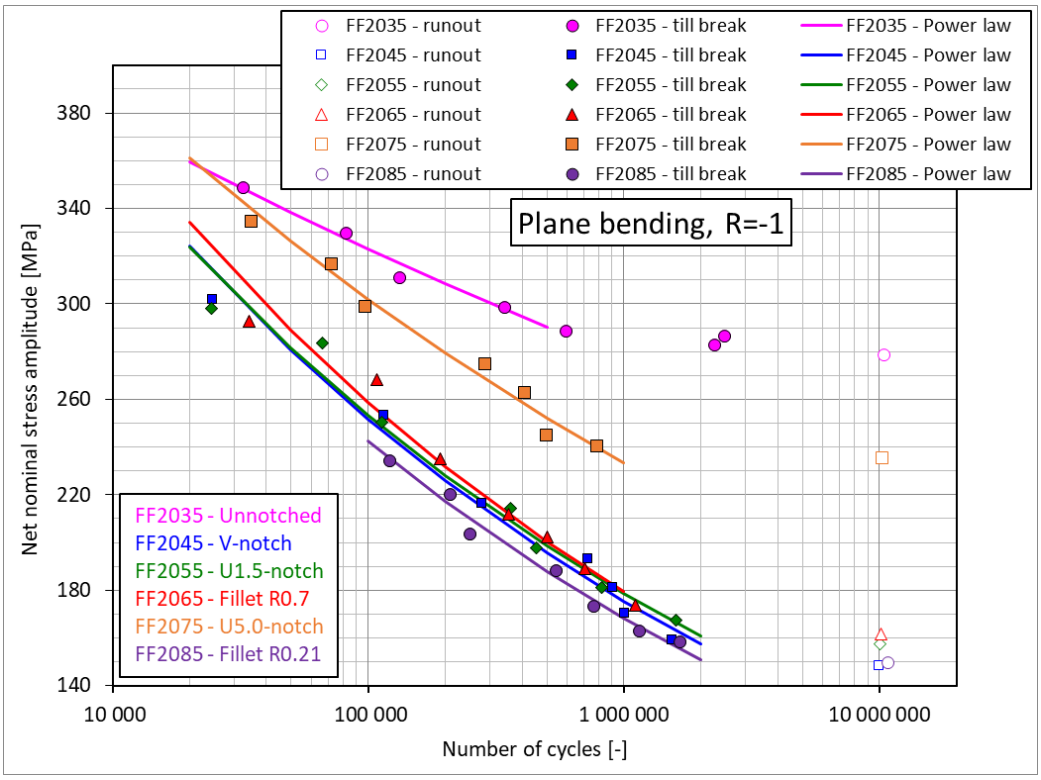

Figure 4.5: S-N curves of fully reversed plane bending tests fitted with Basquin regression model.

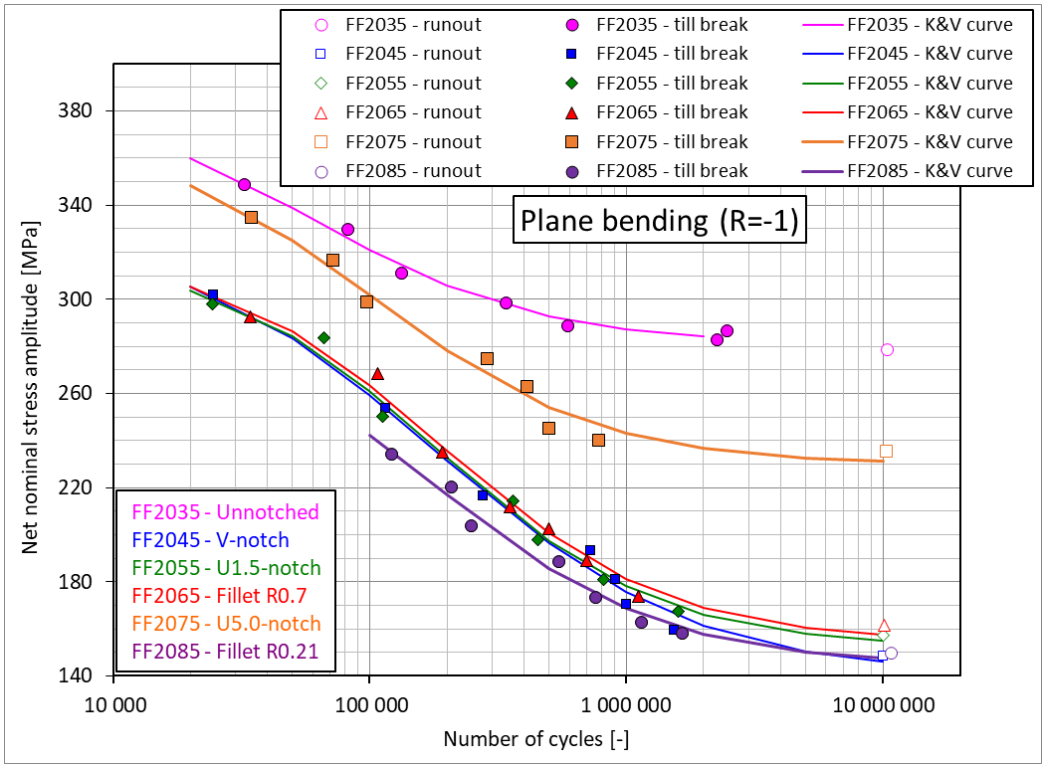

Figure 4.6: S-N curves of fully reversed plane bending tests fitted with K-V regression model.

The S-N plots reported above showed that not all experimental points can be fitted by a power law model without qualitative compromises. This is the reason why all the runout points and some break points, e.g. the ones standing in the transition region to the fatigue limit, were not included in the Basquin regressions. Such points are clearly out of the linear trend that the Wöhler curve would exhibit if plotted in a log-log diagram. On the contrary, the K-V regression can include a wider set of data which involves also the outermost points, which define the Wöhler knee: this fitting model clearly results in a more realistic and extended representation of the typical S-shaped S-N curve, demonstrating that the K-V fit is a valid alternative to the more traditional Basquin fit. The reason why both models are anyway presented is because the power law model is still widely used when assessing fatigue, while the K-V function is a less common model for this purpose [22].

5 IMPLEMENTATION OF CRITICAL VOLUME APPROACH

In order to address the influence of critical volume on the fatigue behaviour of the investigated material, dependencies between fatigue strength and critical volume (which possible existence was highlighted in previous work by Fojtík and Papuga [17], described in Section 2.5) have been sought. At first, a preliminary study based on the application of the simple Manson-McKnight fatigue criterion was conducted. Later, a more sophisticated procedure which includes the Dang Van multiaxial fatigue strength criterion was implemented.

Introducing the evaluation of critical volume in the fatigue assessment, it is evident that the problem acquires three degrees of freedom:

1. fatigue strength, for instance expressed in terms of net nominal stress amplitude ($\sigma_{a,net}$);
2. fatigue life, thus number of cycles to failure (N_f);
3. critical volume (CV).

To evaluate these dependencies in a two axes graph, where such axes refer to fatigue strength and critical volume respectively, the value of fatigue life N_f must be fixed (as it was done in [17]). Constant-life cuts of S-N curves of all specimens tested under the three types of loading were carried out, as illustrated in Figures 5.1 – 5.3: these graphs report net nominal stress amplitude vs. fatigue life curves, fitted with K-V regression model (since it better fits experimental points). It can be observed that the best confidence with experimental data is found in the HCF region, especially in the interval:

$$10^5 \leq N_f \leq 10^6 \tag{5.1}$$

where experimental points are gathering more. The value $N_f = 5 \cdot 10^5$ was fixed for further calculations involving the critical volume.

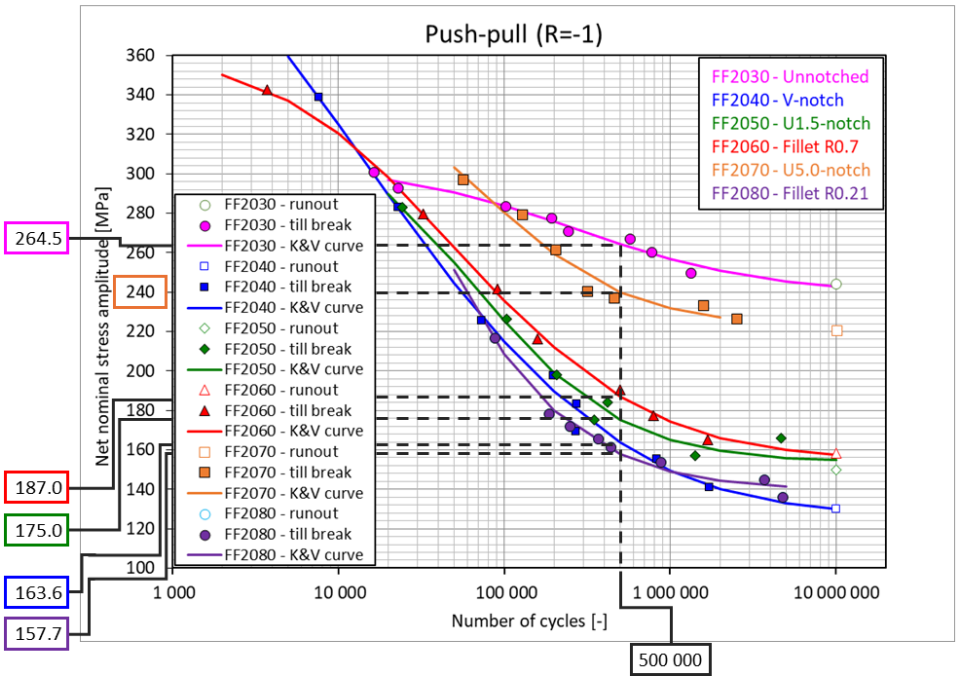

Figure 5.1: Net nominal stress amplitudes in fully reversed push-pull at $N_f = 5 \cdot 10^5$.

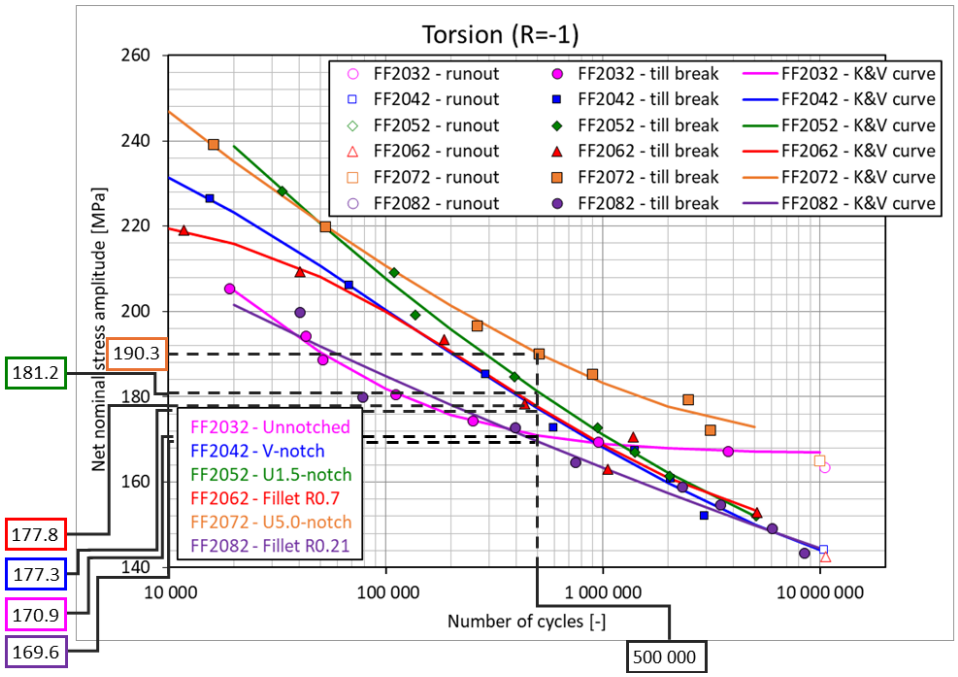

Figure 5.2: Net nominal stress amplitudes in fully reversed torsion at $N_f = 5 \cdot 10^5$

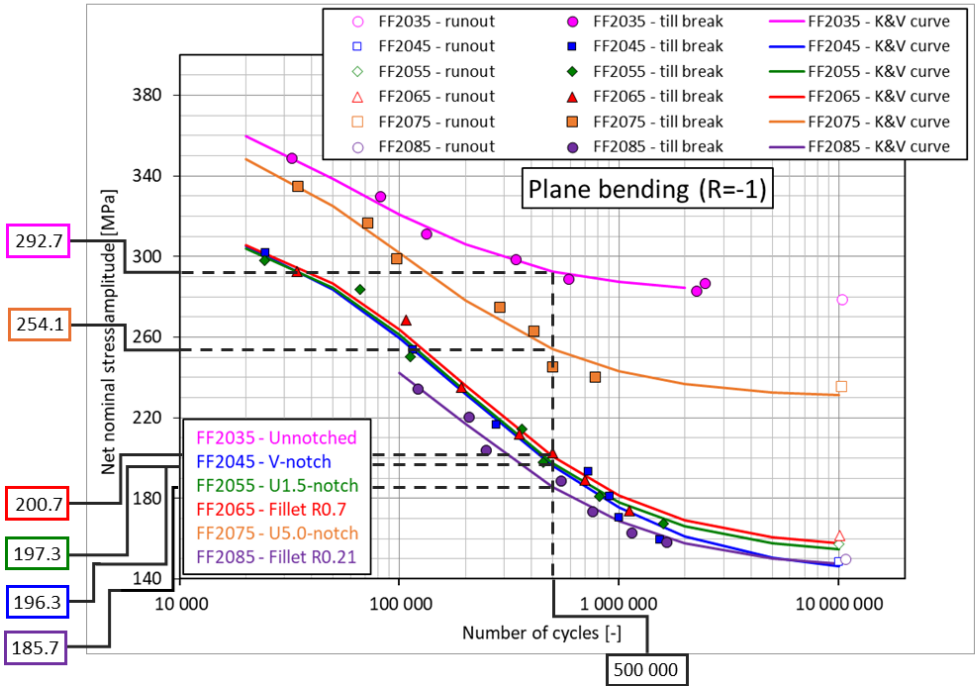

Figure 5.3: Net nominal stress amplitudes in fully reversed plane bending at $N = 5 \cdot 10^5$

5.1 PRELIMINARY STUDY USING MMK CRITERION

5.1.1 Remark on the equivalence between MMK and von Mises criteria

As previously mentioned, MMK criterion is a uniaxial fatigue strength criterion derived directly from the classic von Mises criterion, which is widely used when assessing static loads. For the sake of clarity, it is important to point out that when there is no effect of mean stress, like in the current case (load ratio is $R = -1$), the equivalent stress amplitude formulation proposed by MMK is totally equivalent to the von Mises one. This is easily demonstrable looking at equations 2.16 and 2.17, which can be readapted into:

$$\sigma_{i,m} = 0 \tag{5.2}$$

$$\tau_{ij,m} = 0 \tag{5.3}$$

for $i,j = x,y,z$. So, the equivalent mean stress value according to MMK criterion results to be:

$$\sigma_m^* = 0 \tag{5.4}$$

Moreover, the stress amplitudes along all directions are equal to the corresponding maximum values of stress state components:

$$\sigma_{i,a} = \max_t \sigma_i = \left|\min_t \sigma_i\right| \tag{5.5}$$

$$\tau_{i,a} = \max_t \tau_i = \left|\min_t \tau_i\right| \tag{5.6}$$

for $i = x,y,z$. Hence, the equivalent stress amplitude formula becomes known as the classic von Mises formulation:

$$\sigma_a = \sqrt{\frac{1}{2}\left[\left(\sigma_x - \sigma_y\right)^2 + \left(\sigma_y - \sigma_z\right)^2 + (\sigma_z - \sigma_x)^2 + 6\left(\tau_{xy}^2 + \tau_{yz}^2 + \tau_{zx}^2\right)\right]} \tag{5.7}$$

In the end, processing the stress tensor with MMK or von Mises does not make any difference for the reason above: thus, the two criteria can be confused with each other without doing any mistake. It is worth opening a bracket about how the equivalent von Mises stresses were calculated. As any commercial FE software, Abaqus can provide in the analysis results the values of von Mises stresses, that can also be visualized with the coloured map in the results visualization environment. But in this context, computation of von Mises equivalent stresses (needed to calculate the elastic peak at the root of the notch and the related critical volume within the material) was performed by the Python script developed in this work. The code reads the not averaged nodal stress components from the mesh, averages them and processes them obtaining the equivalent stress value at the considered node. It can be anticipated that when the code evolves into the new version with Dang Van incorporated, the same operations are performed again through the script.

5.1.2 Notch fatigue strengths

Processing the results of FE analyses with von Mises criterion allowed:

- to calculate the net nominal stress concentration factors (K_{t_Mises}), already reported in Table 3.5 in Section 3.2 for what concerns involving the equivalent von Mises stress;
- to calculate the elastic peak stress amplitudes at the root of the notch for each specimen.

In particular, elastic peak stress amplitude at the notch tip was obtained multiplying the net nominal stress amplitude of each specimen read from the S-N curves (as illustrated in Figure 5.1 to Figure 5.3) by the corresponding K_{t_Mises} factor. According to the nomenclature adopted in the reference paper [17], these elastic peak stress amplitudes are called “component fatigue strengths”, but, henceforth in the present work, they will be referred to as notch fatigue strengths (i.e. expressed as elastic peak stress amplitudes). The latter name better emphasises the fact that the fatigue strength of the mechanical notched component is governed by the elastic peak stress amplitude at the root of the notch (and the relative critical volume beneath it). Notch fatigue strengths calculated with the MMK criterion are reported in Table 5.1 below.

Specimen	Load	Mark	Notch fatigue strength [MPa]
Unnotched	Push-pull	FF2030	264.5
	Torsion	FF2032	170.9
	Plane bending	FF2035	292.7
V-notch R1.3	Push-pull	FF2040	325.6
	Torsion	FF2042	254.2
	Plane bending	FF2045	321.3
U-notch R1.5	Push-pull	FF2050	330.0
	Torsion	FF2052	252.0
	Plane bending	FF2055	307.4
Fillet R0.7	Push-pull	FF2060	391.9
	Torsion	FF2062	263.2
	Plane bending	FF2065	362.5
U-notch R5	Push-pull	FF2070	312.9
	Torsion	FF2072	217.0
	Plane bending	FF2075	298.9
Fillet R0.2	Push-pull	FF2080	526.5
	Torsion	FF2082	348.5
	Plane bending	FF2085	513.3

Table 5.1: Notch fatigue strengths evaluated with MMK criterion for all specimen series.

A quick observation can be made looking at the notch fatigue strengths reported in Table 5.1. Relying on the MMK criterion (or one the von Mises one, it makes no difference), no one of these stress amplitudes exceed the material yield strength ($\mathrm{R_e} = 401\ \mathrm{MPa}$), except for two cases which are series FF2080 and FF2085 that refer to push-pull loading and plane bending loading of the Fillet R0.2 specimen, respectively.

5.1.3 Critical volume calculation

Once the equivalent stresses are obtained, critical volumes can be calculated if the value of parameter z is also fixed. Actually, one of the objectives of the current analysis is to find the value of z which allows to obtain the best fitting law between notch fatigue strength and critical volume. This means that z acts like a fitting parameter that needs to be optimized. Therefore, since its value is unknown, a wide discrete set of values was considered for the analysis:

$$z \in \{0.50, 0.55, 0.60, 0.65, 0.70, 0.75, 0.80, 0.85, 0.90, 0.95, 0.99\} \tag{5.8}$$

Critical volumes of all series of specimens were evaluated adopting the procedure described in Section 3.3, which was implemented in the Python script reported in Appendix 9.3. Values of critical volume evaluated at the different z values listed above are reported in Table 9.3 in Appendix 9.4.

5.1.4 Notch fatigue strength vs. critical volume

From previous discussion, it is known that the purpose of the critical volume approach is to define the notch fatigue strength vs. critical volume dependencies in axial and torsion load cases, in order to use them for evaluating the fully reversed axial and torsion fatigue strengths, f_{-1} and t_{-1} respectively, which depend on the evaluated magnitude of critical volume. These fatigue strengths are required to calculate the material parameters (generally referred to as a and b), which are given as input to the multiaxial fatigue strength criterion. MMK solution does not represent a typical multiaxial fatigue criterion. Thus, the aim of this first analysis is just to enhance the existence of the sought-after dependencies and make some considerations about them.

It is interesting to study how the experimental data lie on the notch fatigue strength vs. critical volume graphs and if they generate appreciable curves to be fitted later or not. The various plots, obtained for different z parameter, are observed in search of the optimum value of such a parameter which guarantees the best alignment of points along a possible fitting curve. Notch fatigue strengths evaluated at the given lifetime of $N_f = 5 \cdot 10^5$ (Table 5.1) were combined with the calculated critical volumes. Even if [17] adopted a “critical volume vs. component fatigue strength” graphical representation, as described in Section 2.5, in the present work the order of axes has been inverted. From now, all graphs represent the “notch fatigue strength vs. critical volume“ representation, which turns out to be more logic for the purpose of the study. Indeed, the objective is to evaluate the critical volume of a notched component because its value (input of the dependency) affects the fatigue strength of the component at the given lifetime N_f (output of the dependency). Logarithmic scale is adopted for the horizontal axis, since the critical volumes cover several orders of magnitude (varying from few decimal points to thousands of mm^3), while fatigue strengths are in a much smaller range.

At first, the relationship between notch fatigue strength and critical volume under axial loading of the specimens was observed: related graphs are illustrated in pictures grouped in Figure 5.4. Data from fully reversed push-pull and fully reversed plane bending tests were involved, since these loading modes induce normal stresses in the material along the specimen axis. An additional reason why these loading modes are studied together is because push-pull and plane bending fatigue loads are supposed to cause the same type of crack initiation. Some interesting observations, which can be made observing the graphs and scrolling them through the different values of z parameter, are reported hereafter.

- A general decreasing trend is found over all the graphs, whereby the fatigue strength diminishes with the critical volume. This is reasonable because it is in accordance with the principle of size effect, which states that the larger the highly stressed volume (i.e. critical volume), the more likely the crack initiation: therefore, a specimen with a large critical volume will withstand a lower axial fatigue strength (for a constant fatigue life).

- Moreover, plots show that the two series of points (the blue one referring to data from push-pull tests and the orange one referring to data from the plane bending tests) seem to reach a horizontal plateau for large critical volume entities, and thus small values of notch fatigue strength. The existence of such a horizontal asymptote is found out to be rational, again on the basis of the size effect which governs the experimental reality. Over a certain dimension of critical volume, its size can no longer influence the component fatigue strength causing it to diminish more and more. For instance, consider an axisymmetric unnotched specimen tested under push-pull loading: this scenario is characterized by a large value of critical volume (the rightmost point in the considered diagrams). Increasing its diameter, critical

volume will surely increase and fatigue strength decrease. But at a certain point the statistical size effect would reach a kind of saturation. Indeed, fatigue strength will stabilize around a minimum value rather than continuing to decrease until reaching zero for huge critical volume dimensions: a scenario like this would not make any sense from the physical point of view.

- However, it is not straightforward to imagine the shape of the possible curve that would fit such points, at least according to the available experimental data. Starting from the end, the $z = 0.99$ graph presents two series of points which seem to create two separate, clearly delineated curves: this makes difficult (practically impossible) to fit all these points with a single law in an acceptable manner, which means with a reduced scatter around the fitting curve.

- Switching to lower values of parameter z, experimental points are arranged in a different way. The good point is that the two data series start crossing and overlapping each other, but only for small values of notch fatigue strength and thus large values of critical volume. In general, the situation seems to be more chaotic, especially for the very lowest z values, with the dots that do not follow a smooth trend as seen before. But on the other hand, the two series got closer to each other than before, so it should result easier to fit them with a single curve.

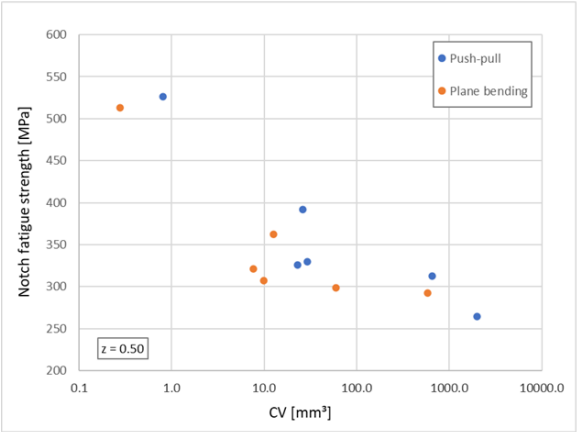

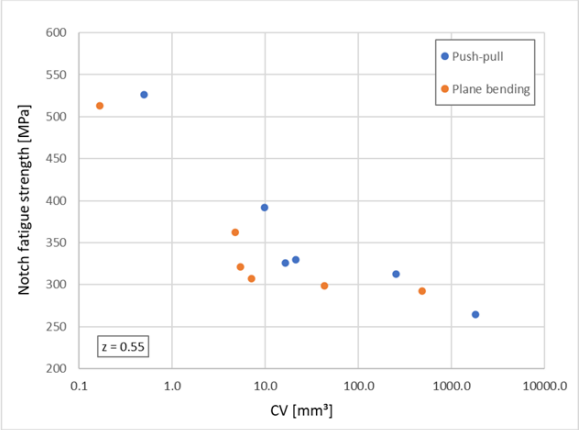

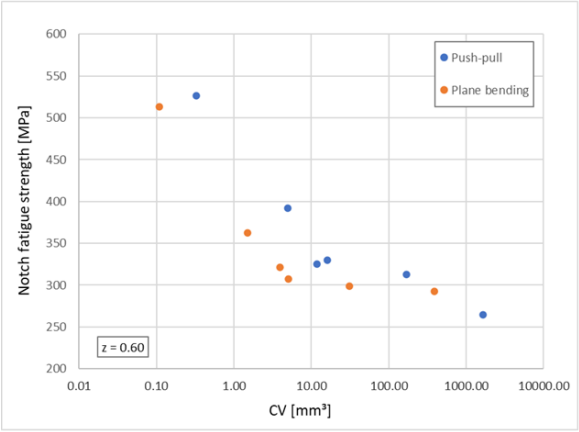

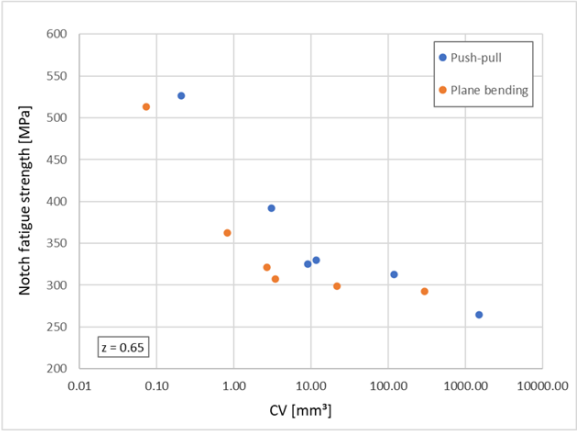

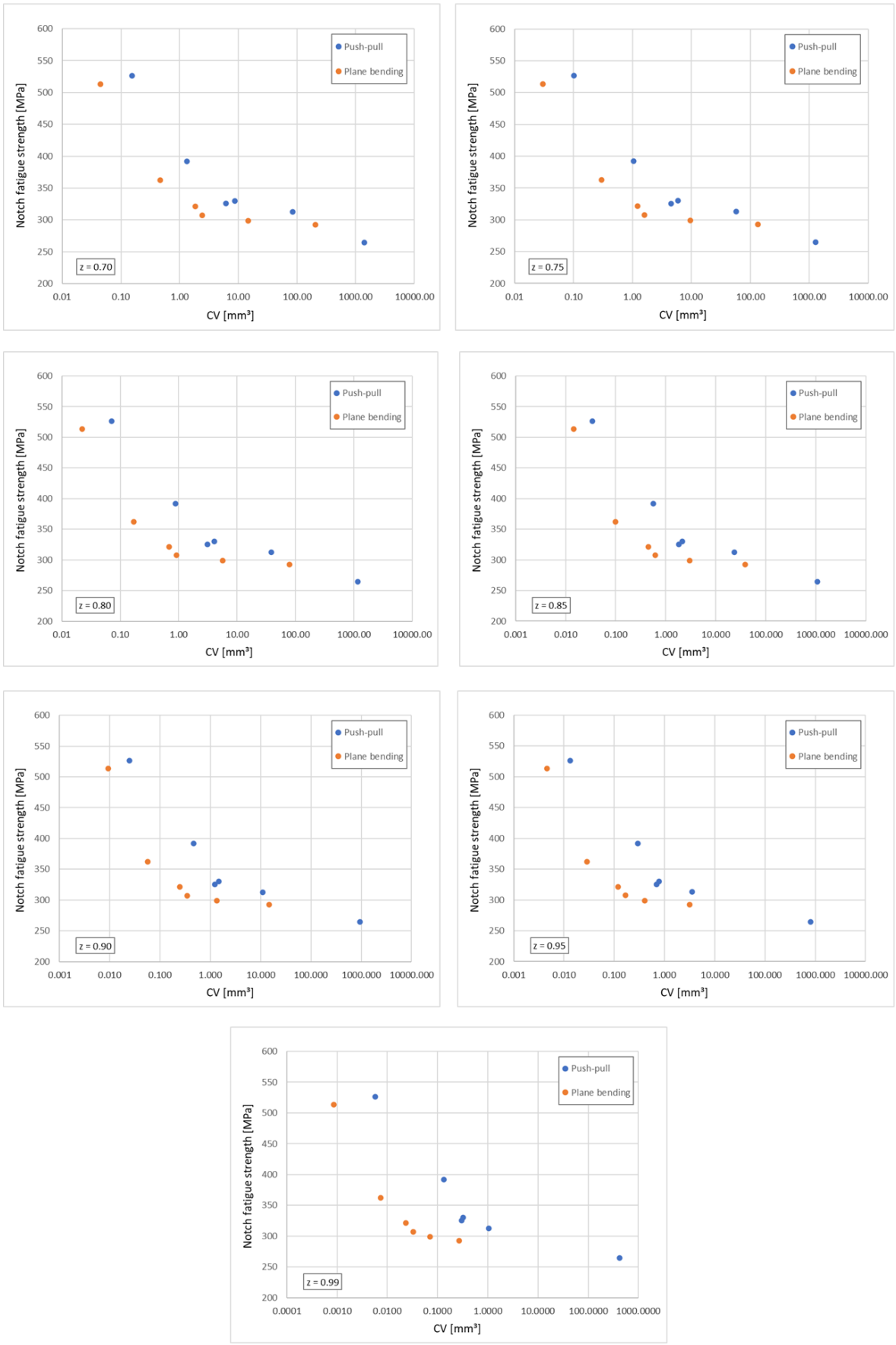

Figure 5.4: Diagrams of Notch fatigue strength vs. Critical volume dependencies evaluated for different z values, referring to axial loading (R=-1) and fatigue life of $N_f = 5 \cdot 10^5$.

Subsequently, the relationship between notch fatigue strength and critical volume under torsion loading condition was investigated, considering data available only from the fully reversed torsion tests: relative graphs are grouped in Figure 5.5. Also in this case, points distribution reflects the expected behaviour, in accordance with the size effect. They lie along a monotonic descending curve showing a low scatter, which, however, seems to increase a bit for the lowest z values due to one point starting to misbehave. No more other particular observations emerge from these diagrams, a part the fact that it is immediate to understand that data can be easily fitted with a power law.

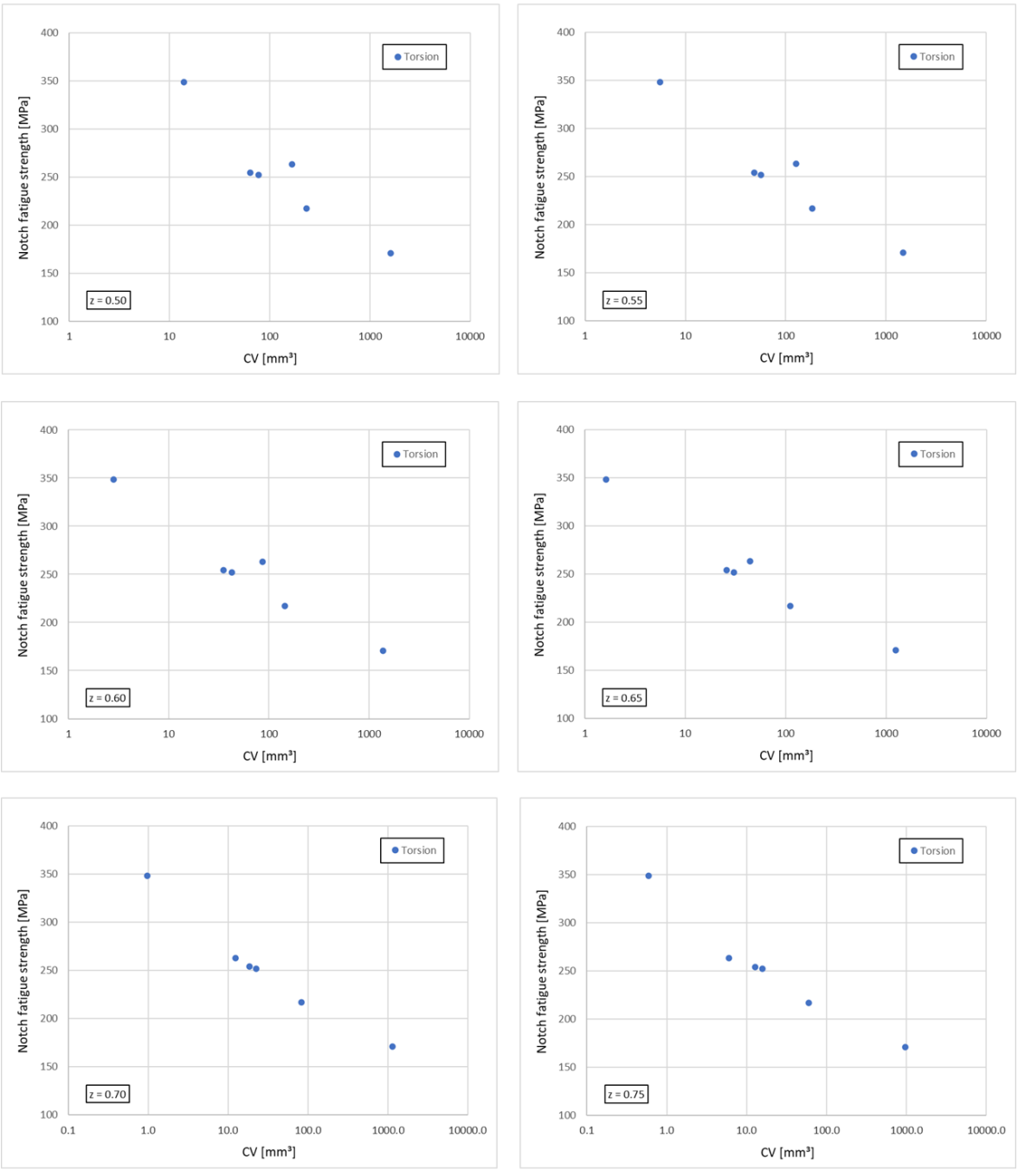

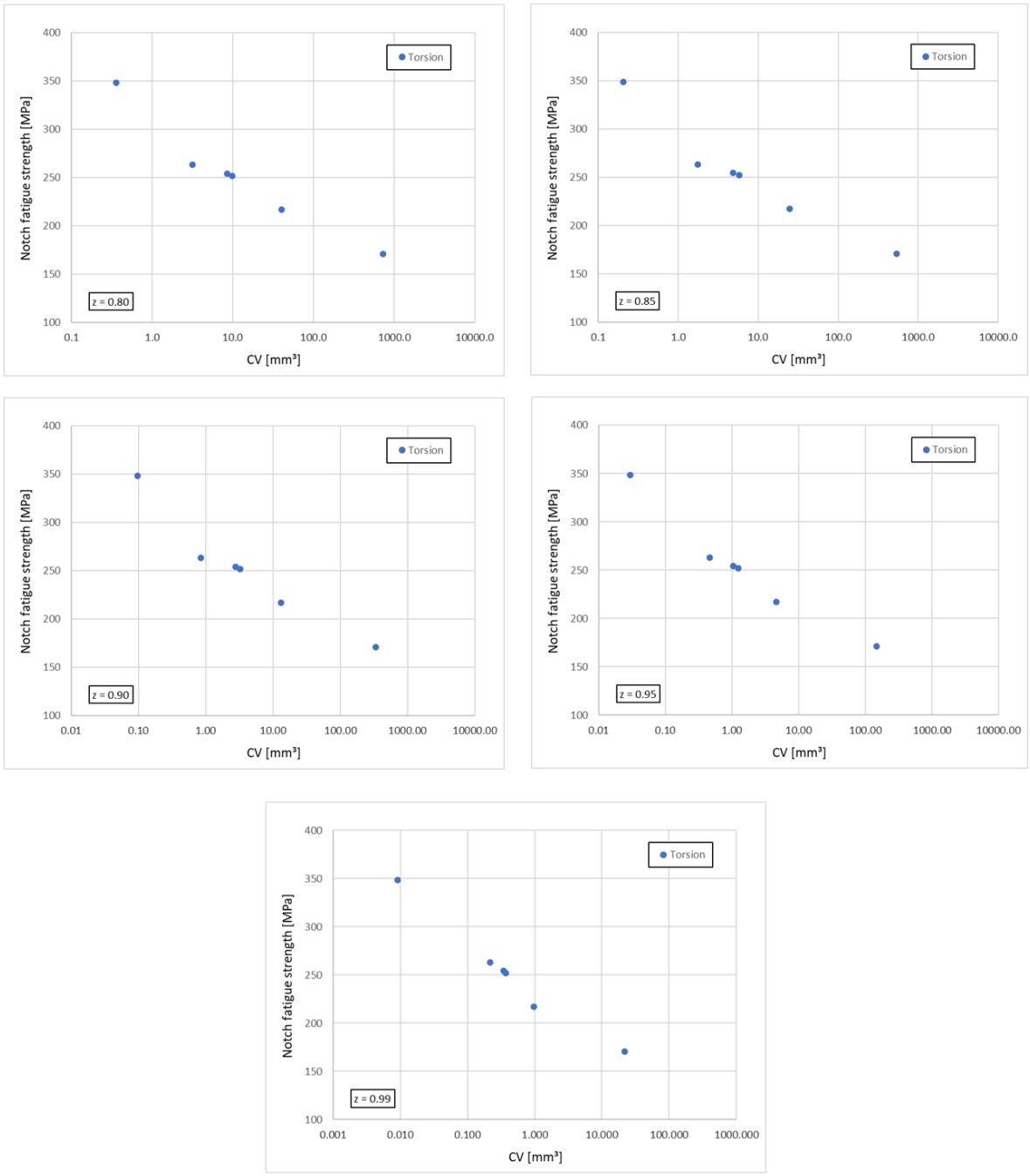

Figure 5.5: Diagrams of Notch fatigue strength vs. Critical volume dependencies evaluated for different z values, referring to torsion loading (R=-1) and fatigue life of $N_f = 5 \cdot 10^5$.

In order to evaluate the goodness of such dependencies and to find the optimum z, the experimental data were fitted. In fatigue it is quite common to deal with power laws, so the first idea was to try to fit the points with the Basquin regression (as was done in [17]). Furthermore, concerning the axial load case, the non-linear K-V regression was also considered as a viable option at the beginning. The idea came from the fact that, if it is assumed that there is a horizontal asymptote for very large critical volumes, the equation of a non-linear model (like the K-V one) could capture the “knee” of the curve. As a consequence, same Excel macros already used for computing regression of S-N curves were adopted for fitting the dependencies, for convenience. At first, the best fit according to both power law and K-V model was obtained for $z = 0.55$, so further decision was to investigate the neighbouring z values. In the end, the best fit was confirmed for $z = 0.56$. Regression curves obtained with both models are illustrated in Figure 5.6 with respect to the mentioned best-fit condition.

Coefficients of determination and RMSE values are also reported in the graph, while regression parameters used to fit those functions are collected in Tables 9.4 and 9.5 in Appendix 9.4.

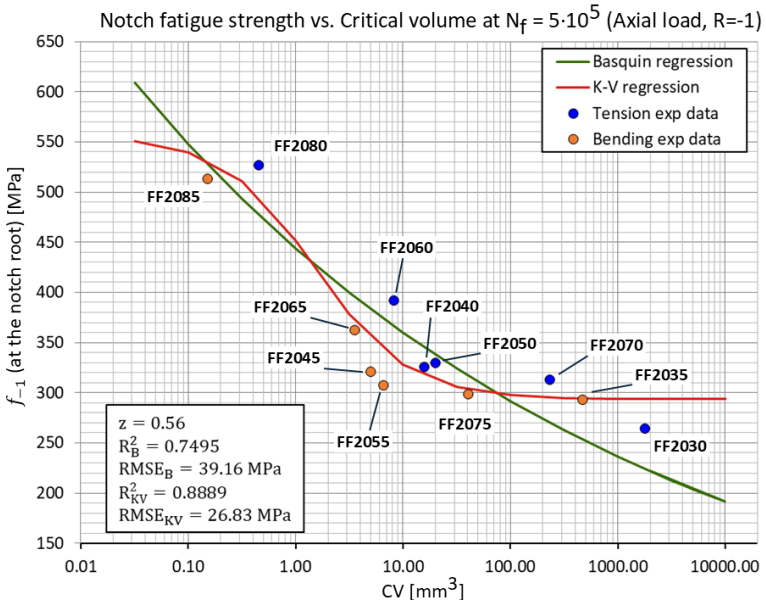

Figure 5.6: Notch fatigue strength vs. Critical volume dependency for axial load case, fitted with both power law model (green) and K-V model (red).

Looking at Figure 5.6, a considerable dispersion of experimental points can be observed: if this scatter were not present, even the simple power law model would have been sufficient to capture the data trend well. One more hypothesis was discussed in this phase, and concerned the way how the bending load is transferred to the specimen. As explained in Paragraph 3.1.2, every sample under plane bending load can be schematized as a cantilever beam fixed at one end which is flexed by a shear force applied to the other free end. Specimens are certainly not considerable as slender beams: it is known from the continuum mechanics theory that shear deformability cannot be neglected in these cases. Therefore, it is curious to wonder whether this might have an influence in some way on the scattering problem, or not, especially with regard to the fact that the experimental plane bending data were considered as representative of a fully axial loading mode. In the subsequent phase, involving the implementation of the multiaxial fatigue strength criterion, an attempt was made to solve this scattering problem, based on the fact that the multiaxial criterion could better assess the effect of the critical volume also in this case of axial fatigue loading through plane bending.

Meanwhile, concerning the torsion case things went smoothly as expected. Monitoring values of coefficient of determination for each power law regression associated to a specific value of z, the best fit was found for $z = 0.70$. Regression curve obtained with power law model is illustrated in Figure 5.7 with respect to the best-fit condition. Coefficient of determination and RMSE value are also reported in the figure, while regression parameters related to the fitting function are reported in Table 9.6 in Appendix 9.4.

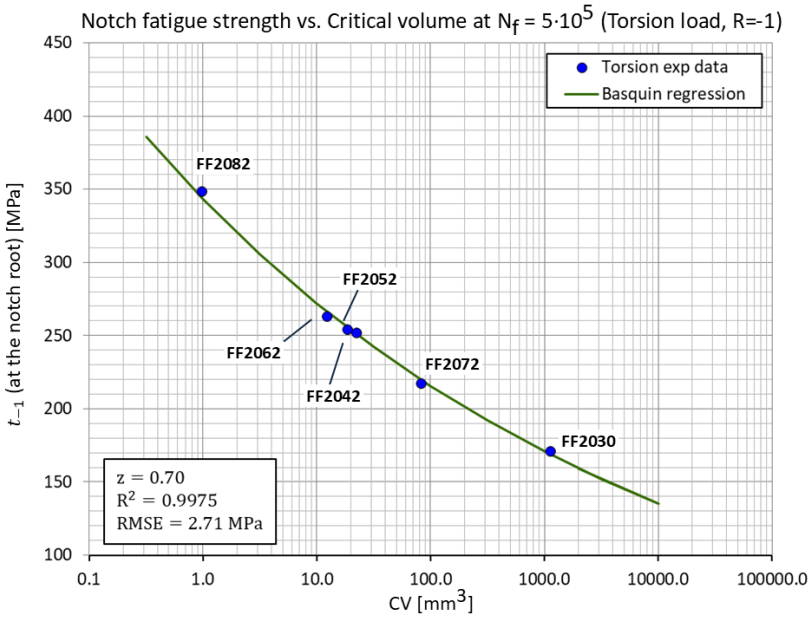

Figure 5.7: Notch fatigue strength vs. Critical volume dependency for torsion load case, fitted with power law model.

A few additional comments can be made about these outcomes regarding the fitted dependencies. Though the optimum z parameter found for torsion case is partially in line with expectations, since it assumes a quite high value, the same parameter related to the axial load case assumes an exceptionally low value. Low levels of z parameter were investigated (see the range reported in 5.8) because the hypothesis was that larger critical volumes could better assess the fatigue damage of a very ductile steel alloy like the one studied here. Indeed, it is well known that ductile materials typically show a deeper fatigue process zone under the notch than in case of fragile materials, due to the plasticity effects that blunt the elastic peak stress at the notch. However, this foresight seems to have helped at bit fitting the dependency but not in a very good way, because the $z = 0.56$ is extremely low, and nevertheless data scattering is still evident. Moreover, another issue is quite noticeable: if the relationship between notch fatigue strength and critical volume were working perfectly, in both cases of axial and torsion loading, the same optimum z parameter would come out from the analysis. In this way, the engineer would use that z value for assessing the critical volume calculation and using the two dependencies calibrated on the same z. These considerations are echoed in the next Section 5.2 and resumed later in final Section 5.3.

5.2 STUDY USING THE DANG VAN CRITERION

Since the aim of this work is to implement the critical volume approach for the evaluation of the multiaxial fatigue problem, the study proceeded with the application of this approach to the Dang Van criterion. Relevant information on the family of critical plane-based criteria to which Dang Van belongs and on the criterion itself has already been reported in Sections 2.2 and 2.3, respectively. The choice fell on Dang Van criterion because it represents one of the most popular and widely used solutions for assessing multiaxial fatigue of mechanical components, for what concerns both research papers and commercial applications. Therefore, it was selected as a proper tool to start working on the critical volume approach implementation in multiaxial fatigue strength criteria. It is important to remember that the type of multiaxial loading studied here is classified as proportional loading (also known as in-phase loading). Hence, the discussion on how to deal with multiaxial fatigue of engineering materials enters more into the heart of the problem: the challenge is to understand how the selected criterion can be modified and adapted to assess the critical volume, in order to make the criterion capable of considering both size and stress gradient effects, thus providing more accurate fatigue strength estimates.

To use the multiaxial fatigue strength criterion, it is necessary to calculate its material parameters which depend on fully reversed fatigue strengths in axial (f_{-1}) and torsion load cases (t_{-1}), as already expressed in equations 2.23 and 2.24. Instead of taking these fatigue strengths from the respective plain S-N curves as usual, the idea here introduced is to find them using the notch fatigue strength vs. critical volume dependencies. So, a calibration procedure of Dang Van criterion must be performed in order to find the dependencies for both loading cases, which will be expressed by some kind of formulations like $f_{-1} = f_{-1}(CV)$ and $t_{-1} = t_{-1}(CV)$. Once the criterion calibration is completed, the two calibrated dependencies are ready to use. As it was conceptualized in the work by Fojtík and Papuga [17] (reviewed in Section 2.5), the user would give as input to these two functions the value of critical volume experienced by the notched component he/she is designing. Thus, the output would be the f_{-1} and t_{-1} to be used to calculate the updated material parameters a_{DV} and b_{DV}, needed for the multiaxial fatigue strength analysis. Once Dang Van criterion has been applied to the FE model, values of equivalent stress amplitude for the given fatigue life (N_f) are available. Scheme reported in Figure 5.8 resumes the critical volume approach workflow explained few lines above.

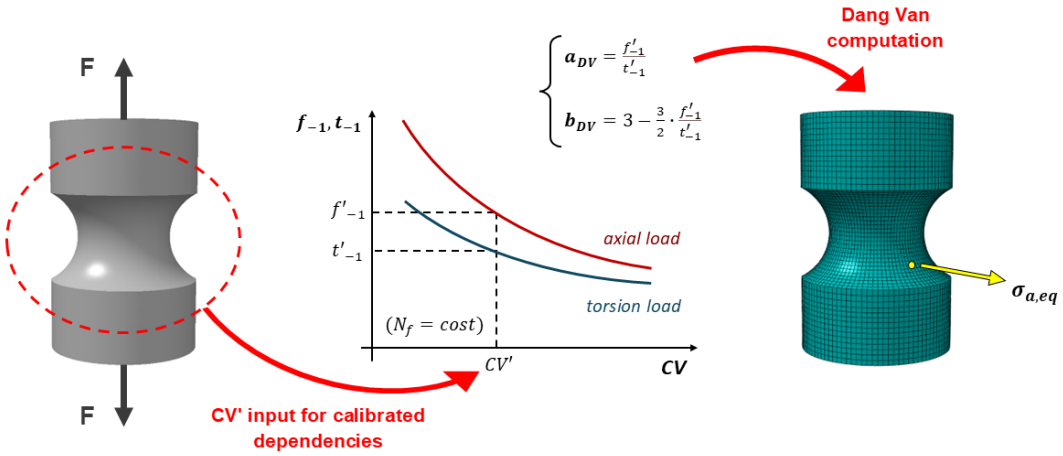

Figure 5.8: How the multiaxial fatigue strength criterion (i.e. Dang Van) should be used in conjunction with the critical volume approach.

It is worth noting the existence of a blind spot of the whole idea illustrated until this point, which is related to the constant number of cycles to failure that was considered. As declared at the beginning of Chapter 5, the decision of keeping the fatigue life at $5 \cdot 10^5$ cycles raised from the necessity to fix one degree of freedom in order to start with the critical volume analysis.

Concerning the current analysis, critical volumes and notch fatigue strengths were calculated again using the Python code, which was adapted to this new level of the analysis which involves Dang Van multiaxial criterion. In particular, the more modern version of Dang Van formulation was applied in this context (refer to equation 2.26): it was implemented in the Python script using the Fatigue Prediction Utility (FPU2019), which development and functioning is detailed in [26].

5.2.1 Iterative procedure of calibration

Dealing with the calibration of Dang Van criterion, an issue arises. To calculate the sought-after dependencies, it is necessary to process numerical results from the FE analysis of each specimen series in order to compute the critical volume. But the calculation of this quantity requires the use of a functional criterion that allows to compute equivalent stress amplitudes at every node of the mesh: this tool is clearly still not available, since the criterion's material parameters have not yet been updated according to the critical volume approach. The direct solution for this closed loop problem is the implementation of an iterative procedure, described by following the block sequence reported hereafter.

1. Initial conditions. First, initial conditions must be fixed in order to have a starting point for the iterative procedure. Thus, Dang Van criterion is applied in its basic version where the material parameters are computed with equations 2.23 and 2.24, referring to the fully reversed plain fatigue strengths f_{-1} and t_{-1}, obtained from the corresponding Unnotched S-N curves (refer to Figures 5.1 and 5.2, respectively). Then, the equivalent stress amplitudes (that have been derived from the criterion) are used to calculate the first attempt critical volumes (CV_0) for every specimen series (6 geometries and 3 testing loads, for a total of 18 critical volumes). Since the optimum value of z parameter is still unknown (analogously to what was seen in the preliminary study with MMK criterion), critical volume computation must be repeated for all the investigated values of z contained in the following range:

$$z = \{0.50,\ 0.525,\ 0.55,\ 0.575,\ 0.60,\ 0.625,\ 0.65,\ 0.675,\ 0.70,\ 0.725,\ 0.75,\ 0.775,\ 0.80,\ 0.825,\ 0.85,\ 0.875,\ 0.90,\ 0.925,\ 0.95,\ 0.975,\ 0.99\} \tag{5.9}$$

   It is also possible to compute the new stress concentration factors according to Dang Van (K_{t_DV}), which allow to derive the notch fatigue strengths (thanks multiplying K_{t_DV} factors by the net nominal fatigue strengths). Thus, raw dependencies between notch fatigue strength and critical volume are fitted for both axial and torsion load cases, for every z value considered in 5.9. It is important to point out that these dependencies are kept valid as they are till the end of the calibration: this means that the next steps will use them, so they are not updated at each iteration using with the new available values of critical volumes and elastic peak stress amplitudes at the notch. Therefore, such dependencies are fitted again only at the end of the procedure, as detailed later.

2. Iteration loop. At this point, the effective iterative calibration procedure can begin. It is fundamental to start with fixing one value of z parameter and considering the two related dependencies, fitted at the previous stage. Focusing on one specimen under a specific type of loading at a time, it is possible to enter in the functions $f_{-1} = f_{-1}(CV)$ and $t_{-1} = t_{-1}(CV)$ with the value of critical volume computed at the previous iteration and related to the considered series: as a result, new notch fatigue strengths are obtained from the dependencies, and the new material parameters can be calculated (again following the formulations 2.23 and 2.24). Running Dang Van criterion again with the new a_{DV} and b_{DV} that have been modified according to the observed value of CV, new equivalent fatigue strengths are computed over the whole specimen's mesh, and this allows to evaluate the new critical volumes. This procedure must be repeated for all specimen series, and of course

also for all values of z parameter. Scheme reported in Figure 5.9 remarks the need of calculating notch fatigue strengths and relative material parameters for every specimen series.

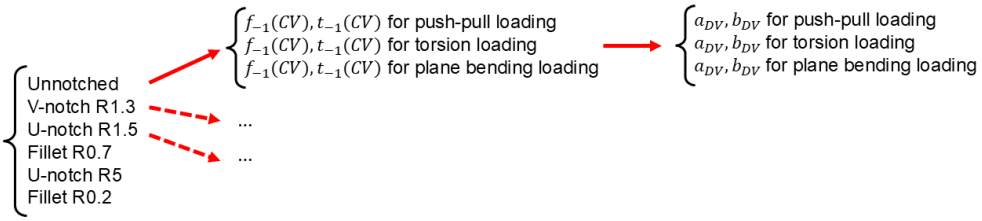

Figure 5.9: Scheme illustrating how the calculation of material parameters for Dang Van criterion splits across the various specimen series when critical volume is involved.

This second block called “Iteration loop” is repeated as many times as necessary to the iterative calibration procedure for reaching a convergence. The condition of convergence is verified on the critical volume for all specimens. At the end of each iteration the relative percentage error between the critical volume computed at the current i^{th} iteration (CV_i) and the volume computed at the previous one (CV_{i-1}) is checked:

$$\frac{CV_i - CV_{i-1}}{CV_{i-1}} \cdot 100 \leq error\ [\%] \tag{5.10}$$

No specific value of the error was set a priori. The objective of the procedure is to reduce as much as possible the error on critical volume, reducing it gradually to few percentage points over all specimen series. If these errors result to be sufficiently small, the convergence is assumed to be reached and current values of critical volume are assumed to be the definitive one. Moreover, also stress concentration factors calculated at the current iteration ($K_{t\_DV,i}$) are deemed definitive. Otherwise, if errors are not small enough it means that at least another iteration is necessary, so the current block must be repeated.

3. Final fittings. The very final stage, once the convergence is reached, consists in collecting all the definitive values of fatigue strengths and critical volumes, in order to fit the final dependencies $f_{-1} = f_{-1}(CV)$ and $t_{-1} = t_{-1}(CV)$. Note that notch fatigue strengths are calculated as the product of the net nominal fatigue strengths at $5 \cdot 10^5$ cycles (from S-N curves in Figures 5.1 to 5.3) with the new values of stress concentration factors (K_{t_DV}) computed according to the Dang Van criterion. Once here, the calibrated version of Dang Van criterion can be used to assess the multiaxial fatigue analysis of any notched component made with the same material and withstanding the same load ratio. Multiaxial fatigue calculations are expected to be more accurate than other traditional methods since this new version of the criterion should properly address both stress gradient and size effects simultaneously, merging them into a single “critical volume effect”.

The iterative procedure, which has been schematized in the three blocks above, is illustrated in figure 5.10 below.

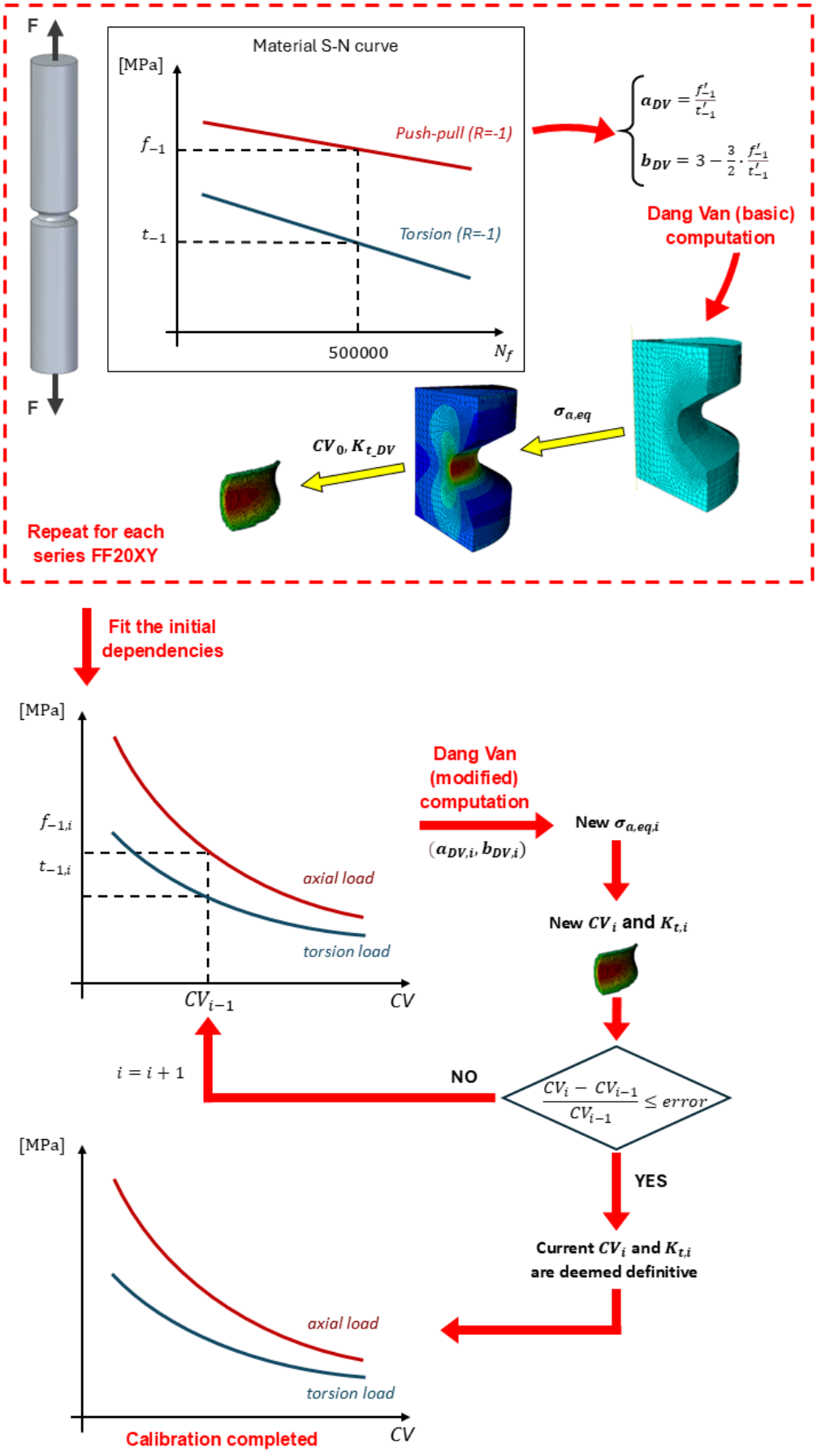

Figure 5.10: Procedure for calibrating Dang Van criterion in conjunction with the critical volume approach.

5.2.2 Notch fatigue strength vs. critical volume

Addressing the Dang Van calibration procedure, it is worth discussing some aspects related to the fitting of the dependencies, both the initial ones (necessary to start with the iterative loop) and the finals ones (which can be used to apply the criterion in its updated version which involves the critical volume). First of all, the idea of fitting experimental data with the non-linear K-V regression model was not pursued here, despite its application in the preliminary study. Main reason behind this choice was that some struggles and numerical issues were encountered while implementing this regression model in the Python code. In order to avoid possible compiler's warnings and wrong fittings of data, and also to streamline the process, the simpler power law regression model was adopted. Diagrams in Figure 5.11 present a couple of examples of initial data fits (referred to as "raw dependency" in the graphs) for axial loading mode. In particular, the two extreme cases of $z = 0.55$ and $z = 0.99$ are reported as examples of the dependency that relates critical volume to the notch fatigue strength in case of axial loading.

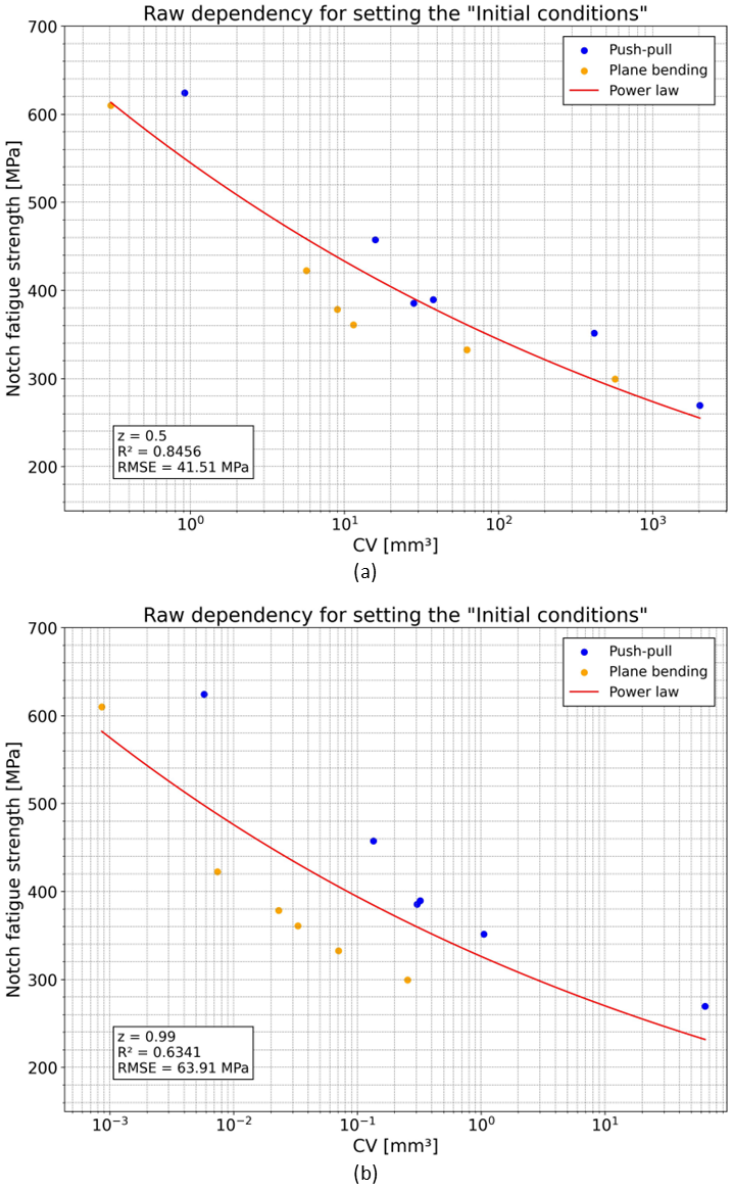

Figure 5.11: Notch fatigue strength vs. Critical volume dependencies for axial load case, fitted to fix the initial conditions for the Dang Van calibration procedure referring to parameters: (a) $z = 0.50$, (b) $z = 0.99$.

Typical decreasing trend of this kind of dependency can be appreciated. Similarly to previous results, for high values of z the two push-pull and plane bending series diverge, while they seem to get closer to each other when z decreases from the highest value to lower ones. As can easily be imagined, power law regression was also used for fitting the raw dependencies related to torsion load. Again, a couple of examples for different considered z values is reported in Figure 5.12: specifically, considering $z = 0.55$ and $z = 0.99$ for the sake of consistency with previous discussion on the axial load case.

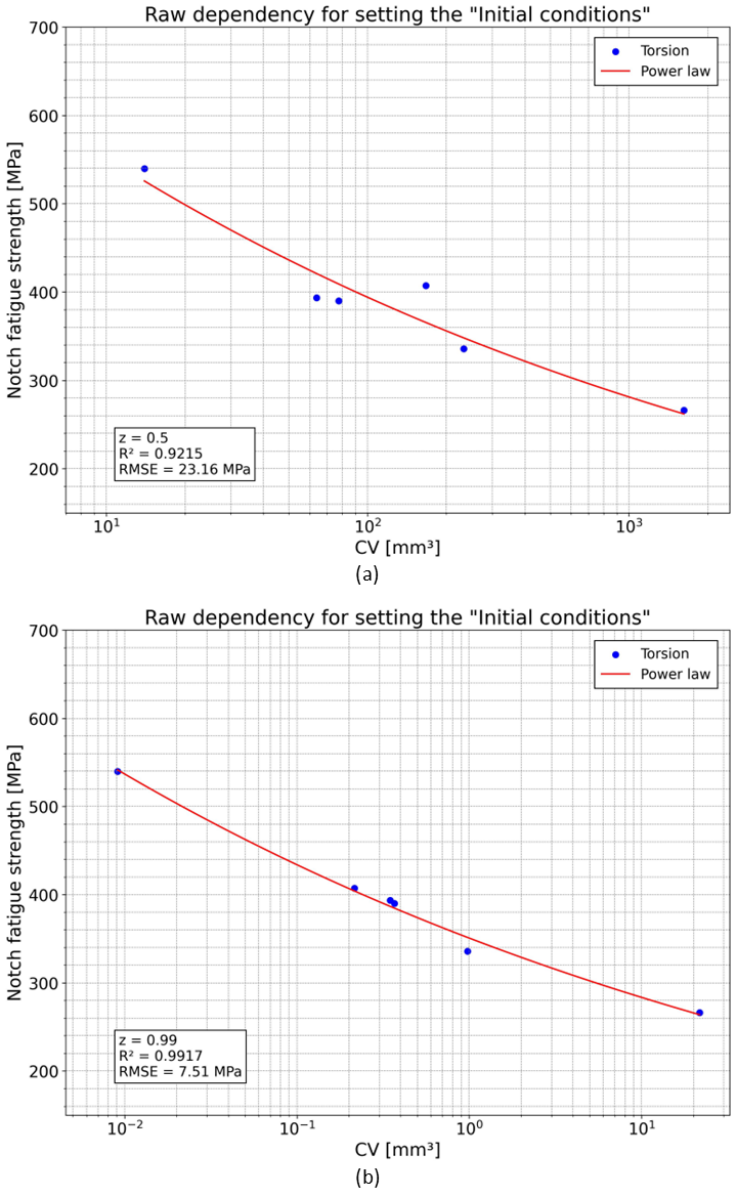

Figure 5.12: Notch fatigue strength vs. Critical volume dependencies for torsion load case, fitted to fix the initial conditions for the Dang Van calibration procedure referring to parameters: (a) $z = 0.50$, (b) $z = 0.99$.

Cases illustrated above refer to the very first raw dependencies calculated to fix the initial conditions for starting with the iterative calibration procedure. Once this calibration is completed (over all the several z values), it is possible to find the optimum z based on the fitted results. As anticipated when describing operations performed in the second block of the procedure (“Iteration loop”), the dependencies fitted at the beginning were kept fixed till the end without updating them in the meanwhile. This decision came out in order to keep the procedure the clearest and simplest as possible, at least for this first attempt of adapting Dang Van criterion to the critical volume approach. To give an idea to the reader about the complexity of updating the dependencies every time, it is

sufficient to think that: 1 specimen loaded under 1 specific load configuration needs 2 notch fatigue strengths (axial and torsion ones) to define its material parameters (a_{DV}, b_{DV}). Every specimen was tested under 3 different loading conditions, and there are 6 different specimen geometries, thus 2·3·6=36 notch fatigue strengths (and corresponding material parameters) must be monitored through the several iterations, which become 756 if all the selected z values (21 in total, see 5.8) is considered.

Going back to the calibration procedure, it was found that two iterations were enough to reach the convergence. This means that, if the first stage named “Initial conditions” is not considered in the count, the “Iteration loop” block was repeated two times carrying out iterations No.1 and No.2. In particular:

- checking the error calculated on the critical volume between iteration No.2 and the previous No.1, it was observed that such an error is close to zero in almost all cases, assuming absolute values of few decimals or cents of percentage error. The biggest absolute value comes from the error computed on the V-notch R1.3 specimen in case of push-pull loading (FF2040), when considering $z = 0.55$: this error turns out to be equal to -2.26%, which can be anyway neglected. Moreover, it was observed that the higher the value of z, the larger the number of specimens series which error tends to zero;

- another interesting observation can be made about torsion loading. It was noted in this case that critical volume never changes, thus the error is always equal to zero. This behaviour can be explained looking at how the Dang Van criterion works. According to equation 2.26, the equivalent stress amplitude is a linear combination of the shear stress and the hydrostatic stress evaluated on the critical plane. But in pure torsion, like here, there is no active hydrostatic stress and thus the equivalent stress amplitude is just a multiple of the shear stress amplitude: the multiplication factor involved in this case corresponds to the criterion’s material parameter a_{DV}. Therefore, the pure shear stress state is just scaled from one iteration to another, without producing any variations of the critical volume. Two iterations were nevertheless carried out, for consistency with the iterations performed in case of axial load.

It is finally time to assess the definitive notch fatigue strength vs. critical volume dependencies obtained from the calibration procedure of the multiaxial fatigue criterion. Starting with the axial load dependency, the best fit over all the various investigated z parameters was found for $z = 0.60$, to which corresponds a coefficient of determination $\mathrm{R}^2 = 0.8615$. The corresponding best-fit curve is presented in Figure 5.13, together with the related coefficient of determination and RMSE values. This optimum was confirmed after having checked neighbouring values such as $z = 0.575$ and $z = 0.625$, that showed worse fits. Similar considerations to the one already made for dependencies obtained through MMK criterion can be done here.

- The typical decreasing trend of notch fatigue strength with critical volume can be recognized also here, thus experimental data can be fitted by the power law. The optimum z value increased a bit with respect to the optimum one obtained from the MMK analysis, tending to higher values that should be more suitable for this purpose. However, 0.60 is still a very low value which could hide some possible unknown issues.

- In addition, coefficient R^2 obtained from this analysis with Dang Van is better than the one obtained with the power law fitting performed with the MMK analysis. Despite these positive points have been highlighted, it is inevitable to state that the data scattering persists.

- A final consideration is made about the experimental data trend to reach the horizontal plateau (that was previously theorized), which seems to be less evident in this context. Despite this, the hypothesis about its existence has no reason to be cancelled.

Critical volumes obtained from the approach are collected in Table 9.7 in Appendix 9.4, with respect to the optimum value of z parameter, meanwhile relative regression parameters used to fit those data are collected in Table 9.8. in Appendix 9.4.

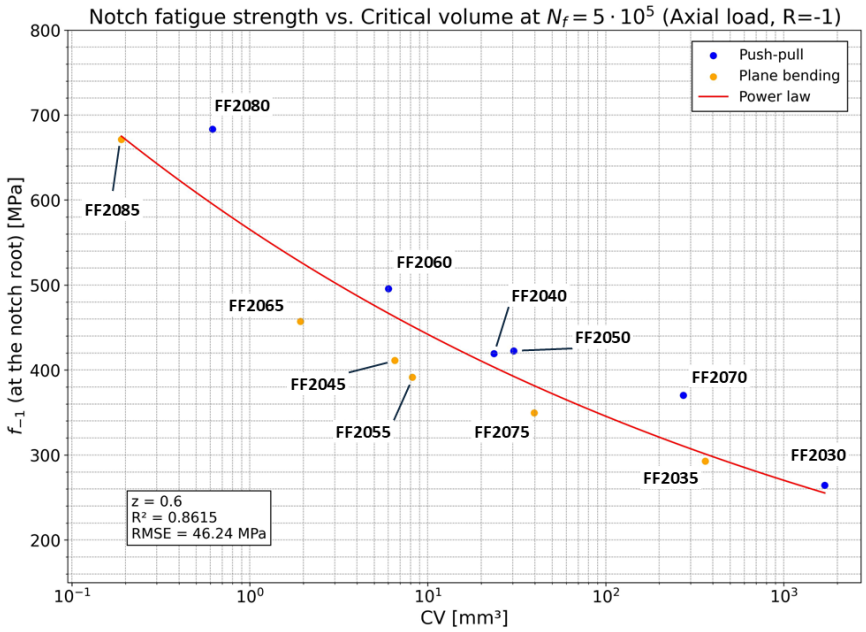

Figure 5.13: Notch fatigue strength vs. Critical volume dependency for axial load, to be used when applying Dang Van criterion in conjunction with the critical volume approach.

Regarding the torsion load case, the best fit over all the considered z values was found for $z = 0.70$, to which corresponds a coefficient of determination $\mathrm{R}^2 = 0.9858$. The fitted curve is reported in Figure 5.14, together with the related coefficient of determination and RMSE values. As done previously, neighbouring values such as $\mathrm{z} = 0.675$ and $\mathrm{z} = 0.725$ were investigated, but they exhibited lower fitting goodness. Following comments can be advanced.

- The value of the fitting parameter is confirmed to be the same already found in the preliminary MMK analysis, this $z = 0.70$. So, the final consideration is that, for what concerns the torsion load case, the critical volume approach (in its formulation presented in this work) seems to stabilize the z parameter at such a value.

- Coefficient R^2 has reduced slightly, but the quality of the power law fitting is certainly good.

Critical volumes obtained from the approach are collected in the same in Table 9.7 in Appendix 9.4, referring to the best-fit z parameter, meanwhile relative regression parameters used to fit those functions are collected in Table 9.9 in Appendix 9.4.

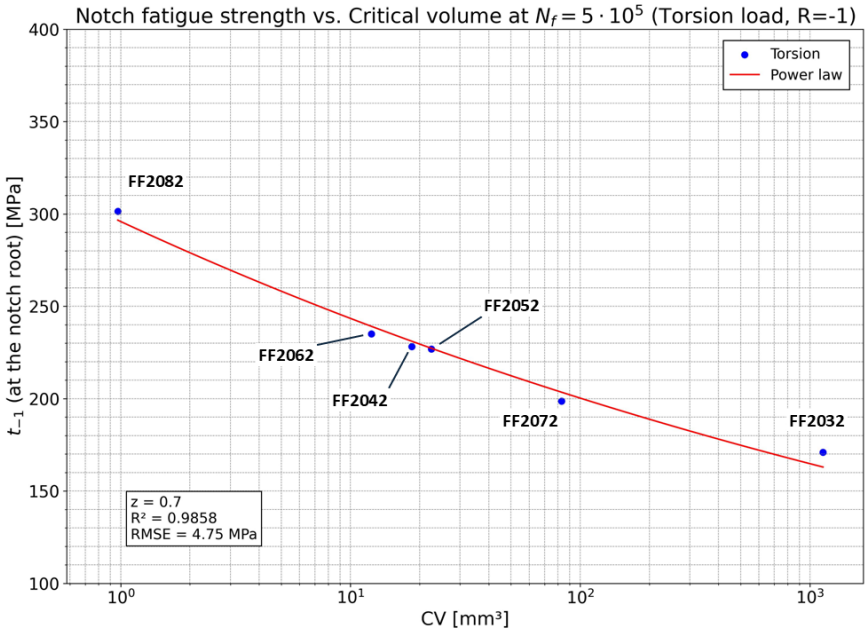

Figure 5.14: Notch fatigue strength vs. Critical volume dependency for torsion load, to be used when applying Dang Van criterion in conjunction with the critical volume approach.

At the end of this discussion, it is possible to state that some slight improvements of the notch fatigue strength vs. critical volume dependencies, resulting from this approach based on Dang Van criterion, can be noted with respect to the ones got from the preliminary analysis based on MMK criterion. But the approach in general still presents some important issues that does not make it work properly as expected. The outcomes are still far from the optimal scenario where the user can evaluate the critical volume of a generic notched component referring only to one value of z, and then use it in the two axial load and torsion load dependencies which should fit well the experimental data used for the criterion calibration.

5.2.3 Derived stress concentration factors

Besides the already discussed dependencies, another interesting outcome of the multiaxial fatigue analysis based on critical volume regards the calculation of stress concentration factors. They have been used to compute the notch fatigue strengths, mentioned above concerning the fitting of the final dependencies, multiplying these K_{t_DV} by the net nominal fatigue strengths read from the S-N curves. As already evidenced in previous Paragraph 5.2.2, axial load and torsion load dependencies do not converge on a common value of z parameter. So, K_{t_DV} factors presented in Table 5.2 refer to the optimum z condition corresponding to the considered load configuration.

Specimen	Tension	Plane bending	Torsion
V-notch R1.3	2.56	2.10	1.29
U-notch R1.5	2.41	1.98	1.25
Fillet R0.7	2.65	2.28	1.32
U-notch R5	1.54	1.38	1.04
Fillet R0.2	4.33	3.62	1.78

Table 5.2: Stress concentration factors evaluated according to the critical volume approach implemented using the Dang Van criterion. adapted to the critical volume approach.

5.3 ENCOUNTERED ISSUES

Analysing the outcomes of the implementation of the critical volume approach, both with MMK and Dang Van criteria, it is possible to observe some criticalities that deserve to be addressed, especially for what concerns the axial load mode.

5.3.1 Push-pull vs. plane bending test data

In the preliminary study using the MMK criterion, the issue of experimental data scattering, particularly evident in the dependency related to axial load case, was identified. This observation was further confirmed through subsequent analyses involving the Dang Van criterion. The switch from the MMK uniaxial solution to the Dang Van multiaxial one was expected to address this scattering problem by better capturing the multiaxiality of the stress tensor around the notch, which is distorted due to the presence of the stress concentrator. However, as the results revealed, this change did not significantly improve the situation.

The general observation is that by varying the parameter z, the plane bending series overlaps with the push-pull series only at lower notch fatigue strengths, corresponding to larger critical volumes (bottom-right region of graphs obtained with both MMK, Figures 5.4 and 5.6, and Dang Van, with reference to Figure 5.13). Both series exhibit a monotonic decreasing trend that can be effectively modelled by a power law. However, the plane bending points consistently deviate from the push-pull points, lying further to the left on the graph. This divergence leads to considerable data dispersion, which is highlighted by the statistical indicator R^2, the coefficient of determination. Implementing Dang Van criterion in the critical volume analysis, the power-law fitting achieves a moderate R^2 value of 0.8615 for the best-fit dependency, indicating a necessary compromise in fitting quality when both series are analysed simultaneously. Combining the two series into a single fitting model is unavoidable, as they represent the two kinds of axial loading configurations evaluated in the current experimental work. However, the observed dispersion and the relatively low R^2 suggest the potential influence of additional variables that affect the correlation between fatigue strength and critical volume.

One possible explanation for this issue could involve plasticity effects. An attempt was made to incorporate this phenomenon into the analysis, as described at the end of Section 5.1, by reducing the z factor which directly affects the critical volume size. The hypothesis was that considering larger portions of high cyclic stressed material might account for potential plastic deformation below the notch root. This adjustment was expected to shift the plane bending points to the right, closer to the push-pull points, thereby reducing the observed scatter. Unfortunately, this strategy provided only marginal improvements both using the MMK criterion and the Dang Van one: the two series came slightly closer together at lower z, but the overlap remained insufficient to achieve a high-quality fit. The results indicate that for relatively high values of notch fatigue strength, the two series do not overlap at any of the considered z parameters. This might suggest there are additional mechanisms governing material damage, which are not captured by the current definition of critical volume. These mechanisms could potentially involve plasticity effects as said, which remain unaccounted for in this analysis since it is likely that the critical volume, as it is defined, cannot assess them. Notch fatigue strengths in axial load case evaluated relying on the modified Dang Van approach, and referring to $z = 0.6$, are reported in Table 5.3 below for every series tested under axial load. Plastic deformation should be supposed to occur in a quite wide set of series, specifically FF2040, FF2045, FF2050, FF2060, FF2065, FF2080 and FF2085 where the elastic peak stress amplitude at the notch tip goes over the yield strength of 401 MPa.

Specimen	Load	Mark	Notch fatigue strength [MPa]
Unnotched	Push-pull	FF2030	264.52
	Plane bending	FF2035	292.74
V-notch R1.3	Push-pull	FF2040	419.25
	Plane bending	FF2045	411.31
U-notch R1.5	Push-pull	FF2050	422.40
	Plane bending	FF2055	391.54
Fillet R0.7	Push-pull	FF2060	495.81
	Plane bending	FF2065	457.13
U-notch R5	Push-pull	FF2070	370.20
	Plane bending	FF2075	349.75
Fillet R0.2	Push-pull	FF2080	683.34
	Plane bending	FF2085	671.26

Table 5.3: Notch fatigue strengths evaluated with the modified Dang Van criterion which involves critical volume, computed for all specimen series tested under axial loading.

5.3.2 Further discussion

It has previously been observed that the push-pull and plane bending series do not collapse into a single curve describing well the dependency between notch fatigue strength and critical volume. Some additional considerations on this issue can be made by focusing on the critical volume evaluation performed for axial loading configurations. The following approach is undoubtedly qualitative, as every specimen is characterized by its two critical volumes, one under tension load and the other under plane bending load, which are associated with two different notch fatigue strengths (even if these fatigue strengths slightly differ as shown in Figure 5.13). However, few interesting insights can still be drawn. For this purpose, CV vs. z graphs are proposed in Figure 5.15, where the critical volume values (represented on a log scale) are those calculated in the preliminary analysis using the MMK criterion. Specimen series have been grouped based on their notch “sharpness” as follows:

- the Unnotched geometry (characterized by an infinite notch radius) forms its own distinct group (Figure 5.15a);
- blunt notch geometries (with a medium notch radius) include the U-notch and V-notch specimens (Figure 5.15b);
- sharp notch geometries (with a very small notch radius) consider the two Fillet specimens (Figure 5.15c).

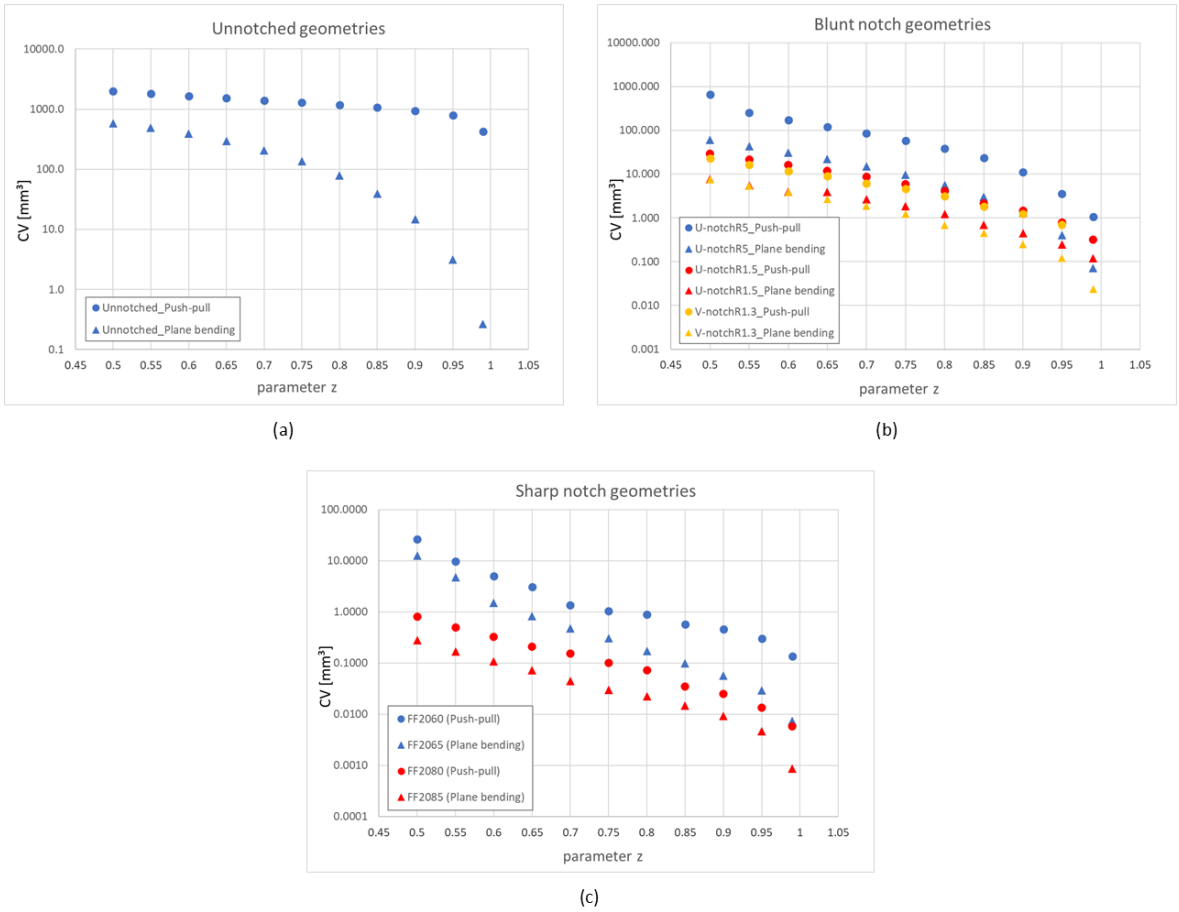

Figure 5.15: Diagrams showing the relationship between the critical volume (evaluated with MMK criterion) and the z parameter.

The first noticeable outcome is that the ratio between the critical volume in push-pull and plane bending configurations can vary with the parameter z. Starting from the "Unnotched geometries" case (Figure 5.15a), critical volume values generally remain substantially higher across the entire z-range: this is line with expectations, since smooth specimens do not present stress concentration phenomena. But it is also evident that in this case the two curves clearly diverge significantly as z increases. While the FF2030 curve exhibits an initial plateau (with CV remaining relatively unchanged with z) followed by an abrupt decrease at very high z values, the FF2035 curve decreases continuously with the downward trend accelerating as z increases. This could suggest that in unnotched specimen geometries the z parameter has a more pronounced effect on the plane bending loading mode than push-pull one, because of the different stress gradients. Looking at the other diagrams in Figures 5.15b and 5.15c, the relationship between the push-pull and plane bending curves depends on the considered series:

- for some series, such as FF2060-FF2065 and FF2070-FF2075, the push-pull and plane bending curves approach each other or diverge depending on the z value;

- in other cases, like FF2040-FF2045, FF2050-FF2055, and FF2080-FF2085, the two curves exhibit nearly identical trends, appearing as if one is simply shifted vertically relative to the other;

- it is both interesting and reasonable to observe the similarity between the V-notch R1.3 and U-notch R1.5 specimens (FF204Y and FF205Y, respectively). The curves for these series, under one of the two axial loads, almost superpose each other. This can be attributed to their

similar notch radii, which induce comparable stress gradients and critical volumes across both configurations.

In order to give an alternative visualization of the data presented in previous graphs, the ratios between critical volumes for each notch geometry under push-pull and plane bending loading modes have been computed and summarized in Table 5.4 below.

z (MMK criteron)	0.50	0.55	0.60	0.65	0.70	0.75	0.80	0.85	0.90	0.95	0.99
Unnotched (FF203Y)	3.42	3.72	4.28	5.18	6.72	9.50	14.83	27.19	64.09	254.79	1591.45
V-notch R1.3 (FF204Y)	3.01	3.01	3.03	3.39	3.29	3.74	4.57	4.10	4.96	5.84	12.91
U-notch R1.5 (FF205Y)	2.95	3.02	3.19	3.40	3.53	3.72	4.51	3.45	4.27	4.63	9.89
Fillet R0.7 (FF206Y)	2.09	2.05	3.28	3.73	2.86	3.47	5.16	5.79	8.13	10.25	18.18
U-notch R5 (FF207Y)	10.88	5.82	5.48	5.51	5.73	6.08	6.80	7.90	8.30	8.78	14.73
Fillet R0.2 (FF208Y)	2.89	2.97	3.01	2.88	3.46	3.38	3.23	2.39	2.68	2.89	6.78

Table 5.4: Ratios between critical volumes under tension load and under plane bending load, calculated for the various z parameters using MMK criterion.

For consistency, equivalent graphs based on results obtained using the Dang Van criterion are shown in Figure 5.16. Switching to this other criterion does not significantly alter the trends observed. The behaviours are largely similar to those illustrated above, with minor differences. For example, FF206Y and FF207Y series, in Figures 5.16b and 5.16c, no longer bend upwards at very low z values.

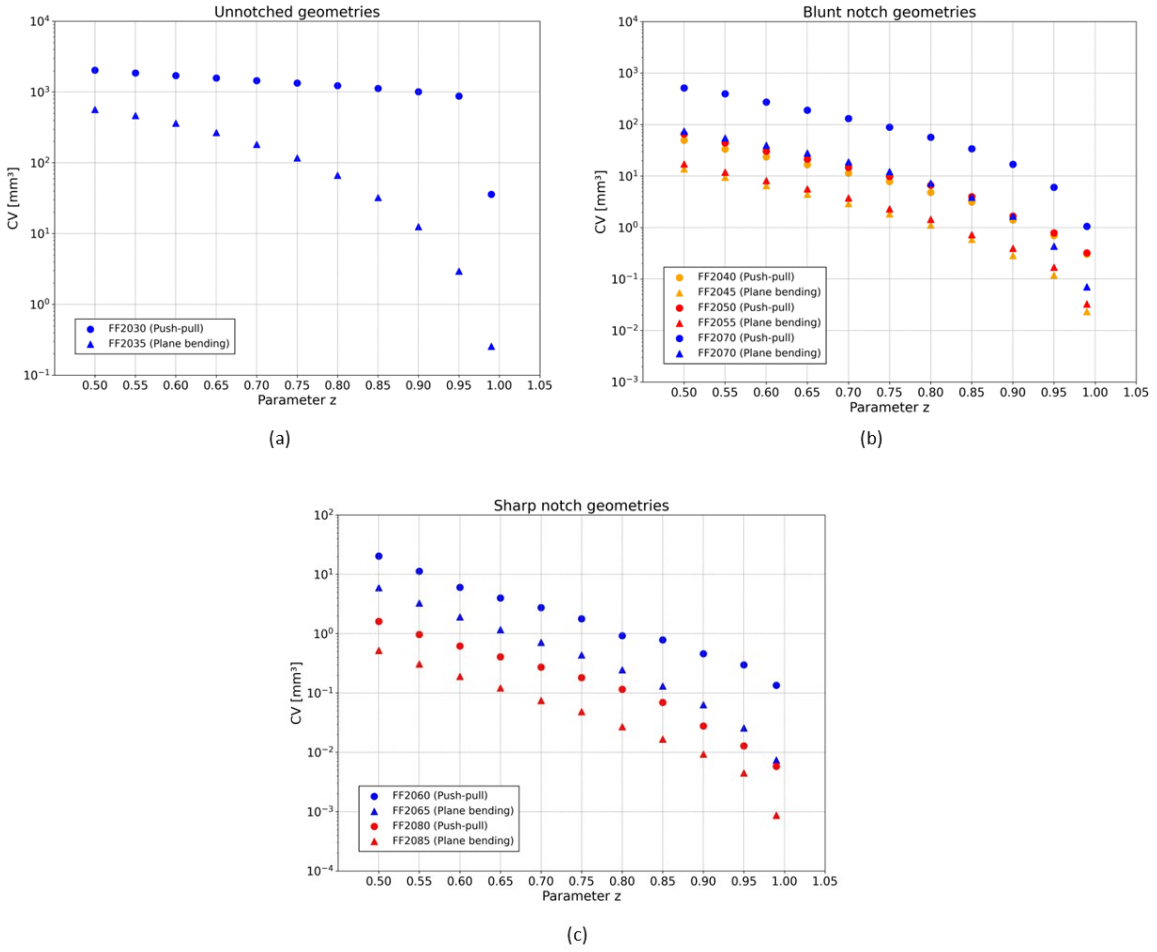

Figure 5.16: Diagrams showing the relationship between the critical volume (evaluated with the modified Dang Van criterion) and the parameter z.

As already done before, table with values of ratios computed between critical volumes of push-pull and plane bending series are reported also for this case in Table 5.5.

z (Dang Van criteron)	0.50	0.55	0.60	0.65	0.70	0.75	0.80	0.85	0.90	0.95	0.99
Unnotched	3.59	3.99	4.70	5.90	7.93	11.43	18.41	34.64	80.69	297.10	140.28
V-notch R1.3	3.58	3.51	3.60	3.75	3.91	4.24	4.29	5.29	4.87	5.86	13.01
U-notch R1.5	3.81	3.70	3.72	3.78	3.91	4.24	4.62	5.46	4.22	4.64	9.82
Fillet R0.7	3.41	3.45	3.13	3.42	3.85	4.08	3.73	5.99	7.23	11.49	18.18
U-notch R5	6.86	7.21	6.89	6.78	6.91	7.27	7.77	8.71	10.16	13.89	14.90
Fillet R0.2	3.09	3.15	3.25	3.34	3.65	3.76	4.28	4.13	2.97	2.86	6.68

Table 5.5: Ratios between critical volumes under tension load and under plane bending load, calculated for the various z parameters using Dang Van criterion in conjunction with the critical volume approach.

It is challenging to extract further critical insights from these data. However, one thing is clear: the relationship between critical volumes in push-pull and plane bending configurations changes with z parameter and varies across the different notch geometries, increasing the complexity of understanding how to correlate the fatigue strength to the critical volume.

6 APPLICATION OF THEORY OF CRITICAL DISTANCES

6.1 POINT METHOD

The implementation of the critical volume approach has shown weak results for what concerns the study of the notch fatigue strength vs. critical volume dependency, especially under axial loading conditions. Therefore, the subsequent idea was to investigate the axial load configurations using a more stable method, capable of better capturing and summarizing all the stress gradient effects related to the considered specimen geometries. For this purpose, the Theory of Critical Distances (TCD) was applied to data from both push-pull and plane bending tests. Among the various variants of TCD, the Point Method (PM) was chosen due to its widespread use and straightforward application. For clarity, PM is briefly reviewed here. This method involves determining the effective stress amplitude (σ_{eff}), which is representative of the entire linear elastic stress field damaging the fatigue process zone. The σ_{eff} is evaluated at the critical distance (D_{PM}), located beneath the notch tip along the bisector of the notch opening angle, as recalled in Figure 6.1. Equations for σ_{eff} and D_{PM} are provided in 2.29 and 2.30, respectively.

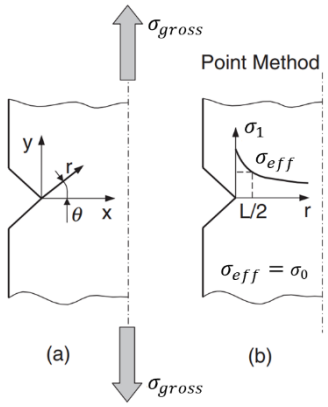

Figure 6.1: Reference to the definition of the Point Method, already addressed in Paragraph 2.4.2 while introducing the Theory of Critical Distances [7].

The critical distance is a material property that can be defined at the material fatigue limit or, alternatively, at the material fatigue strength for a given life N_f. Taylor and Susmel [7], [14] extended the TCD to the medium-cycle fatigue domain, proposing that the critical distance varies with the fatigue life according to a power law. Based on this and the definitions previously outlined in Paragraph 2.4.2, the PM can be enunciated as follows: if the local stress amplitude, evaluated at the critical distance below the notch root, equals the material fatigue limit (or the material fatigue strength at a specific number of cycles N_f), the notched component is designed to last for an infinite life (or the specified life N_f).

6.1.1 Critical distance vs. fatigue life

According to the original formulation of the TCD approach, the critical distance should be calculated using parameters derived from the LEFM theory. It is worth remembering that D_{PM} is a function of L, the material characteristic length as defined by El Haddad. However, it is possible to implement a procedure for calibrating this critical distance using data obtained from fatigue tests. Authors of latest advancements of TCD, Taylor and Susmel, state that a material S-N curve and at least one notched S-N curve are required to calibrate the critical distance, and further construct the S-N curve of

arbitrary notches. Thereby, direct calculation of any fracture mechanical parameter, like L, is avoided [15].

In the present study, the extension of TCD to the finite fatigue life domain was employed to analyse axial loading conditions, encompassing both push-pull and plane bending tests. To determine the D_{PM} vs. N_f relationship, which expresses the dependency of the critical distance on the number of cycles to failure, the following five fatigue life values were selected:

$$N_f \in [50000, 100000, 200000, 500000, 1000000] \tag{6.1}$$

This set of N_f values defines a fatigue life interval for which experimental data are available for all specimen series. This fact can be verified by examining the K-V regressions shown in Figures 4.2, 4.4 and 4.6. Linear elastic stress fields were plotted to facilitate visualization of the problem and to enable preliminary considerations. Since calibrating the critical distance at the material fatigue limit was not feasible, it turned out to be pertinent to investigate the stress fields corresponding to the highest fatigue life considered, thus $N_f = 10^6$. Stresses computed through FE analyses need to be scaled according to the specified fatigue life, in order that the fatigue load which generates that stress distribution matches the real experimental load (that led the specimen to fatigue failure after N_f cycles). Figures 6.2 and 6.3 illustrate the linear elastic stress fields (expressed in terms of maximum principal stress) for tension and bending cases, respectively, at this fatigue life.

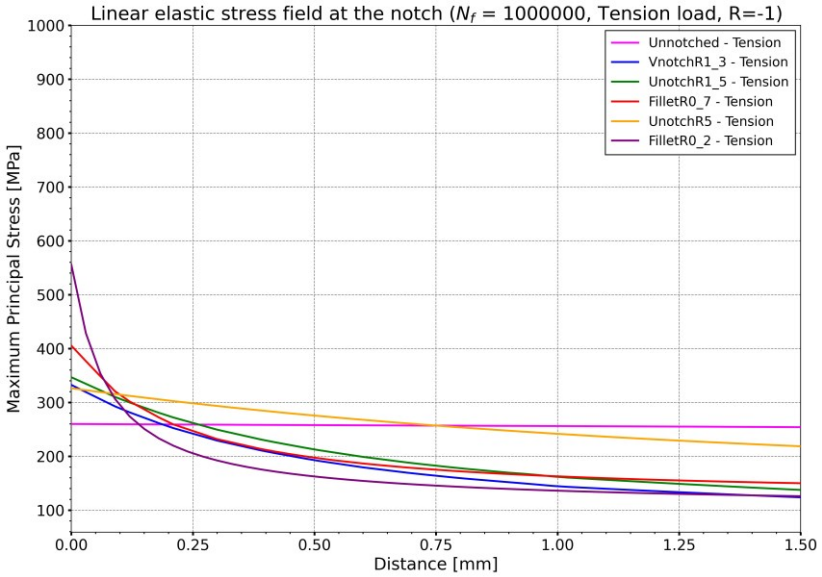

Figure 6.2: Maximum principal stress under tension load plotted along the x-coordinate, originating at the most stressed point at the notch root.

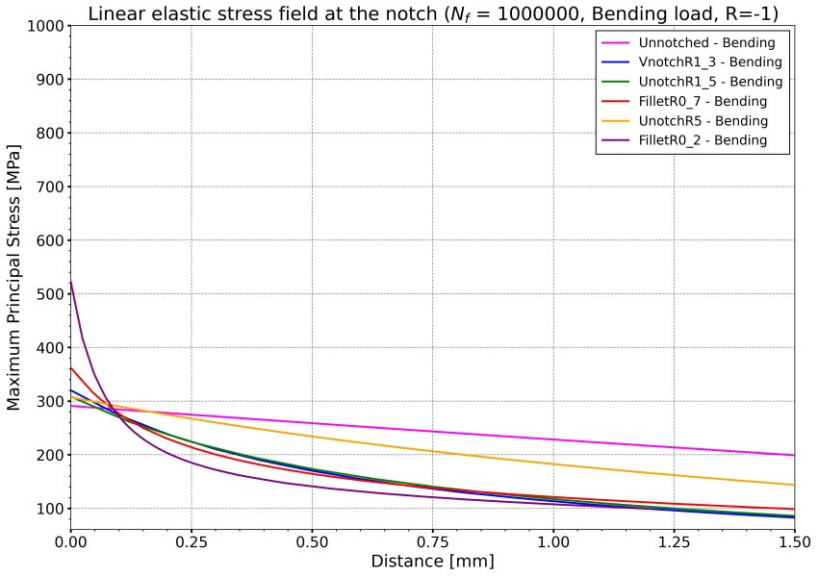

Figure 6.3: Maximum principal stress under bending load plotted along the x-coordinate, originating at the most stressed point at the notch root.

Plain fatigue strength under axial loading at $N_f = 10^6$ is equal to $f_{-1} = 256.87$ MPa, as determined from the Unnotched S-N curve (Figure 4.2). According to PM, each specimen is expected to exhibit a linear elastic stress field which matches the value of f_{-1} at the critical distance D_{PM}. If PM perfectly captured experimental reality, all the considered stress fields would intersect at a single point with an x-coordinate equal to D_{PM} (according to the reference frame defined in Figure 6.1): also the stress field of the smooth specimen under tension load would pass through this common point. Nevertheless, experimental results deviate significantly from theoretical expectations, as for example shown in Figure 6.2, with respect to the tension load case: intersection points are scattered, and the Unnotched stress profile crosses the notched stress profiles at different locations, complicating the determination of a precise value for D_{PM}. In contrast, the situation appears less scattered for plane bending case (see Figure 6.3) where the intersections are closer to a possible common point of intersection. Returning to the tension load case, initial estimates of the critical distance were made by calculating the intersection points between the Unnotched stress field and notched stress fields. Concerning V-notch R1.3, U-notch R1.5, Fillet R0.7 and Fillet R0.2 specimens, the D_{PM} values under tension load ranged between 0.14 mm and 0.27 mm. Instead, the U-notch R5 specimen emerged as an outlier with a D_{PM} equal to 0.75 mm. An additional observation concerns the stress distribution within the Unnotched specimen, which was assumed constant over the entire cross-section so far. Though this sample has a smooth geometry, there exist very small stress concentration factors both under tension and bending loads (this fact was anticipated in Paragraph 3.1.1). Referring to the maximum principal stress, stress concentration factor assumes the value of:

$$K_{t,ten\_PS1} = 1.012 \tag{6.2}$$

under tension load, while of:

$$K_{t,ben\_PS1} = 1.013 \tag{6.3}$$

under plane bending. Consequently, the linear elastic stress field of the Unnotched specimen under tension load is not entirely flat, and its intersection with the plain fatigue strength in axial loading (f_{-1}) occurs at a D_{PM} equal to 0.77 mm. To address these inconveniences, an alternative “engineering” approach was proposed. Since PM claims that all stress fields should pass through a single intersection point (as remarked above), the idea was to calculate critical distance as the average x-

coordinate of all possible intersections between linear elastic stress fields for axial load cases, including both push-pull and plane bending tests. This approach presents two key advantages:

1. it respects the fundamental principle of PM, as if the method were perfect, all intersections would collapse into a single point;
2. averaging mitigates the impact of outliers, enhancing the robustness of the D_{PM} calculation.

This methodology was applied for each selected fatigue life. The resulting critical distances are summarized in Table 6.1, and plots illustrating the mutual intersections between all stress fields under tension and bending loads are reported in Figures 6.4 to 6.9 for every fatigue lifetime.

N_f	D_{PM} [mm]
50000	0.29
100000	0.24
200000	0.19
500000	0.16
1000000	0.14

Table 6.1: Critical distances evaluated according to the PM at the selected fatigue lives.

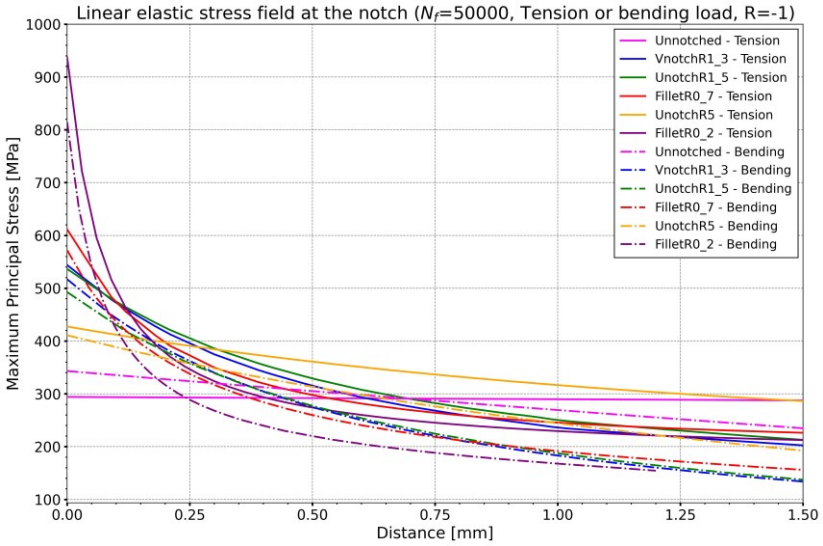

Figure 6.4: Plots of maximum principal stresses along the x-coordinate for both tension and bending load cases at $N_f = 5 \cdot 10^4$, illustrating intersections between the various stress fields.

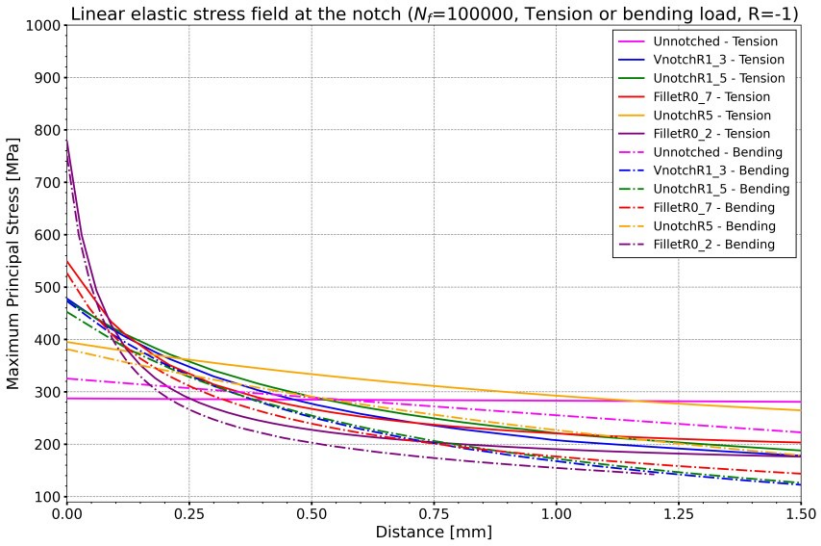

Figure 6.5: Plots of maximum principal stresses along the x-coordinate for both tension and bending load cases at $N_f = 10^5$, illustrating intersections between the various stress fields.

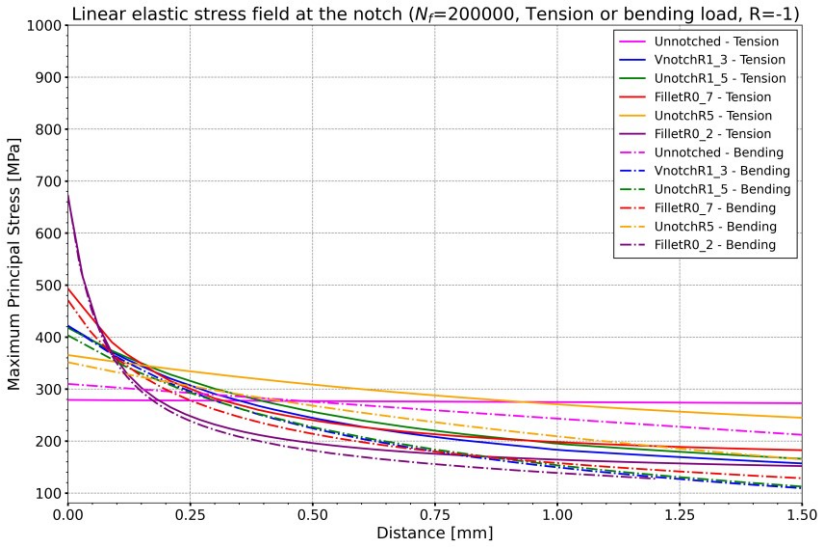

Figure 6.6: Plots of maximum principal stresses along the x-coordinate for both tension and bending load cases at $N_f = 2 \cdot 10^5$, illustrating intersections between the various stress fields.

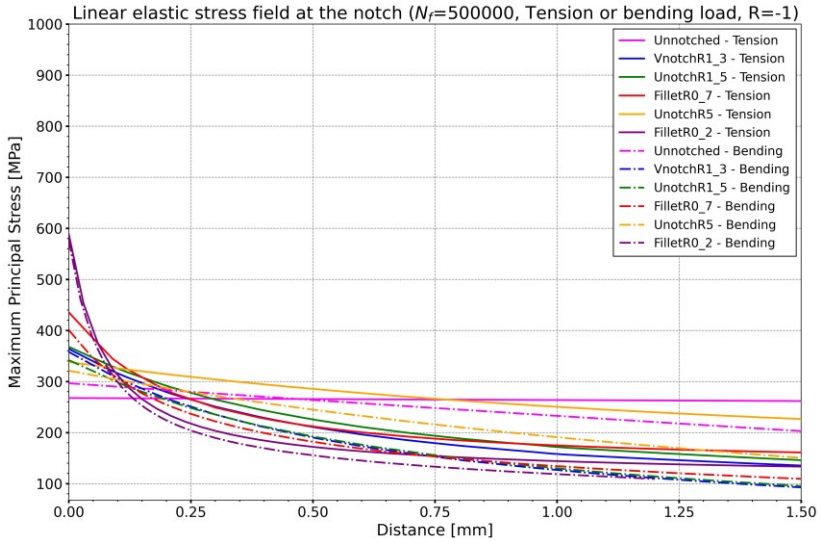

Figure 6.7: Plots of maximum principal stresses along the x-coordinate for both tension and bending load cases at $N_f = 5 \cdot 10^5$, illustrating intersections between the various stress fields.

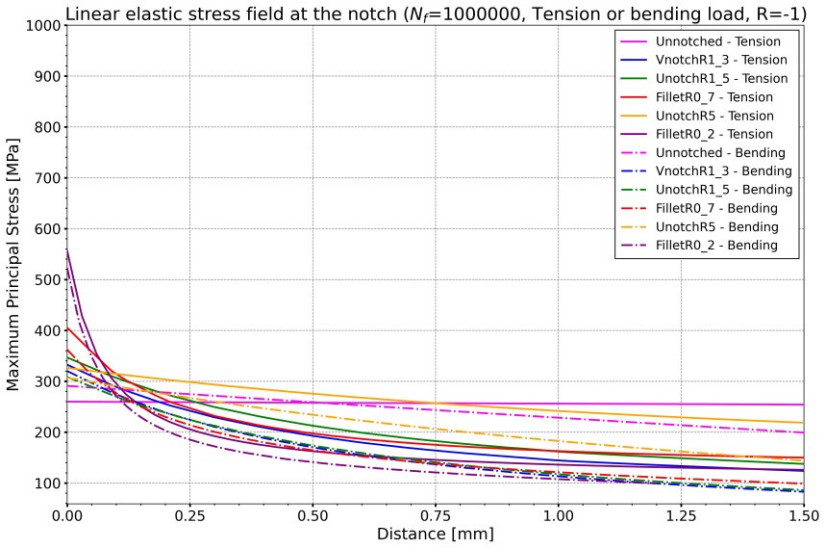

Figure 6.8: Plots of maximum principal stresses along the x-coordinate for both tension and bending load cases at $N_f = 10^6$, illustrating intersections between the various stress fields.

At this point, the dependency between critical distance and fatigue life was expressed according to the power law formulation proposed in equation 2.35, which was used to derive directly the D_{PM} instead of L. Power law regression parameters C_1 and C_2 are collected in Table 9.10 in Appendix 9.5, while the plot of the dependency is illustrated in Figure 6.9.

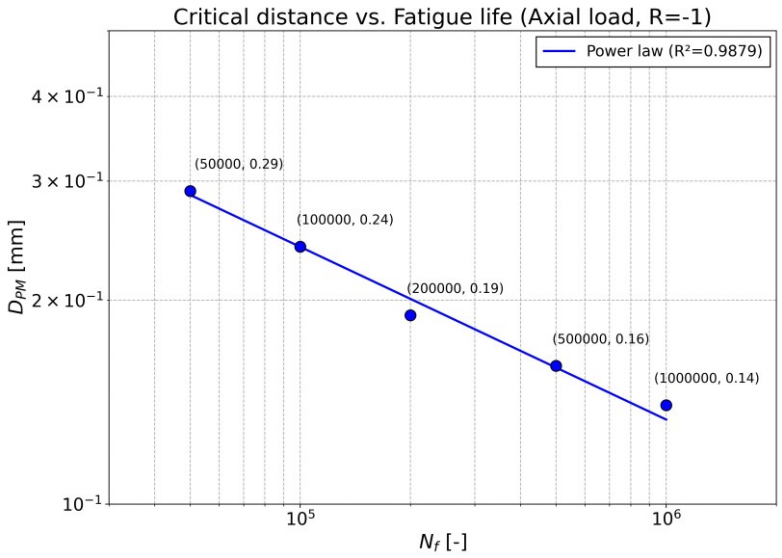

Figure 6.9: Critical distance vs. Fatigue life relationship, fitted by a power law.

6.1.2 S-N diagram reconstruction

The next stage involved reconstructing the Wöhler diagram by processing experimental data obtained from fatigue tests using the PM. Main steps of the procedure are outlined hereafter.

1. Selection of specimen series. Consider a single specimen under a specific axial load configuration. Each series produced a certain number of experimental points (used to derive the S-N curves), each characterized by a distinct value of experimental fatigue life N_f. These points are processed individually in the following steps.

2. Scaling of the stress field. The linear elastic stress field calculated from the FE analysis must be scaled in order to be consistent with the real experimental fatigue load that caused failure at the given N_f. For this purpose, a procedure inspired by the one used for critical distance calibration by Nesládek et al. in [15] was adopted.

   First, maximum principal stress is normalized by the corresponding local maximum value at the notch root (σ_{ep}). If $\sigma_1(x)$ represents the maximum principal stress at coordinate x, dividing it by the elastic peak stress it will result in the dimensionless factor $s(x)$:

$$s(x) = \frac{\sigma_1(x)}{\sigma_{ep}} \tag{6.4}$$

   Then, the stress concentration factor (K_{t_PS1}), referred to the net cross-sectional area, and the specimen fatigue strength at N_f (σ_{N_f}), expressed in terms of net nominal stress amplitude, are considered. The maximum principal stress level at an arbitrary x-coordinate ($\sigma_{1,N_f}(x)$) is determined as follows:

$$\sigma_{1,N_f}(x) = s(x) \cdot \sigma_{N_f} \cdot K_{t\_PS1} \tag{6.5}$$

3. Calculation of critical distance. Critical distance corresponding to the given fatigue life must be calculated using the D_{PM} vs. N_f law previously fitted (refer to power law parameters in Table 9.10).

4. Determination of the effective stress. The effective stress is obtained by evaluating the actual maximum principal stress at the critical distance:

$$x = D_{PM} \tag{6.6}$$

Substituting this into the stress calculation formula (6.5):

$$\sigma_{eff} = \sigma_{1,N_f}(D_{PM}) \tag{6.7}$$

Linear interpolation was employed between the node stress values for this purpose.

This procedure was repeated for all specimen series subjected to axial load. As a results, data points (N_f, σ_{eff}) were obtained for all the analysed cases, enabling the construction of the new S-N diagram. Figure 6.10 presents the graph of local stress amplitudes at the critical distance vs. number of cycles to failure graph, derived using TCD.

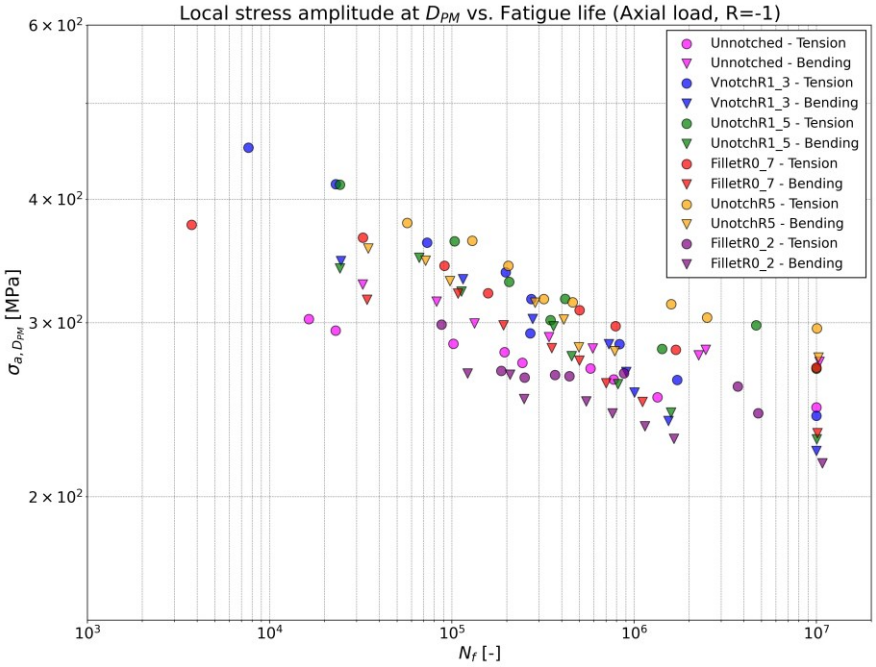

Figure 6.10: S-N diagram derived from the TCD. Local stress amplitudes, referred to as $\sigma_{a,D_{PM}}$ on the y-axis, correspond to the effective stresses calculated using the procedure described above.

6.2 VALIDATION OF POINT METHOD

The TCD, as applied through the PM, aims to synthetize all the stress gradient effects observed across the various specimen series into a single S-N curve, which represents a characteristic curve of the material for the given load ratio ($R = -1$). Ideally, all the experimental data points obtained from fatigue tests should collapse onto this fatigue curve, appearing as a linear function in a log-log diagram. However, the PM does not perform perfectly. This limitation is evident in the scattered representation of data points in Figure 6.10. To validate the PM and assess its effectiveness, the degree of data scattering must be quantified. This can be achieved by calculating the width of the scatter band defined between two reference probabilities of survival. For this study, probabilities of survival of 10% and 90% were considered. The scatter band was determined following the procedure outlined in the international standard ISO 12107 [40]. Calculations were performed using an Excel spreadsheet specifically programmed to implement the method described in the standard. The width of the scatter band is expressed as the ratio (T_σ) between the stress amplitude at 10% probability of survival (σ_{10}) and stress amplitude at 90% probability of survival (σ_{90}):

$$T_\sigma = \frac{\sigma_{10}}{\sigma_{90}} \tag{6.8}$$

6.2.1 Scatter band calculated on PM results

First, the scatter band was calculated using data obtained from the PM. These data points are represented in terms of local stress amplitude at the critical distance ($\sigma_{a,D_{PM}}$). The graphical output of the procedure is illustrated in Figure 6.11, which includes the three band lines corresponding to 10%, 50% and 90% probabilities of survival, along with the calculated value of T_σ.

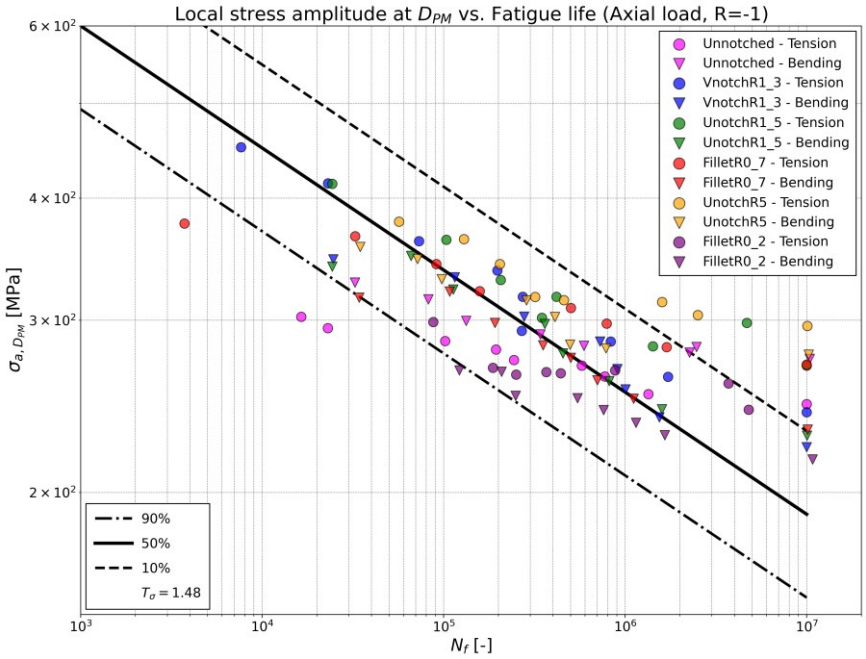

Figure 6.11: Scatter band evaluated on experimental data processed by the Point Method.

6.2.2 Scatter band calculated on raw experimental data

The scatter band was also evaluated for all raw experimental data obtained from the fatigue tests. In this case, data points are represented in terms of net nominal stress amplitude ($\sigma_{a,net}$), as used in the S-N curves discussed in Chapter 4. Graphical outputs for each series are presented in Figures 6.12 to 6.23, displaying the three band lines and the corresponding T_σ values.

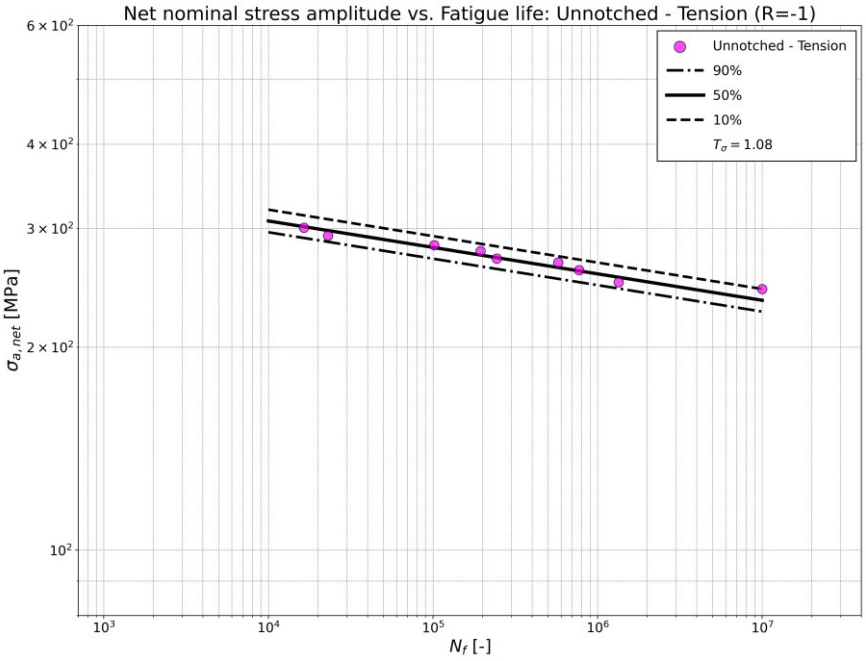

Figure 6.12: Scatter band evaluated on FF2030 experimental data.

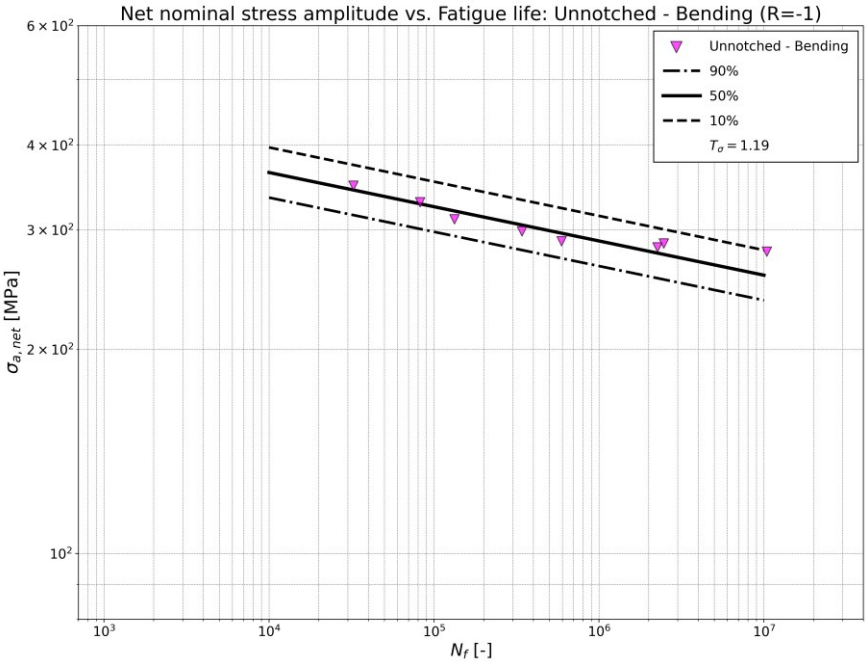

Figure 6.13: Scatter band evaluated on FF2035 experimental data.

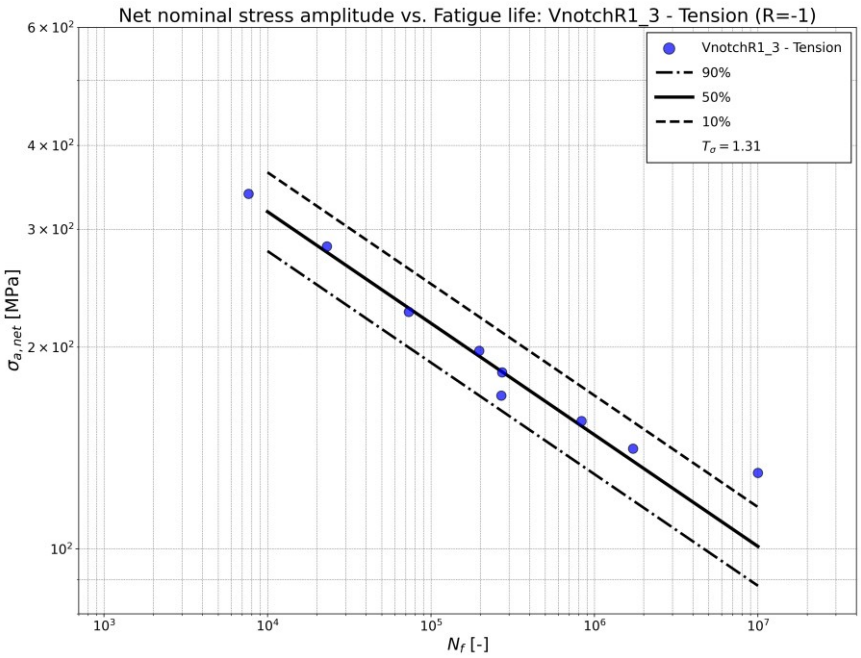

Figure 6.14: Scatter band evaluated on FF2040 experimental data.

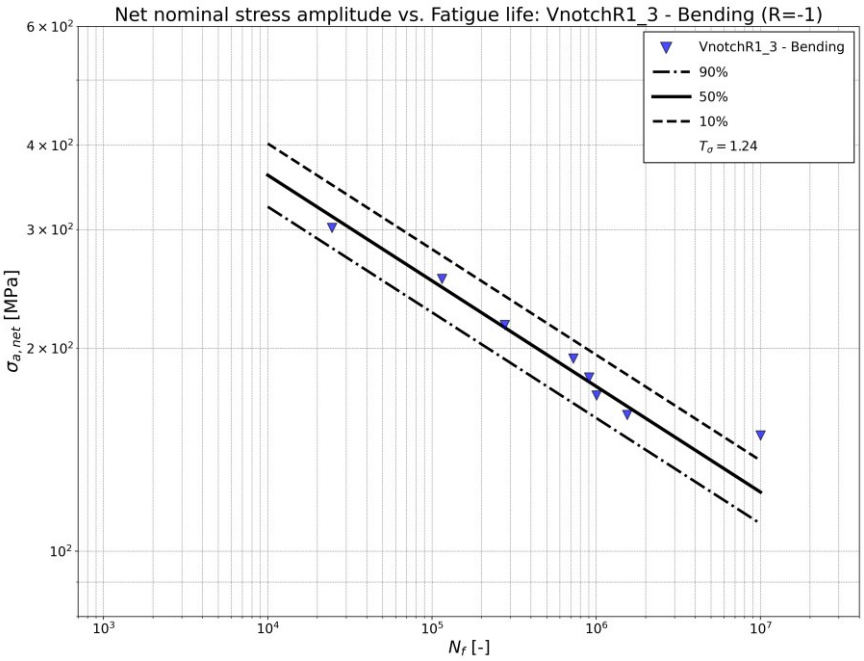

Figure 6.15: Scatter band evaluated on FF2045 experimental data.

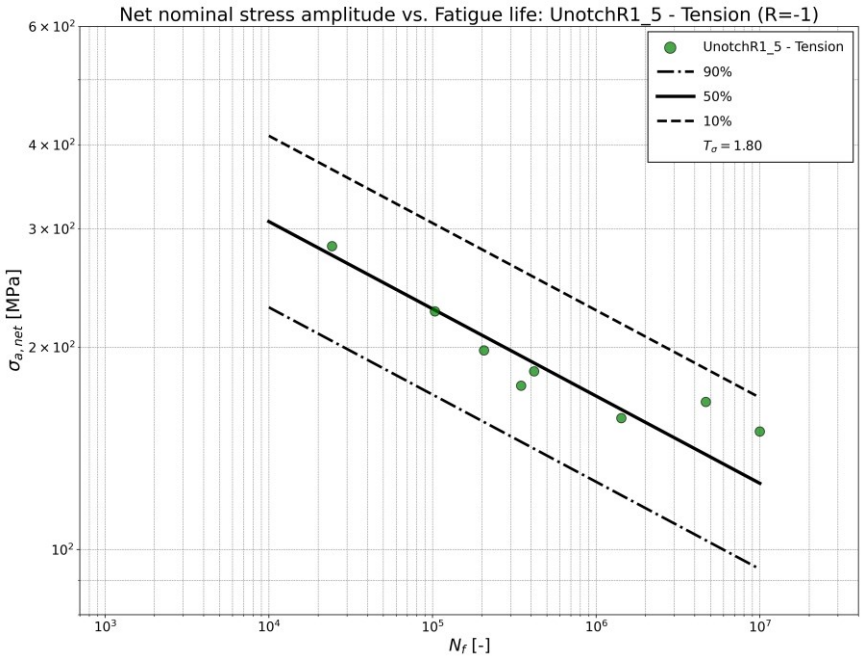

Figure 6.16: Scatter band evaluated on FF2050 experimental data.

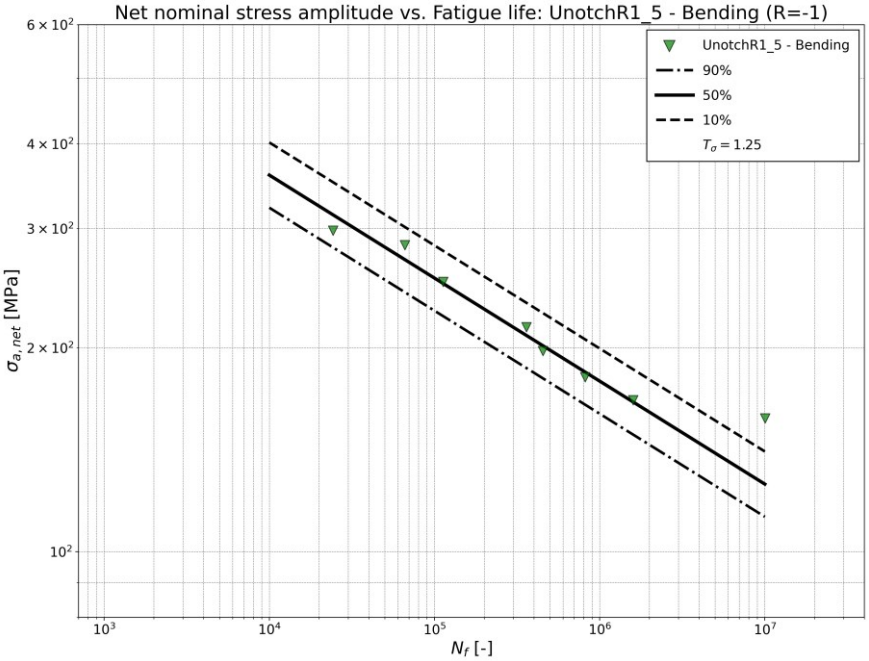

Figure 6.17: Scatter band evaluated on FF2055 experimental data.

Figure 6.18: Scatter band evaluated on FF2060 experimental data.

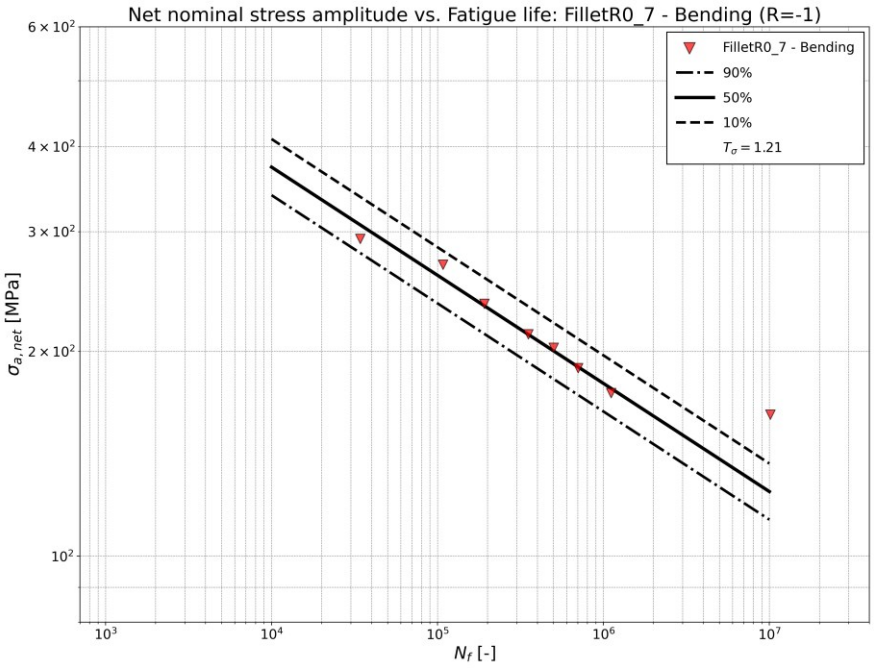

Figure 6.19: Scatter band evaluated on FF2065 experimental data.

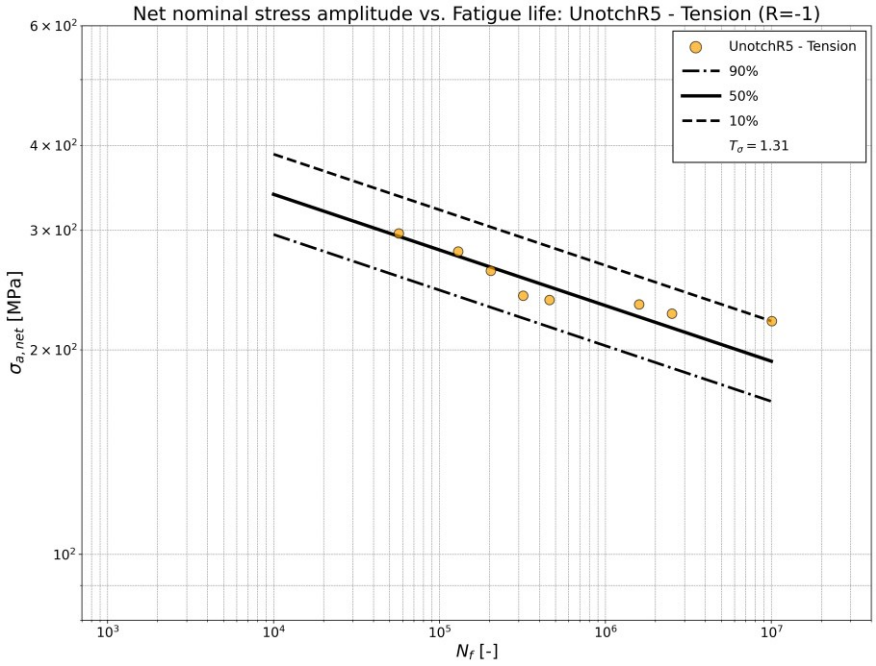

Figure 6.20: Scatter band evaluated on FF2070 experimental data.

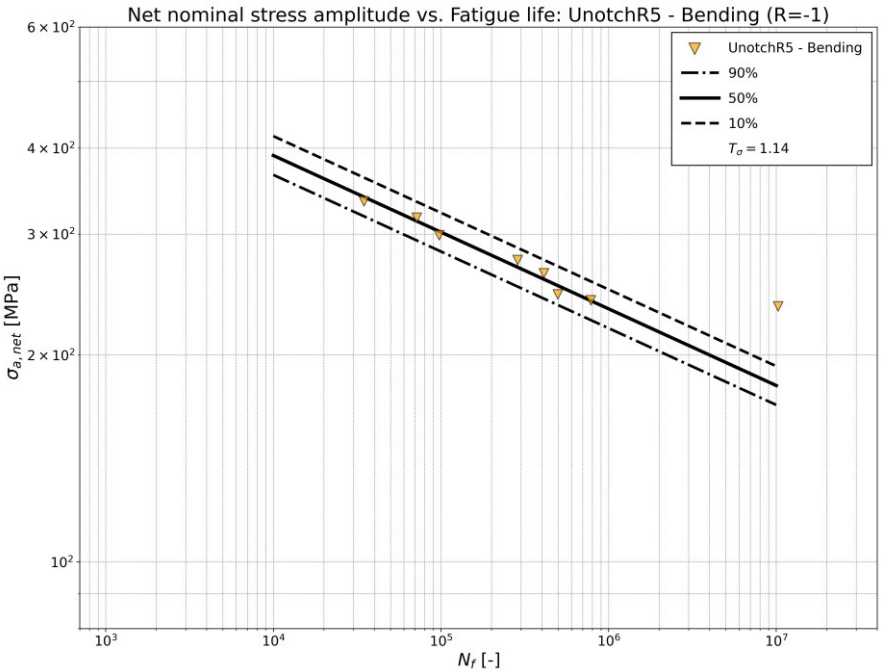

Figure 6.21: Scatter band evaluated on FF2075 experimental data.

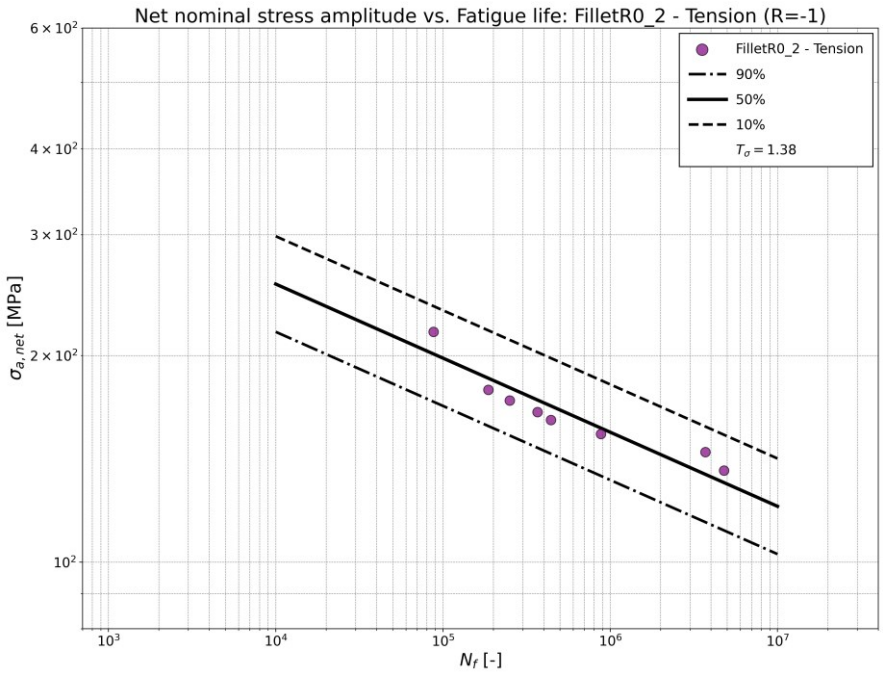

Figure 6.22: Scatter band evaluated on FF2080 experimental data.

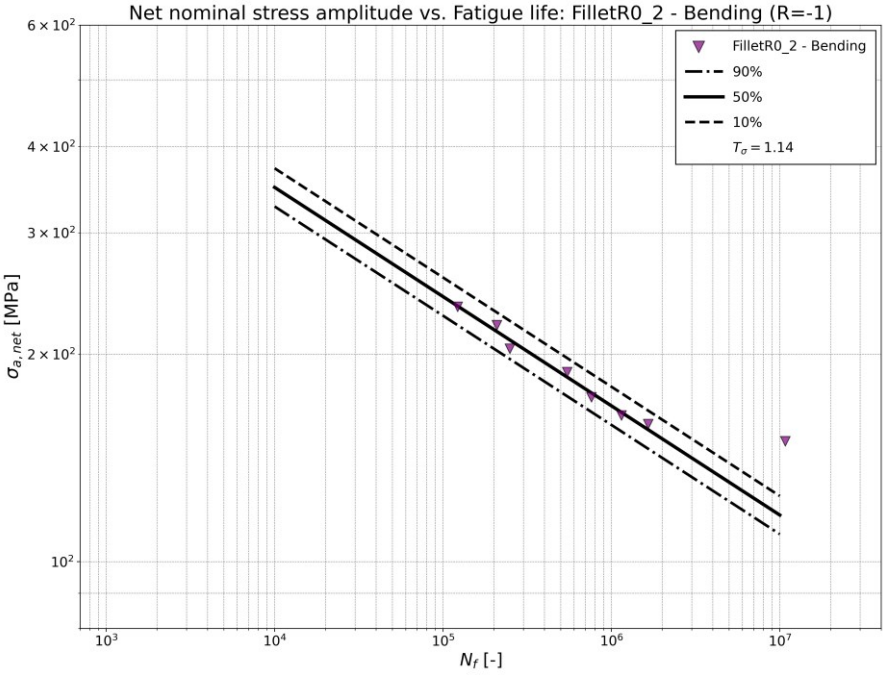

Figure 6.23: Scatter band evaluated on FF2085 experimental data.

6.2.3 Final considerations about the effectiveness of the PM

All T_σ values calculated for the data processed via PM and the raw experimental data are summarized in Table 6.2

Specimen	Load	Mark	T_σ	
			Exp. data	PM
Unnotched	Push-pull	FF2030	1.08	1.48
	Plane bending	FF2035	1.19	1.48
V-notch R1.3	Push-pull	FF2040	1.31	1.48
	Plane bending	FF2045	1.24	1.48
U-notch R1.5	Push-pull	FF2050	1.80	1.48
	Plane bending	FF2055	1.25	1.48
Fillet R0.7	Push-pull	FF2060	1.18	1.48
	Plane bending	FF2065	1.21	1.48
U-notch R5	Push-pull	FF2070	1.31	1.48
	Plane bending	FF2075	1.14	1.48
Fillet R0.2	Push-pull	FF2080	1.38	1.48
	Plane bending	FF2085	1.14	1.48

Table 6.2: Values of ratio T_σ expressing the width of the scatter bands for the various specimen series. Concerning the PM results, T_σ is equal to 1.48.

Comparing the T_σ derived from the PM with those obtained from raw experimental data, it is possible to see that only one case emerges where the scatter band from the PM is narrower than the one observed on experimental data: this occurs for the FF2050 (corresponding to the U-notch R1.5 loaded under push-pull). For all other series, the scatter band derived from experimental data is narrower than that from the PM. Despite this observation, the overall performance of the PM is considered satisfactory. The value of $T_\sigma = 1.48$ aligns with typical values found in fatigue data scatter bands evaluated between 10% and 90% probabilities of survival. In conclusion, the PM variant of TCD synthesized the stress gradient effects associated with the investigated geometries and loading configurations in an acceptable manner. This validates the PM for design purposes, allowing engineers to:

- evaluate the critical distance using the D_{PM} vs. N_f relationship defined during the method calibration;
- compute the local stress amplitude at the critical distance below the notch root of a notched component, e.g. via FE analysis, and use this stress value in the material S-N curve derived from the Unnotched specimen.

Finally, it is worth to point out one advantage of TCD in general. This approach allows fatigue damage estimations by directly post-processing the linear elastic stress field acting on the fatigue process zone below the root of the notch. This aspect is quite significant, since it allows to avoid the need for complex and time-consuming elastoplastic analyses [7]. With this final consideration on the TCD approach, the data elaboration phase of this experimental thesis come to an end. The conclusions of the work are outlined in the next chapter.

7 CONCLUSIONS

7.1 SUMMARY OF THE CURRENT WORK

7.1.1 Outcomes from the critical volume approach

The present work proposed an innovative approach based on the critical volume to assess multiaxial fatigue of notched specimens. Widely used solutions in the literature, such as the Theory of Critical Distances (TCD) or the Relative Stress Gradient (RSG) approach, typically account only for the stress gradient effect while neglecting the statistical size effect, which is undoubtedly significant for the fatigue strength of engineering materials. This study aimed to enhance the accuracy of multiaxial fatigue predictions by simultaneously accounting for both stress gradient and size effects through the definition of the critical volume (CV) and integrating it into a multiaxial fatigue strength criterion.

The experimental campaign was conducted on structural steel S355J2, testing six specimen geometries: one unnotched and five notched configurations (including V-notch R1.3, U-notch R1.5, Fillet R0.7, U-notch R5 and Fillet R0.2). All specimens were tested under push-pull, torsion and plane bending with a load ratio of $R = -1$ (ensuring the absence of mean stress effect).

Critical volume was defined as the highly cyclic stressed region within the material where cracks are most likely to initiate. The CV is parametrized by the factor $z \in [0; 1]$, representing the portion of the material loaded at least z-times the value of the elastic peak stress at the notch. Dependencies between notch fatigue strength and critical volume were established for both axial and torsion load cases, enabling the calculation of new material parameters for multiaxial fatigue criterion. In this way, the criterion accounts for the CV experienced by the component.

After a preliminary study conducted using the Manson-McKnight (MMK) criterion, aimed at ensuring the existence of the mentioned dependencies, the Dang Van criterion was selected as the reference for testing this innovative approach. Among the positive findings of this work, the following can be outlined:

- the study confirmed a dependency between the notch fatigue strength (evaluated as elastic peak stress amplitude at the root of the notch) and the critical volume (found below the notch root) for both axial and torsion fatigue loads. These dependencies exhibit a monotonic descending trend for hotspot fatigue strength as CV increases, which is consistent with the size effect principle. Experimental data can be reasonably fitted with a power law, but other non-linear regression models could potentially be involved to better capture the theorized asymptotic behaviour at large critical volumes;

- the initial MMK-based study identified optimum z values of 0.56 for axial load case and 0.70 for torsion load case. The more sophisticated approach involving Dang Van criterion required the implementation of a calibration procedure, resulting in an optimum z parameter value of 0.60 for axial load, while 0.70 was confirmed for torsion load. Switching to the Dang Van-based approach improved slightly the fit quality of axial load dependency, which resulted in a higher coefficient of determination of $R^2 = 0.8615$. Meanwhile, for torsion load case the coefficient turned out to be $R^2 = 0.9858$ according to the Dang Van method.

Despite the critical volume approach showed no inconvenience for what concerns notch fatigue strength vs. critical volume dependencies in torsion load case, the axial load case presented several challenges:

- the optimum z values for both axial and torsion load cases have been found are lower than typical levels for critical volume evaluation (0.8 – 0.99) suggested in the literature. Switching from MMK to Dang Van criterion did not significantly improve this aspect;

- notch fatigue strength vs. critical volume dependencies for axial loads displayed notable data scattering, observed in both MMK and Dang Van analyses. Exploring lower z values reduced scattering to some extent, trying to move the push-pull data series closer to the plane bending one. But the two data series still struggle to collapse on a common curve, since they only cross each other and overlap at lower fatigue strengths and larger critical volumes, leaving significant scattering at higher fatigue strengths. The moderate R^2 values suggest that additional variables affecting the critical volume effect, most likely plasticity effects, should be considered in more robust way;

- although the two axial load and torsion load dependencies were supposed to converge on a common optimum z parameter, this did not happen. This divergence complicated the development of a convenient engineering approach where both dependencies would result to be calibrated at the same z;

- finally, it is worth to remember that all the study was conducted at a fixed fatigue life of $N_f = 5 \cdot 10^5$. It would be necessary to extend the discussion to different fatigue life ranges, in order to evaluate the consistency of the approach across a wider fatigue life domain.

As a result, the critical volume approach offers attractive contributions to the integration of the size effect in multiaxial fatigue assessment. However, further refinements are required to address the identified issues and advance the approach to the next stage of development.

7.1.2 Outcomes from the application of the Point Method

Since the critical volume approach presented the challenges outlined above, the Theory of Critical Distances (TCD) was introduced in the study as a more stable alternative for fatigue assessment. The Point Method (PM) variant was selected to implement the TCD approach. Results derived from processing experimental data through the PM demonstrated the robustness of this method. This positive outcome is attributed to the ability of PM to effectively synthesize the stress gradient effects evaluated in the experimental work.

The final S-N diagram, which reports all the processed data points expressed in terms of local stress amplitude evaluated at the critical distance, revealed a scatter band width characterized by a ratio of $T_\sigma = 1.48$, calculated between the stress amplitudes for 10% and 90% probabilities of survival, respectively. This scatter band width aligned with typical values commonly observed in fatigue. Consequently, even though PM accounts only for the stress gradient effect, it provides a functional and practical solution for designing against fatigue of notched mechanical components. Its efficacy is further supported by its extensive validation in existing literature.

7.1.3 Future developments

This thesis work offers a wealth of insights that which could inspire future developments of the proposed methodology. Beyond the needed improvements for the critical volume approach already discussed, a few additional aspects could be explored:

- the RSG approach could provide valuable additional information about the material's behaviour concerning the evaluated notched configurations and fatigue tests. Latest editions of the FKM-Guideline define the fatigue factor n as the product of three subfactors. Specifically, the newly introduced subfactors n_{st} and n_{def} should account for statistical size effect and plasticity effect, respectively. It would be interesting to assess whether this more "traditional" (albeit evolving) approach could better assess size and plasticity effects at the notches;

- as mentioned in Paragraph 7.1.1, it would be valuable to evaluate fatigue lives different from the one here considered, to determine if the proposed approach can adapt effectively to both high-cycle and medium-cycle fatigue regimes;

- eventually, expanding the experimental dataset to include a wider variety of steel alloys would enable a more comprehensive assessment of the critical volume approach. This effort would help clarify how far this method can be generalized across different steel classes, providing useful knowledge about its potential strength and limitations.

In conclusion, the results of this thesis work represent a step forward in understanding the fatigue behaviour of engineering materials, paving the way for the development of further experimental methods to enhance multiaxial fatigue assessment in practice.

8 BIBLIOGRAPHY

[1] F. Berto, A. Gagani, R. Aversa, R. V. V. Petrescu, A. Apicella, and F. I. T. Petrescu, 'Multiaxial fatigue strength to notched specimens made of 40CrMoV13.9', 2016, doi: 10.3844/ajeassp.2016.1269.1291.

[2] J. Schijve, *Fatigue of Structures and Materials*. Springer Science & Business Media, 2008.

[3] B. Atzori, 'Appunti di costruzione di macchine'.

[4] A. J. McEvily, 'Metal Failures – Mechanisms, Analysis, Prevention'.

[5] J. Liu, Y. Ran, L. Xie, and W. Xue, 'Multiaxial fatigue life prediction method of notched specimens considering stress gradient effect', *Fatigue & Fracture of Engineering Materials & Structures*, vol. 44, no. 5, pp. 1406–1419, 2021, doi: 10.1111/ffe.13438.

[6] R. Budynas and K. Nisbett, *Shigley's Mechanical Engineering Design*. McGraw-Hill Companies,Incorporated, 2008.

[7] L. Susmel, *Multiaxial Notch Fatigue*. 2009.

[8] J. Kohout and S. Věchet, 'A new function for fatigue curves characterization and its multiple merits', *International Journal of Fatigue*, vol. 23, no. 2, pp. 175–183, 2001, doi: 10.1016/S0142-1123(00)00082-7.

[9] O. H. Basquin, 'The exponential law of endurance tests', *American Society for Testing and Materials Proceedings*, vol. 10, pp. 625–630, 1910.

[10] F. Fojtík, J. Papuga, M. Fusek, and R. Halama, 'Validation of Multiaxial Fatigue Strength Criteria on Specimens from Structural Steel in the High-Cycle Fatigue Region', *Materials*, vol. 14, no. 1, Art. no. 1, Jan. 2021, doi: 10.3390/ma14010116.

[11] W. Weibull, *Fatigue Testing and Analysis of Results*. 1961.

[12] J. Papuga and F. Fojtík, 'Multiaxial fatigue strength of common structural steel and the response of some estimation methods', *International Journal of Fatigue*, vol. 104, pp. 27–42, Nov. 2017, doi: 10.1016/j.ijfatigue.2017.07.001.

[13] J. Papuga, M. Margetin, and V. Chmelko, 'Various parameters of the multiaxial variable amplitude loading and their effect on fatigue life and fatigue life computation', *Fatigue & Fracture of Engineering Materials & Structures*, vol. 44, no. 10, pp. 2890–2912, 2021, doi: 10.1111/ffe.13560.

[14] L. Susmel and D. Taylor, 'A novel formulation of the theory of critical distances to estimate lifetime of notched components in the medium-cycle fatigue regime', *Fatigue & Fracture of Engineering Materials & Structures*, vol. 30, no. 7, pp. 567–581, 2007, doi: 10.1111/j.1460-2695.2007.01122.x.

[15] M. Nesládek, F. Fojtík, M. Mžourek, and J. Papuga, 'Notched structural steel specimens assessed by selected fatigue analysis methods', *Journal of Constructional Steel Research*, vol. 219, p. 108789, Aug. 2024, doi: 10.1016/j.jcsr.2024.108789.

[16] S. A. McKelvey, Y.-L. Lee, and M. E. Barkey, 'Stress-Based Uniaxial Fatigue Analysis Using Methods Described in FKM-Guideline', *J Fail. Anal. and Preven.*, vol. 12, no. 5, pp. 445–484, Oct. 2012, doi: 10.1007/s11668-012-9599-4.

[17] F. Fojtík and J. Papuga, 'Issues encountered in the application of multiaxial fatigue strength methods to experiments with various stress distributions', *International Journal of Fatigue*, vol. 149, p. 106295, Aug. 2021, doi: 10.1016/j.ijfatigue.2021.106295.

[18] A. Fatemi and N. Shamsaei, 'Multiaxial fatigue: An overview and some approximation models for life estimation', *International Journal of Fatigue*, vol. 33, no. 8, pp. 948–958, Aug. 2011, doi: 10.1016/j.ijfatigue.2011.01.003.

[19] L. Susmel, 'Appunti di Progettazione a Fatica Multiassiale'. 2003.

[20] Y. Verreman and H. Guo, 'High-cycle fatigue mechanisms in 1045 steel under non-proportional axial-torsional loading', *Fatigue & Fracture of Engineering Materials & Structures*, vol. 30, no. 10, pp. 932–946, 2007, doi: 10.1111/j.1460-2695.2007.01164.x.

[21] J. Papuga, M. Vargas, and M. Hronek, 'Evaluation of uniaxial fatigue criteria applied to multiaxially loaded unnotched samples', *Engineering MECHANICS*, vol. 19, pp. 99–111, 2012.

[22] J. Papuga, 'Lectures notes on "Design Against Fatigue - Multiaxial Fatigue Analysis"', Faculty of Mechanical Engineering - Czech Technical University, Apr. 2024.

[23] J. Papuga, E. Cízová, and A. Karolczuk, 'Validating the Methods to Process the Stress Path in Multiaxial High-Cycle Fatigue Criteria', *Materials*, vol. 14, no. 1, Art. no. 1, Jan. 2021, doi: 10.3390/ma14010206.

[24] A. Carpinteri *et al.*, ‘Fatigue assessment of notched specimens by means of a critical plane-based criterion and energy concepts’, *Theoretical and Applied Fracture Mechanics*, vol. 84, pp. 57–63, Aug. 2016, doi: 10.1016/j.tafmec.2016.03.003.
[25] J. Papuga, ‘A survey on evaluating the fatigue limit under multiaxial loading’, *International Journal of Fatigue*, vol. 33, no. 2, pp. 153–165, Feb. 2011, doi: 10.1016/j.ijfatigue.2010.08.001.
[26] M. Nesládek and M. Španiel, ‘An Abaqus plugin for fatigue predictions’, *Advances in Engineering Software*, vol. 103, pp. 1–11, Jan. 2017, doi: 10.1016/j.advengsoft.2016.10.008.
[27] V. Dang, ‘Sur la résistance à la fatigue des métaux’, *Sciences et Techniques de l’armement*, vol. 47. p. 641, 1973.
[28] J. Papuga, A. Karkulín, O. Hanžl, and M. Lutovinov, ‘Comparison of several methods for the notch effect quantification on specimens from 2124-T851 aluminum alloy’, *Procedia Structural Integrity*, vol. 19, pp. 405–414, Jan. 2019, doi: 10.1016/j.prostr.2019.12.044.
[29] M. Leitner, M. Vormwald, and H. Remes, ‘Statistical size effect on multiaxial fatigue strength of notched steel components’, *International Journal of Fatigue*, vol. 104, pp. 322–333, Nov. 2017, doi: 10.1016/j.ijfatigue.2017.08.002.
[30] D. Taylor, ‘The theory of critical distances’, *Engineering Fracture Mechanics*, vol. 75, no. 7, pp. 1696–1705, May 2008, doi: 10.1016/j.engfracmech.2007.04.007.
[31] R. Wang, H. Liu, D. Hu, D. Li, and J. Mao, ‘Evaluation of notch size effect on LCF life of TA19 specimens based on the stress gradient modified critical distance method’, *Fatigue & Fracture of Engineering Materials & Structures*, vol. 41, no. 8, pp. 1794–1809, 2018, doi: 10.1111/ffe.12821.
[32] L. Susmel, ‘The theory of critical distances: a review of its applications in fatigue’, *Engineering Fracture Mechanics*, vol. 75, no. 7, pp. 1706–1724, May 2008, doi: 10.1016/j.engfracmech.2006.12.004.
[33] E. Haibach, *FKM Guideline-Analytical Strength Assessment of Components in Mechanical Engineering*, 5th edition, English Version. Forschungskuratorium Maschinenbau (FKM), 2003.
[34] M. Mžourek, J. Papuga, M. Nesládek, M. Matušů, J. Čapek, and V. Mára, ‘Fatigue Damage Analysis On 42CrMo4+QT Via Critical Volume Approach’, *Procedia Structural Integrity*, vol. 42, pp. 457–464, Jan. 2022, doi: 10.1016/j.prostr.2022.12.058.
[35] J. Papuga, M. Mžourek, M. Matušů, V. Mára, and J. Čapek, ‘Investigation of the size effect on 42CrMo4 + QT steel in the high-cycle fatigue domain part I: Experimental campaign’, *International Journal of Fatigue*, vol. 175, p. 107743, Oct. 2023, doi: 10.1016/j.ijfatigue.2023.107743.
[36] N. Gilbert, ‘Structural Steel - S235, S275, S355 Chemical Composition, Mechanical Properties and Common Applications’, AZoM. [Online]. Available: https://www.azom.com/article.aspx?ArticleID=6022
[37] ‘pyLife 2023 Workshop’. [Online]. Available: https://www.pragtic.com/pyLife_w23.php
[38] Bosh Research, ‘pyLife – a general library for fatigue and reliability’. [Online]. Available: https://pylife.readthedocs.io/en/stable/README.html
[39] Bosh, ‘Bringing Open Source to Mechanical Engineering’. [Online]. Available: https://www.bosch.com/stories/bringing-open-source-to-mechanical-engineering/
[40] ISO 12107, ‘Metallic materials — Fatigue testing — Statistical planning and analysis of data’. International Organization for Standardization, 2003.

9 APPENDIX

9.1 TECHNICAL DRAWINGS OF SPECIMENS

Technical drawings of the specimens tested in the experimental campaign are reported hereafter. Codification of specimen series is explained in Table 3.3, Paragraph 3.1.1.

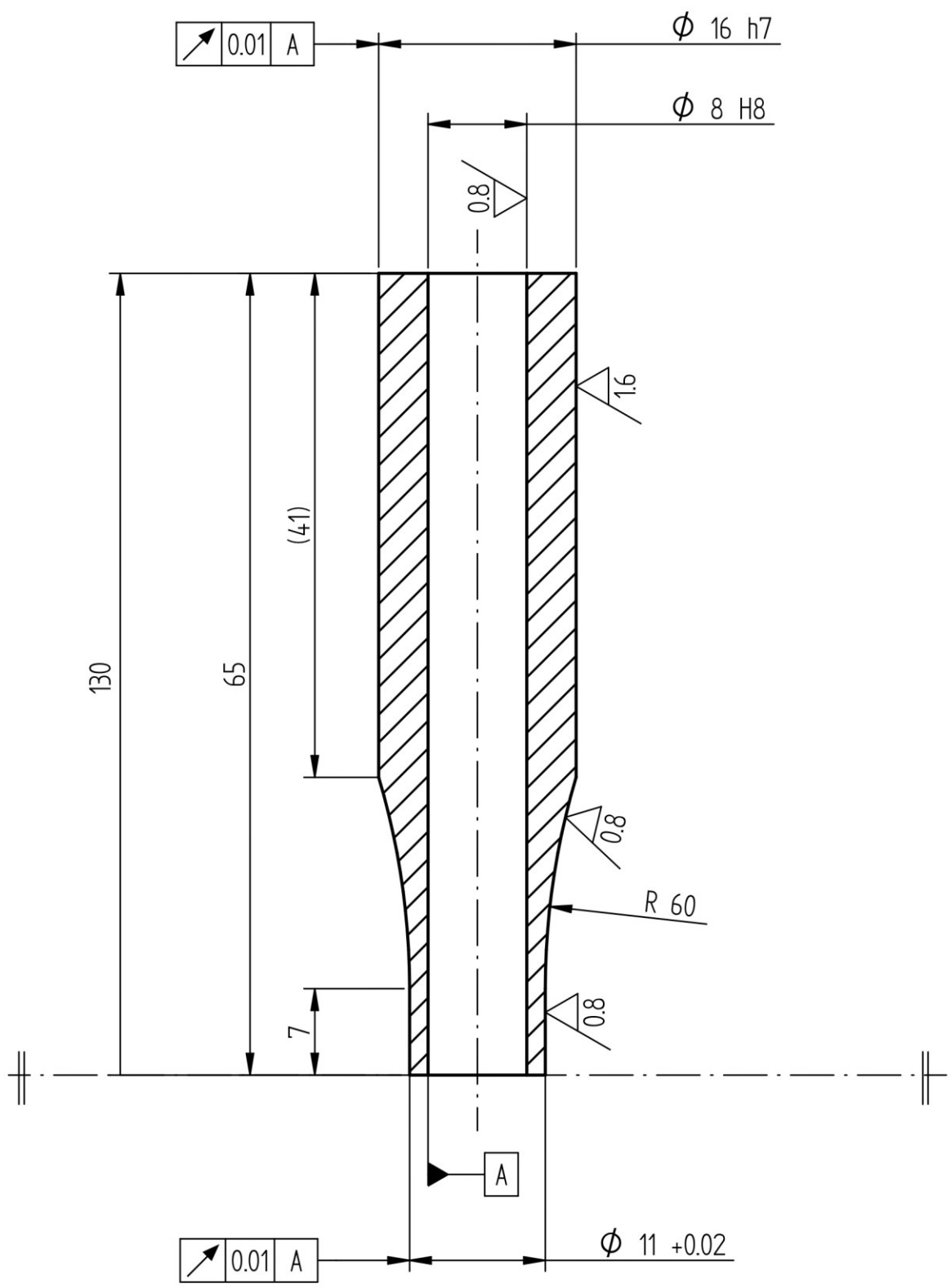

TITLE: UNNOTCHED (FF203_)		MATERIAL: ČSN 411523 (S355J2)	Tolerances according to ISO 8015
SCALE: 2:1	SIZE: A4		
DESIGNER: František Fojtík, Leonardo Serri		DATE: 30/09/2024	FACULTY OF MECHANICAL ENGINEERING CTU IN PRAGUE

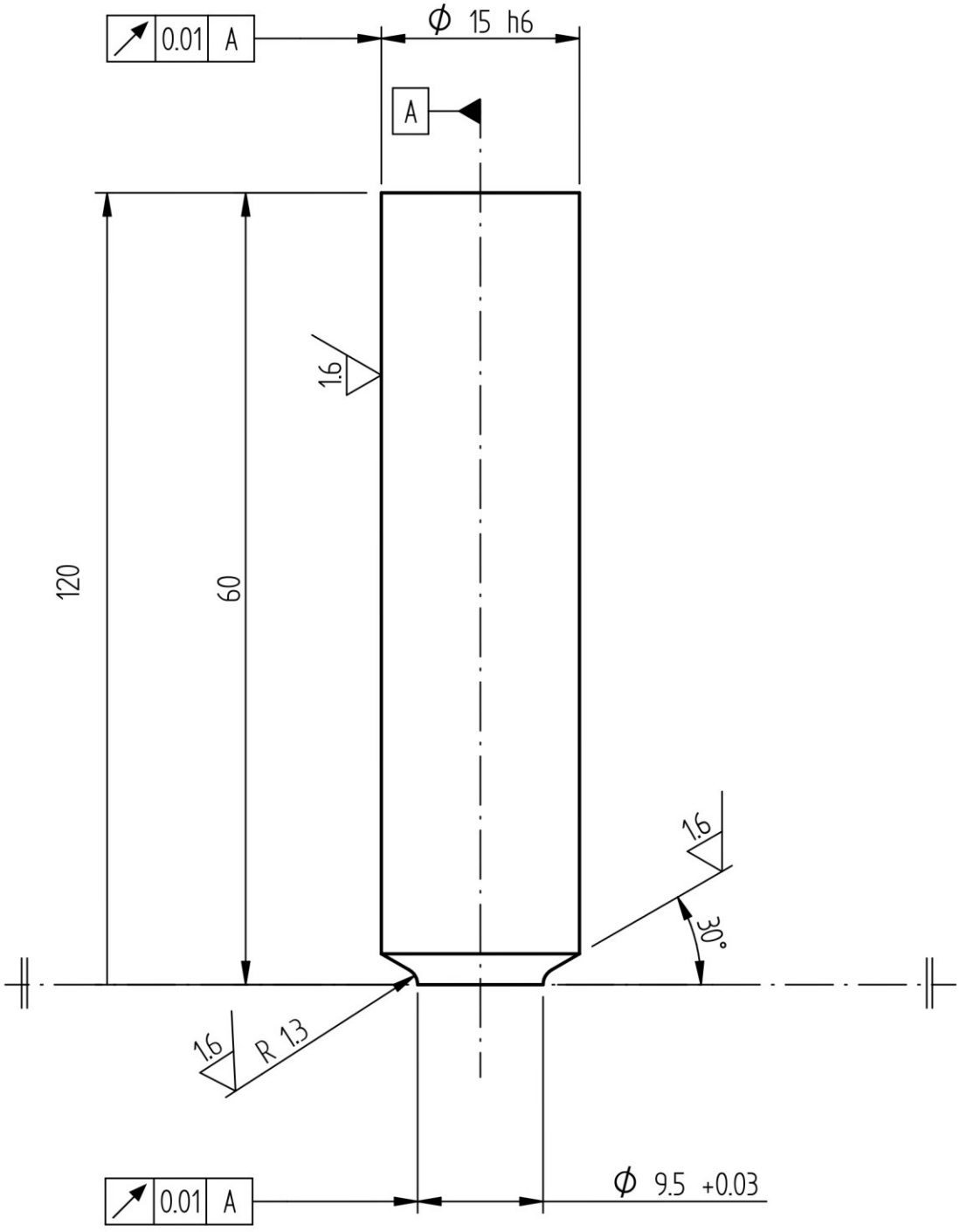

TITLE: V-NOTCH R1.3 (FF204_)		MATERIAL: ČSN 411523 (S355J2)	Tolerances according to ISO 8015
SCALE: 2:1	SIZE: A4		
DESIGNER: František Fojtík, Leonardo Serri		DATE: 30/09/2024	FACULTY OF MECHANICAL ENGINEERING CTU IN PRAGUE

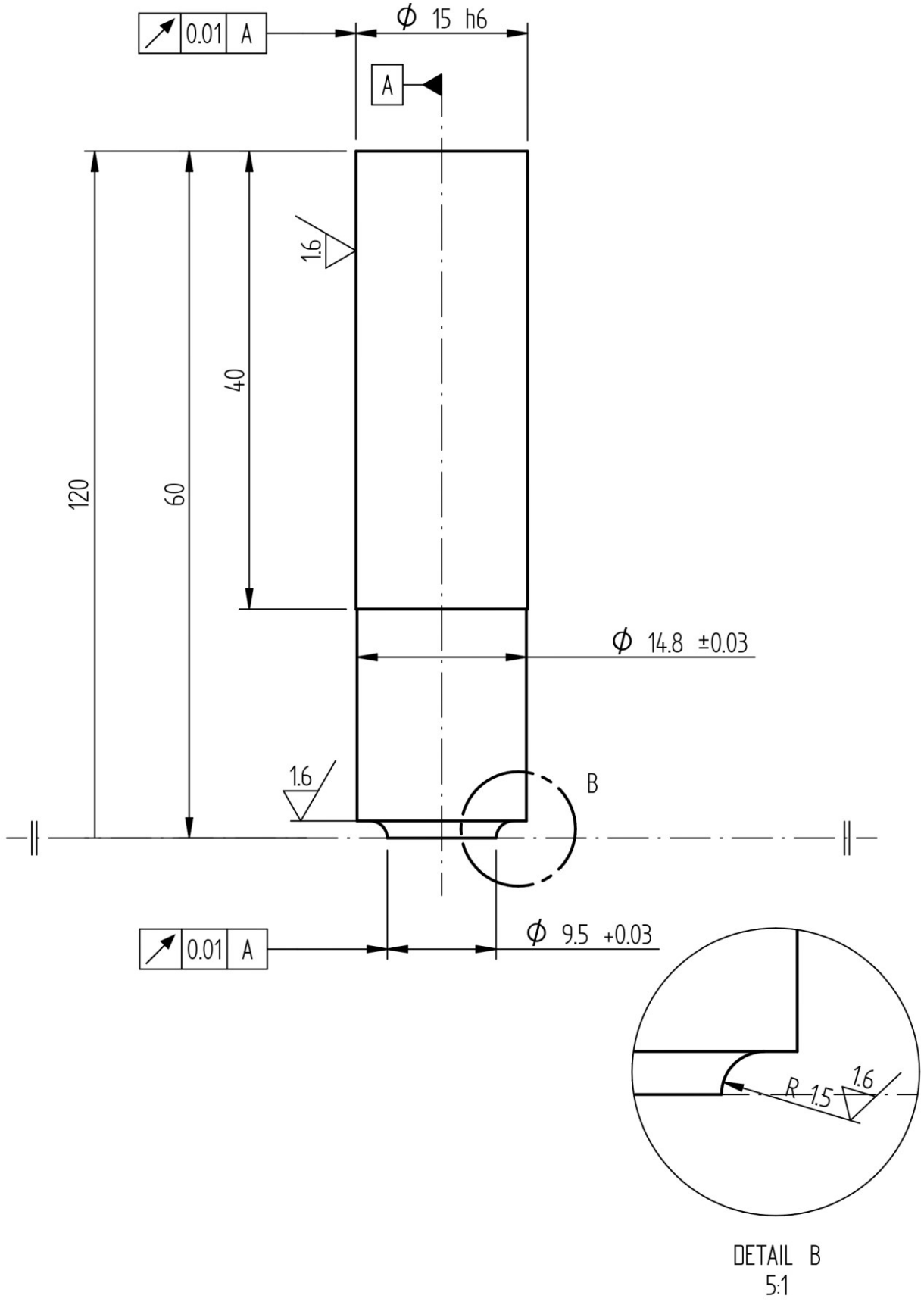

DETAIL B
5:1

TITLE: U-NOTCH R1.5 (FF205_)	MATERIAL: ČSN 411523 (S355J2)	Tolerances according to ISO 8015
SCALE: 2:1 / SIZE: A4		
DESIGNER: František Fojtík, Leonardo Serri	DATE: 30/09/2024	FACULTY OF MECHANICAL ENGINEERING CTU IN PRAGUE

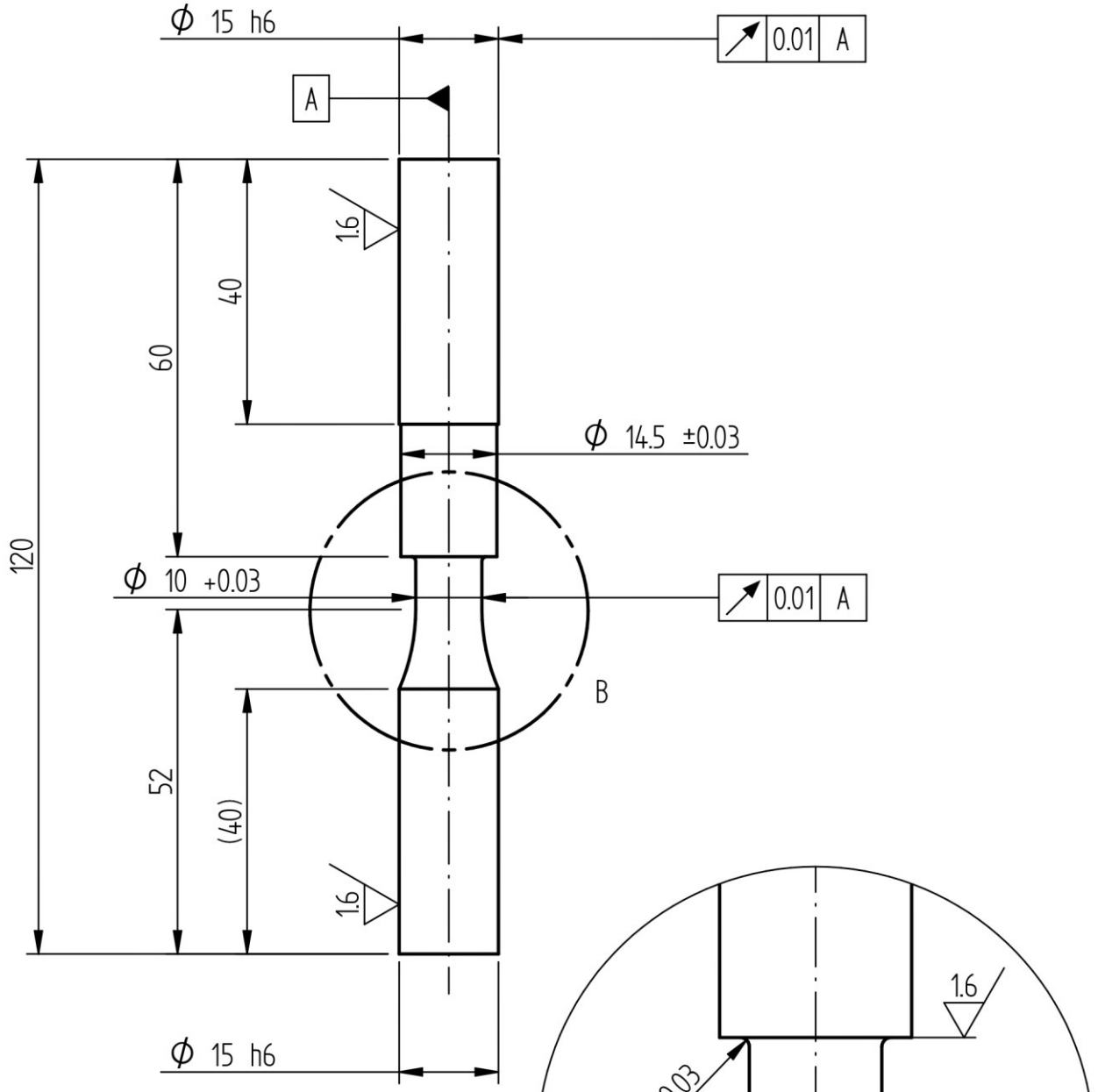

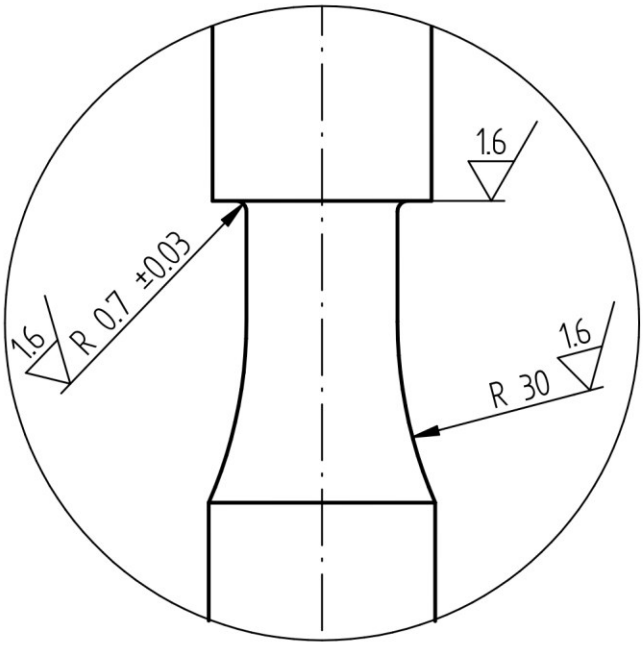

DETAIL B
2:1

TITLE: FILLET R0.7 (FF206_)		MATERIAL: ČSN 411523 (S355J2)	Tolerances according to ISO 8015
SCALE: 2:1	SIZE: A4		
DESIGNER: František Fojtík, Leonardo Serri		DATE: 30/09/2024	FACULTY OF MECHANICAL ENGINEERING CTU IN PRAGUE

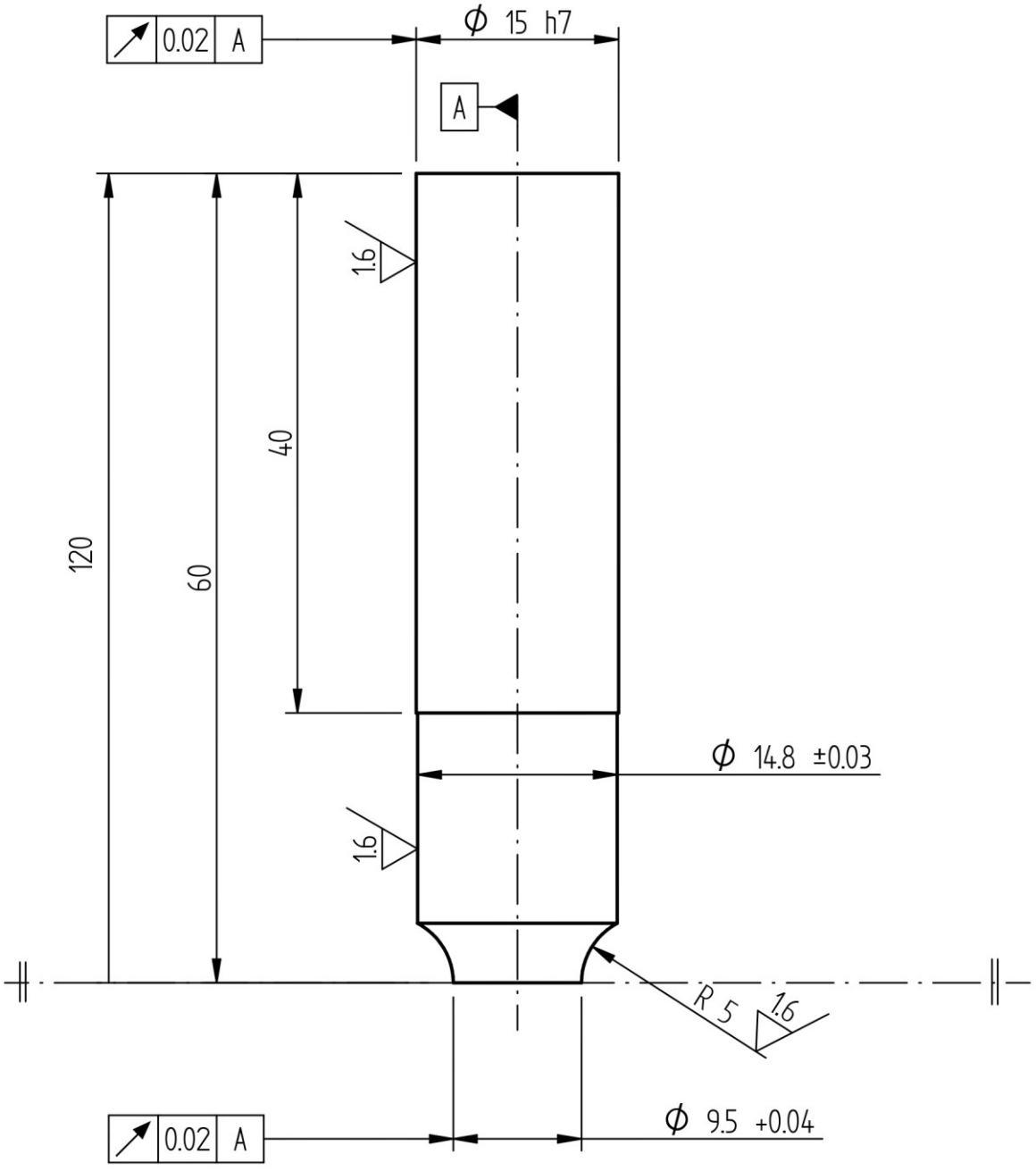

TITLE: U-NOTCH R5 (FF207_)	MATERIAL: ČSN 411523 (S355J2)	Tolerances according to ISO 8015	
SCALE: 2:1	SIZE: A4		
DESIGNER: František Fojtík, Leonardo Serri	DATE: 30/09/2024	FACULTY OF MECHANICAL ENGINEERING CTU IN PRAGUE	

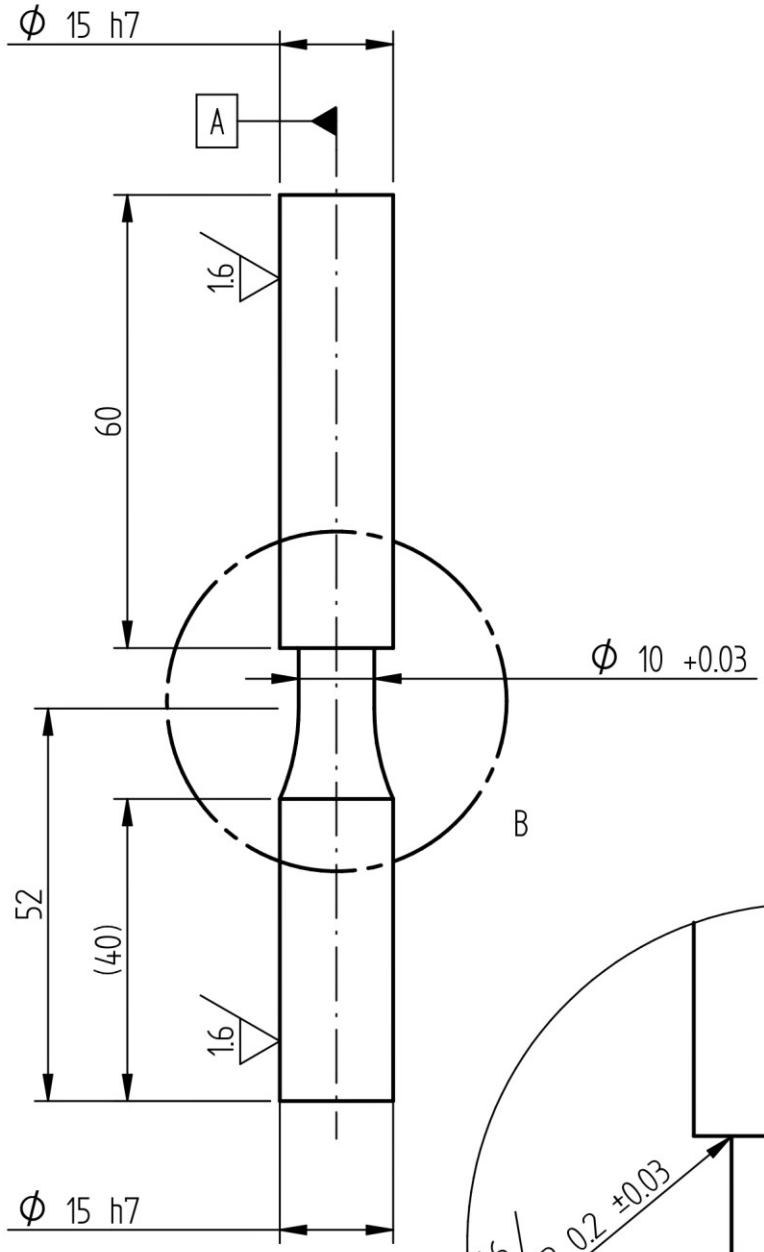

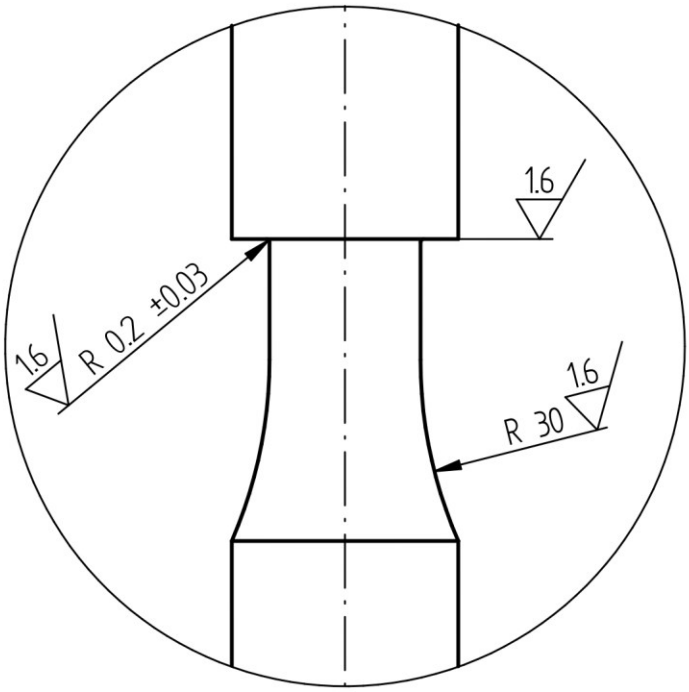

DETAIL B
2:1

TITLE: FILLET R0.2 (FF208_)		MATERIAL: ČSN 411523 (S355J2)	Tolerances according to ISO 8015
SCALE: 2:1	SIZE: A4		
DESIGNER: František Fojtík, Leonardo Serri		DATE: 30/09/2024	FACULTY OF MECHANICAL ENGINEERING CTU IN PRAGUE

9.2 FATIGUE DATA

9.2.1 Experimental data from fatigue tests

Specimen	Load	ID	$\sigma_{a,net}$ [MPa]	N_f
Unnotched	Push-pull	FF2030_8	300.8	16 430
Unnotched	Push-pull	FF2030_13_1	292.7	23 026
Unnotched	Push-pull	FF2030_7	283.4	101 809
Unnotched	Push-pull	FF2030_6	277.7	194 250
Unnotched	Push-pull	FF2030_4	270.8	243 850
Unnotched	Push-pull	FF2030_2	267.1	576 227
Unnotched	Push-pull	FF2030_5	260.3	772 578
Unnotched	Push-pull	FF2030_3	249.7	1 341 204
Unnotched	Push-pull	FF2030_13	243.9	10 000 000

Specimen	Load	ID	$\sigma_{a,net}$ [MPa]	N_f
Unnotched	Torsion	FF2032_11	205.4	19 103
Unnotched	Torsion	FF2032_16	194.3	42 861
Unnotched	Torsion	FF2032_1	188.6	51 540
Unnotched	Torsion	FF2032_10	180.4	111 593
Unnotched	Torsion	FF2032_14	174.4	251 361
Unnotched	Torsion	FF2032_9	169.3	952 356
Unnotched	Torsion	FF2032_15	167.2	3 785 946
Unnotched	Torsion	FF2032_12	163.5	10 546 600

Specimen	Load	ID	$\sigma_{a,net}$ [MPa]	N_f
Unnotched	Plane bending	FF2035_1	348.6	32 443
Unnotched	Plane bending	FF2035_6	329.6	82 355
Unnotched	Plane bending	FF2035_8	311.1	132 912
Unnotched	Plane bending	FF2035_3	298.5	340 900
Unnotched	Plane bending	FF2035_5	288.7	592 773
Unnotched	Plane bending	FF2035_7	282.8	2 260 633
Unnotched	Plane bending	FF2035_2	286.5	2 471 180
Unnotched	Plane bending	FF2035_4	278.6	10 387 380

Specimen	Load	ID	$\sigma_{a,net}$ [MPa]	N_f
V-notch R1.3	Push-pull	FF2040_19_1	338.6	7 652
V-notch R1.3	Push-pull	FF2040_2	282.8	23 066
V-notch R1.3	Push-pull	FF2040_18	225.7	73 189
V-notch R1.3	Push-pull	FF2040_17	197.5	197 350
V-notch R1.3	Push-pull	FF2040_3	169.3	268 983
V-notch R1.3	Push-pull	FF2040_1	183.4	272 597
V-notch R1.3	Push-pull	FF2040_6	155.2	831 710
V-notch R1.3	Push-pull	FF2040_13	141.1	1 722 168
V-notch R1.3	Push-pull	FF2040_19	129.8	10 000 000

Specimen	Load	ID	$\sigma_{a,net}$ [MPa]	N_f
V-notch R1.3	Torsion	FF2042_21	226.4	15 582
V-notch R1.3	Torsion	FF2042_20	206.2	68 182
V-notch R1.3	Torsion	FF2042_10	185.3	289 431
V-notch R1.3	Torsion	FF2042_4	172.8	590 415
V-notch R1.3	Torsion	FF2042_8	167.4	1 402 747
V-notch R1.3	Torsion	FF2042_5	160.9	2 045 825
V-notch R1.3	Torsion	FF2042_14	152.0	2 927 960
V-notch R1.3	Torsion	FF2042_15	144.2	10 399 220

Specimen	Load	ID	$\sigma_{a,net}$ [MPa]	N_f
V-notch R1.3	Plane bending	FF2045_24	301.7	24 632
V-notch R1.3	Plane bending	FF2045_16	253.5	115 058
V-notch R1.3	Plane bending	FF2045_22	216.6	277 631
V-notch R1.3	Plane bending	FF2045_7	193.1	726 100
V-notch R1.3	Plane bending	FF2045_11	181.0	904 290
V-notch R1.3	Plane bending	FF2045_9	170.2	1 004 311
V-notch R1.3	Plane bending	FF2045_12	159.3	1 543 887
V-notch R1.3	Plane bending	FF2045_23	148.5	10 001 000

Specimen	Load	ID	$\sigma_{a,net}$ [MPa]	N_f
U-notch R1.5	Push-pull	FF2050_4_1	282.8	24 328
U-notch R1.5	Push-pull	FF2050_6	226.2	103 397
U-notch R1.5	Push-pull	FF2050_5	197.9	206 246
U-notch R1.5	Push-pull	FF2050_7	175.3	347 519
U-notch R1.5	Push-pull	FF2050_1	184.2	417 841
U-notch R1.5	Push-pull	FF2050_3	156.9	1 422 452
U-notch R1.5	Push-pull	FF2050_2	165.8	4 675 375
U-notch R1.5	Push-pull	FF2050_4	149.9	10 000 000

Specimen	Load	ID	$\sigma_{a,net}$ [MPa]	N_f
U-notch R1.5	Torsion	FF2052_14	228.2	33 514
U-notch R1.5	Torsion	FF2052_13	209.2	109 594
U-notch R1.5	Torsion	FF2052_12	199.1	137 104
U-notch R1.5	Torsion	FF2052_11	184.7	393 575
U-notch R1.5	Torsion	FF2052_10	172.8	944 204
U-notch R1.5	Torsion	FF2052_15	166.9	1 401 089
U-notch R1.5	Torsion	FF2052_16	161.4	2 028 130
U-notch R1.5	Torsion	FF2052_17	152.0	5 061 586

Specimen	Load	ID	$\sigma_{a,net}$ [MPa]	N_f
U-notch R1.5	Plane bending	FF2055_23	297.9	24 328
U-notch R1.5	Plane bending	FF2055_20	283.6	66 175
U-notch R1.5	Plane bending	FF2055_9	250.3	112 864
U-notch R1.5	Plane bending	FF2055_8	214.5	360 574
U-notch R1.5	Plane bending	FF2055_18	197.8	453 570
U-notch R1.5	Plane bending	FF2055_21	181.0	816 061
U-notch R1.5	Plane bending	FF2055_22	167.4	1 594 720
U-notch R1.5	Plane bending	FF2055_19	157.3	10 034 350

Specimen	Load	ID	$\sigma_{a,net}$ [MPa]	N_f
Fillet R0.7	Push-pull	FF2060_12_1	342.4	3 733
Fillet R0.7	Push-pull	FF2060_20	279.6	32 502
Fillet R0.7	Push-pull	FF2060_19	241.4	91 007
Fillet R0.7	Push-pull	FF2060_15	216.0	157 876
Fillet R0.7	Push-pull	FF2060_6	190.6	501 709
Fillet R0.7	Push-pull	FF2060_13	177.5	790 845
Fillet R0.7	Push-pull	FF2060_2	165.2	1 691 222
Fillet R0.7	Push-pull	FF2060_12	158.5	10 000 000

Specimen	Load	ID	$\sigma_{a,net}$ [MPa]	N_f
Fillet R0.7	Torsion	FF2062_21	219.0	11 761
Fillet R0.7	Torsion	FF2062_7	209.4	40 256
Fillet R0.7	Torsion	FF2062_14	193.5	186 330
Fillet R0.7	Torsion	FF2062_9	178.3	437 652
Fillet R0.7	Torsion	FF2062_3	163.0	1 055 529
Fillet R0.7	Torsion	FF2062_10	170.6	1 384 400
Fillet R0.7	Torsion	FF2062_4	152.8	5 113 600
Fillet R0.7	Torsion	FF2062_8	142.6	10 648 000

Specimen	Load	ID	$\sigma_{a,net}$ [MPa]	N_f
Fillet R0.7	Plane bending	FF2065_5_1	292.7	34 243
Fillet R0.7	Plane bending	FF2065_18	268.3	107 938
Fillet R0.7	Plane bending	FF2065_22	235.0	191 810
Fillet R0.7	Plane bending	FF2065_11	212.0	353 050
Fillet R0.7	Plane bending	FF2065_16	202.5	500 812
Fillet R0.7	Plane bending	FF2065_17	189.0	702 710
Fillet R0.7	Plane bending	FF2065_1	173.7	1 112 103
Fillet R0.7	Plane bending	FF2065_5	161.5	10 120 000

Specimen	Load	ID	$\sigma_{a,net}$ [MPa]	N_f
U-notch R5	Push-pull	FF2070_7	296.9	56 807
U-notch R5	Push-pull	FF2070_12	279.2	129 441
U-notch R5	Push-pull	FF2070_6	261.5	203 985
U-notch R5	Push-pull	FF2070_1	240.3	319 252
U-notch R5	Push-pull	FF2070_10	236.8	460 029
U-notch R5	Push-pull	FF2070_4	233.3	1 595 598
U-notch R5	Push-pull	FF2070_3	226.2	2 514 579
U-notch R5	Push-pull	FF2070_2	220.5	10 069 860

Specimen	Load	ID	$\sigma_{a,net}$ [MPa]	N_f
U-notch R5	Torsion	FF2072_25_1	239.1	16 157
U-notch R5	Torsion	FF2072_26	219.8	52 690
U-notch R5	Torsion	FF2072_21	196.6	264 473
U-notch R5	Torsion	FF2072_27	190.1	510 645
U-notch R5	Torsion	FF2072_29	185.3	896 354
U-notch R5	Torsion	FF2072_23	179.3	2 472 800
U-notch R5	Torsion	FF2072_24	172.2	3 120 860
U-notch R5	Torsion	FF2072_25	165.0	10 000 000

Specimen	Load	ID	$\sigma_{a,net}$ [MPa]	N_f
U-notch R5	Plane bending	FF2075_11	334.8	34 724
U-notch R5	Plane bending	FF2075_13_1	316.8	71 669
U-notch R5	Plane bending	FF2075_8	298.9	97 529
U-notch R5	Plane bending	FF2075_22	275.0	286 033
U-notch R5	Plane bending	FF2075_5	263.0	410 519
U-notch R5	Plane bending	FF2075_9	245.1	497 055
U-notch R5	Plane bending	FF2075_19	240.3	783 158
U-notch R5	Plane bending	FF2075_13	235.5	10 263 910

Specimen	Load	ID	$\sigma_{a,net}$ [MPa]	N_f
Fillet R0.2	Push-pull	FF2080_8	216.5	87 714
Fillet R0.2	Push-pull	FF2080_9	178.3	186 714
Fillet R0.2	Push-pull	FF2080_18	172.0	250 612
Fillet R0.2	Push-pull	FF2080_10	165.5	367 533
Fillet R0.2	Push-pull	FF2080_12	161.1	441 500
Fillet R0.2	Push-pull	FF2080_13	153.7	879 166
Fillet R0.2	Push-pull	FF2080_15	144.7	3 707 398
Fillet R0.2	Push-pull	FF2080_16	136.0	4 791 521

Specimen	Load	ID	$\sigma_{a,net}$ [MPa]	N_f
Fillet R0.2	Torsion	FF2082_24	199.8	40 432
Fillet R0.2	Torsion	FF2082_17	179.9	78 110
Fillet R0.2	Torsion	FF2082_21	172.7	396 420
Fillet R0.2	Torsion	FF2082_7	164.5	747 751
Fillet R0.2	Torsion	FF2082_20	158.8	2 316 295
Fillet R0.2	Torsion	FF2082_6	154.6	3 487 906
Fillet R0.2	Torsion	FF2082_22	149.0	6 026 119
Fillet R0.2	Torsion	FF2082_23	143.3	8 509 360

Specimen	Load	ID	$\sigma_{a,net}$ [MPa]	N_f
Fillet R0.2	Plane bending	FF2085_3	234.3	121 977
Fillet R0.2	Plane bending	FF2085_19	220.3	208 620
Fillet R0.2	Plane bending	FF2085_2	203.7	249 204
Fillet R0.2	Plane bending	FF2085_4	188.4	545 826
Fillet R0.2	Plane bending	FF2085_1	173.2	760 536
Fillet R0.2	Plane bending	FF2085_5	163.0	1 145 826
Fillet R0.2	Plane bending	FF2085_11	158.3	1 653 993
Fillet R0.2	Plane bending	FF2085_14	149.5	10 783 752

9.2.2 Parameters for Basquin and Kohout-Věchet regression models

Table 9.1 and Table 9.2 report the regression parameters obtained from fitting the experimental fatigue data with the Basquin formula and the K-V model, respectively.

Specimen	Load	Mark	Basquin model		
			C_B	w	s_{logN}
Unnotched	Push-pull	FF2030	2.75E+67	25.49	0.155
	Torsion	FF2032	5.64E+47	18.85	0.182
	Plane bending	FF2035	4.78E+42	15.02	0.080
V-notch R1.3	Push-pull	FF2040	7.16E+18	5.93	0.108
	Torsion	FF2042	1.13E+36	13.50	0.093
	Plane bending	FF2045	2.10E+20	6.38	0.099
U-notch R1.5	Push-pull	FF2050	8.75E+18	5.93	0.088
	Torsion	FF2052	1.36E+33	12.14	0.055
	Plane bending	FF2055	6.41E+20	6.58	0.105
Fillet R0.7	Push-pull	FF2060	8.13E+23	7.98	0.093
	Torsion	FF2062	1.21E+41	15.74	0.178
	Plane bending	FF2065	1.51E+20	6.29	0.086
U-notch R5	Push-pull	FF2070	2.04E+25	8.29	0.076
	Torsion	FF2072	4.12E+43	16.60	0.111
	Plane bending	FF2075	1.71E+27	8.97	0.084
Fillet R0.2	Push-pull	FF2080	3.00E+19	6.26	0.114
	Torsion	FF2082	6.76E+45	18.00	0.187
	Plane bending	FF2085	1.13E+20	6.31	0.058

Table 9.1: Basquin regression parameters used for fitting S-N curves.

Specimen	Load	Mark	Kohout-Věchet model				
			A	B	C_{K-V}	β	$s_{log\sigma}$
Unnotched	Push-pull	FF2030	601.5	52163	2031734	-0.06	0.006
	Torsion	FF2032	536.2	1	141699	-0.10	0.003
	Plane bending	FF2035	120822.9	53722	97628	-0.53	0.005
V-notch R1.3	Push-pull	FF2040	2292.9	2919	1215313	-0.21	0.015
	Torsion	FF2042	506.9	7855	19555358	-0.08	0.008
	Plane bending	FF2045	11294.1	80459	1139115	-0.31	0.016
U-notch R1.5	Push-pull	FF2050	1672202.5	61624	165465	-0.77	0.020
	Torsion	FF2052	562.5	1	13738873	-0.09	0.005
	Plane bending	FF2055	77601640.1	186365	386711	-1.02	0.012
Fillet R0.7	Push-pull	FF2060	2428.7	12138	781268	-0.20	0.007
	Torsion	FF2062	614.4	42653	4074053	-0.09	0.012
	Plane bending	FF2065	2221613.4	166863	452851	-0.74	0.011
U-notch R5	Push-pull	FF2070	339672.1	65902	142164	-0.62	0.013
	Torsion	FF2072	469.6	1	2405596	-0.07	0.006
	Plane bending	FF2075	776008.0	92145	189220	-0.67	0.013
Fillet R0.2	Push-pull	FF2080	12031.1	1	200865	-0.37	0.012
	Torsion	FF2082	342.7	1	5644842901	-0.05	0.012
	Plane bending	FF2085	1250085.6	159636	443231	-0.70	0.011

Table 9.2: K-V regression parameters used for fitting S-N curves

9.3 SCRIPTS

As explained in Section 3.3, PyLife package (implemented in Python coding language) was used for the implementation of the scripts used to evaluate the critical volume. The *odbclient* class is one of the most important ones because it allows to read .odb files from FE analyses computed in Abaqus, and it can also perform several additional operations on those data. A brief description of main functionalities of this class are presented hereafter:

- *OdbClient()*: it reads the .odb file, once the file path has been specified together with the "bin path" (a system information related to Abaqus installation) and the "environment path" (related to the virtual environment where the python script operates);
- *step_names()*: it reads the steps of the analysis. For what concerns the axisymmetric models, step No.1 was related to the tension analysis, while step. No.2 to the torsion analysis. Instead, plane bending analysis had only one step;
- *variable()*: it reads the specified variable from the .odb ('S': nodal stresses, 'EVOL': element volumes), once the instance (related to the Abaqus model), the step and the frame (a single step can be made by several frames in Abaqus) are given as inputs to the function.

Moreover:

- from the *pylife.stress* class the *equistress* module can be imported. This module is used to calculate von Mises stresses while developing the critical volume approach using the MMK criterion (calling the *equistress.mises()*);
- from the *pylife.mesh* class the *hotspot.calc()* module can be imported. This module is used to detect the hotspot in the mesh, after having specified the value of parameter z.

For further information about PyLife functionalities, it is possible to refer to the official documentation provided by Bosh Research in [38].

9.3.1 Python script for critical volume evaluation using MMK criterion

The main operations are performed inside the function named *critical_volume*. The breakdown of this function is reported hereafter:

1. One step (Tension, Torsion or Bending) and one value of z parameter are selected.
2. Nodal stresses, element volumes and nodal coordinates are read from the mesh and collected inside the DataFrame called *mesh_notavg*.
3. Nodal stresses are averaged, thus a new DataFrame named *mesh_avg* is created.
4. The *mesh_avg* DataFrame is filtered in order to keep only elements included in the element set called 'SET-NOTCH' defined in the Abaqus models. The aim of this operation is to focus only on one subset of the mesh located around the notch, in order to speed up the operations (there is no need to check the hotspot in points which are far from the notch hotspot).
5. Calculation of the equivalent stress using von Mises.
6. Detection of the hotspot by PyLife function *hotspot.calc()*. The new column of *mesh_avg* named 'hotspot' contains ne number of the hotspot to which the node belongs: since all specimens have one notch, only one possible hotspot can exist. The dimension of such hotspot depends of the value of z parameter.
7. For each mesh element, nodes included inside the hotspot (and thus inside the CV) are counted (the number is collected in 'hs_nodes' of the 'crit' DataFrame)
8. Critical volume of each element (CV_i) is calculated according to equation 3.15.
9. Overall critical volume for the specific specimen series is obtained according to equation 3.16.

```python
import pandas as pd
from pylife.stress import equistress
from pylife.mesh import hotspot
import time
import odbclient as CL

### > > > ACCESS TO THE ODB FILE
startP = time.time()

abqBinPath = 'C:\\SIMULIA\\CAE\\2019\\win_b64\\code\\bin\\SMALauncher.exe'
envPath = 'C:\\Users\\Utente\\anaconda3\\envs\\odbserver\\'
# path where odb files are stored
abqWorkDir = 'D:\\DATI\\OneDrive - Università degli Studi di Padova\\Università\\MAGISTRALE\\INGEGNERIA MECCANICA\\THESIS\\FEA\\Spec

# > Select the folder where the odb is stored
abqOdbFolder = 'Unnotched'

# > Select the specimen's odb to analyse
abqOdb = 'Job-Unnotched_axisym'

abqOdbPath = abqWorkDir + abqOdbFolder + '\\' + abqOdb + '.odb'

### > > > SETTINGS FOR THE ANALYSIS
startP = time.time()
print(f'Reading the {abqOdb}.odb file...\n')
client = CL.OdbClient(odb_file = abqOdbPath, abaqus_bin = abqBinPath, python_env_path = envPath)

bool_var = input('Is the model axisymmetric? Type \'y\' if Yes, type anything else if No ')
if bool_var == 'y' or bool_var == 'Y':
    instance = client.instance_names()[-1]
    elNodes = 8         # number of nodes in a planar element
else:
    instance = 'PART-NOTCH-1'
    elNodes = 20        # number of nodes in a brick element

steps = client.step_names()
frame = 1
setName = 'SET-NOTCH'   # name of the set which includes the notch

threshold = [0.50, 0.52, 0.53, 0.54, 0.55, 0.56, 0.57, 0.60, 0.65, 0.70, 0.75, 0.80, 0.85, 0.90, 0.95, 0.97, 0.99]

end = time.time()
print(f'Completed in: {str(end-startP)}s \n--------------------\n')

### > > > CRITICAL VOLUME EVALUATION: FUNCTION DEFINITION
def critical_volume(instance, steps, frame, setName, elNodes, threshold):
    # This function takes as input the variables related to Abaqus model setting:
        # 'instance', 'steps', 'frame', 'setName', the number of element nodes 'elNodes',
        # and also the values of factor z contained in 'threshold'

    result = []
    for step in steps:

        first_iter = 1
        for z in threshold:

            # It checks if it is the first iteration. If yes, it reads the mesh only once. If no, it does not read again the mesh.
            if first_iter == 1:

                first_iter = 0

                # > MESH DATAFRAME CREATION: elements and nodes of the whole model are imported
                start = time.time()
                print(f'## Analysing step: {step}, threshold: {str(z)} ##\n')
                print('Creating \'mesh_notavg\' DataFrame...\n')

                mesh_notavg = client.variable('S', instance, step_name=step, frame_id=frame)
                mesh_notavg = mesh_notavg.swaplevel()
                mesh_notavg = mesh_notavg.join(client.variable('EVOL', instance, step_name=step, frame_id=frame))
                mesh_notavg = client.node_coordinates(instance).join(mesh_notavg)
                print(f'--> \'mesh_notavg\' DataFrame rows: {str(len(mesh_notavg.index))}')

                end = time.time()
                print(f'Completed in: {str(end-start)}s \n--------------------\n')

                # > STRESS AVERAGING: arithmetic mean value of nodal stresses is computed
                start = time.time()
                print('Averaging the stresses and creating \'mesh_avg\' DataFrame...\n')

                components = ['S11', 'S22', 'S33', 'S12', 'S13', 'S23']
                stress_avg = mesh_notavg.groupby('node_id')[components].mean().reset_index()
                mesh_notavg.reset_index(inplace=True)
                mesh_avg = pd.merge(mesh_notavg[['element_id', 'node_id', 'x', 'y', 'z', 'EVOL']], stress_avg, on='node_id')
                mesh_avg.set_index(['element_id','node_id'], inplace=True)
                #it shifts 'EVOL' column to the last position
                mesh_avg = mesh_avg[['x', 'y', 'z', 'S11', 'S22', 'S33', 'S12', 'S13', 'S23', 'EVOL']]

                end = time.time()
                print(f'Completed in: {str(end-start)}s \n--------------------\n')

                # > FILTERING OF THE AVERAGED SUBSET: only nodes belonging to the set are considered from now
                start = time.time()
                print('Filtering \'mesh_avg\' DataFrame...\n')

                set_element_ids = client.element_ids(setName, instance)
                print(f'--> The set {setName} included in the instance {instance} has {str(len(set_element_ids))} nodes')

                mesh_avg = mesh_avg[mesh_avg.index.get_level_values('element_id').isin(set_element_ids)]
                mesh_avg = mesh_avg.sort_index(level=['element_id', 'node_id'])
```

```
100
101                 end = time.time()
102                 print(f'Completed in: {str(end-start)}s \n--------------------\n')
103
104                 # > EQUIVALENT STRESS CALCULATION (Manson-McKnight = von Mises)
105                 start = time.time()
106                 print('Calculating the equivalent stress in the subset...\n')
107                 mesh_avg['equivalent_S'] = mesh_avg.equistress.mises()
108
109                 end = time.time()
110                 print(f'Completed in: {str(end-start)}s \n--------------------\n')
111
112             # > HOTSPOT DETECTION
113             start = time.time()
114             print('Finding the hotspot according to the threshold: ' + str(z) + '*Sigma_Max...\n')
115             mesh_avg.loc[:, 'hotspot'] = mesh_avg.hotspot.calc('equivalent_S', z)
116             print("%d hotspots found over the threshold" % mesh_avg['hotspot'].max())
117             mesh_avg = mesh_avg[mesh_avg['hotspot'] != 0]
118
119             # optional: node labels included in the critical volume can be saved in a text file,
120             # in order to be visualized later in Abaqus.
121             with open(abqWorkDir + abqOdbFolder + '\\HOTSPOT_node_ids_' + step + '_' + str(z) + '.txt', 'w') as file:
122                 file.write(str(mesh_avg.index.get_level_values('node_id').tolist()))
123
124             end = time.time()
125             print(f'Completed in: {str(end-start)}s \n--------------------\n')
126
127             # > COUNT OF THE HOTSPOT NODES
128             start = time.time()
129             print('Counting the number of hotspot nodes...\n')
130
131             # the 'crit' dataframe collects the nodes inside the critical volume.
132             crit = pd.DataFrame(columns=['element_id', 'EVOL', 'hs_nodes'])
133             rows = []
134
135             for element_id, element in mesh_avg.groupby('element_id'):
136
137                 hotspots = 0
138                 for _, row in element.iterrows():
139
140                     hotspots += 1
141                 row_node = {'element_id': element_id, 'EVOL': element['EVOL'].iloc[0], 'hotspot': element['hotspot'].iloc[0],
142                             'hs_nodes': hotspots}
143                 rows.append(row_node)
144
145             crit = pd.DataFrame(rows)
146             crit.set_index(['element_id'], inplace=True)
147             end = time.time()
148             print(f'Completed in: {str(end-start)}s \n--------------------\n')
149
150             # > CRITICAL VOLUME CALCULATION
151             start = time.time()
152             print('Computing the critical volume...\n')
153
154             cv = []
155             for element_id in crit.index:
156
157                 el_cv = (crit.loc[element_id, 'EVOL']) * (crit.loc[element_id, 'hs_nodes']) / elNodes  # element's critical volume
158                 cv.append(el_cv)
159
160             crit['critical_volume'] = cv
161             crit_vol = crit['critical_volume'].sum()
162             result_row = {'specimen': abqOdbFolder, 'load': step, 'factor_n': z, 'critical_volume': crit_vol}
163             result.append(result_row)
164
165             print(f'LOAD TYPE: {step}, FACTOR: {str(z)}')
166             print(f'--> CRITICAL VOLUME equal to: {str(crit_vol)}\n')
167
168             endP = time.time()
169             print(f'Completed in: {str(end-start)}s \n--------------------\n')
170             print('Total execution time: ' + str((endP - startP)/60) + ' minutes\n--------------------\n')
171
172     result = pd.DataFrame(result)
173     csv_critVol_path = abqWorkDir + abqOdbFolder + '\\' + abqOdb + '_CriticalVolume.csv'
174     result.to_csv(csv_critVol_path)
175
176     return()
177
178 ### > > > RUN THE FUNCTION
179 critical_volume(instance, steps, frame, setName, elNodes, threshold)
180
```

9.4 CRITICAL VOLUME APPROACH DATA

9.4.1 Critical volumes evaluated with MMK criterion

Specimen	Load	Mark	Critical volume [mm^3] according to z parameter (MMK)											
			0.5	0.55	0.6	0.65	0.7	0.75	0.8	0.85	0.9	0.95	0.99
Unnotched	**push-pull**	**FF2030**	1.996E+03	1.805E+03	1.657E+03	1.519E+03	1.395E+03	1.284E+03	1.172E+03	1.062E+03	9.446E+02	7.981E+02	4.250E+02
	plane bending	**FF2035**	5.835E+02	4.856E+02	3.872E+02	2.933E+02	2.074E+02	1.352E+02	7.901E+01	3.906E+01	1.474E+01	3.132E+00	2.671E-01
V-notch	**push-pull**	**FF2040**	2.295E+01	1.626E+01	1.179E+01	9.046E+00	6.111E+00	4.563E+00	3.126E+00	1.835E+00	1.220E+00	6.960E-01	3.039E-01
	plane bending	**FF2045**	7.624E+00	5.395E+00	3.894E+00	2.667E+00	1.858E+00	1.221E+00	6.834E-01	4.477E-01	2.462E-01	1.192E-01	2.353E-02
U-notch R1.5	**push-pull**	**FF2050**	2.913E+01	2.131E+01	1.615E+01	1.172E+01	8.652E+00	5.929E+00	4.112E+00	2.132E+00	1.479E+00	7.840E-01	3.221E-01
	plane bending	**FF2055**	9.889E+00	7.055E+00	5.063E+00	3.448E+00	2.448E+00	1.592E+00	9.121E-01	6.174E-01	3.466E-01	1.694E-01	3.256E-02
Fillet R0.7	**push-pull**	**FF2060**	2.614E+01	9.740E+00	4.950E+00	3.091E+00	1.342E+00	1.042E+00	8.778E-01	5.690E-01	4.595E-01	2.971E-01	1.350E-01
	plane bending	**FF2065**	1.252E+01	4.742E+00	1.509E+00	8.279E-01	4.699E-01	3.004E-01	1.700E-01	9.835E-02	5.652E-02	2.898E-02	7.424E-03
U-notch R5	**push-pull**	**FF2070**	6.502E+02	2.526E+02	1.699E+02	1.199E+02	8.459E+01	5.778E+01	3.847E+01	2.352E+01	1.107E+01	3.542E+00	1.051E+00
	plane bending	**FF2075**	5.976E+01	4.340E+01	3.101E+01	2.177E+01	1.476E+01	9.505E+00	5.659E+00	2.977E+00	1.334E+00	4.032E-01	7.135E-02
Fillet R0.2	**push-pull**	**FF2080**	8.019E-01	4.950E-01	3.252E-01	2.093E-01	1.540E-01	1.014E-01	7.146E-02	3.457E-02	2.472E-02	1.336E-02	5.797E-03
	plane bending	**FF2085**	2.771E-01	1.665E-01	1.080E-01	7.264E-02	4.454E-02	2.999E-02	2.212E-02	1.449E-02	9.234E-03	4.621E-03	8.555E-04

Specimen	Load	Mark	Critical volume [mm^3] according to z parameter (MMK)										
			0.5	0.55	0.6	0.65	0.7	0.75	0.8	0.85	0.9	0.95	0.99
Unnotched	**torsion**	**FF2032**	1.623E+03	1.489E+03	1.368E+03	1.254E+03	1.140E+03	9.648E+02	7.332E+02	5.420E+02	3.370E+02	1.489E+02	2.171E+01
V-notch	**torsion**	**FF2042**	6.381E+01	4.831E+01	3.517E+01	2.577E+01	1.850E+01	1.285E+01	8.503E+00	4.841E+00	2.770E+00	1.044E+00	3.473E-01
U-notch R1.5	**torsion**	**FF2052**	7.751E+01	5.670E+01	4.299E+01	3.065E+01	2.250E+01	1.563E+01	9.945E+00	5.789E+00	3.262E+00	1.246E+00	3.681E-01
Fillet R0.7	**torsion**	**FF2062**	1.670E+02	1.272E+02	8.622E+01	4.429E+01	1.233E+01	6.035E+00	3.156E+00	1.771E+00	8.387E-01	4.595E-01	2.155E-01
U-notch R5	**torsion**	**FF2072**	2.334E+02	1.837E+02	1.447E+02	1.107E+02	8.294E+01	5.961E+01	4.012E+01	2.488E+01	1.304E+01	4.593E+00	9.755E-01
Fillet R0.2	**torsion**	**FF2082**	1.399E+01	5.558E+00	2.845E+00	1.620E+00	9.702E-01	5.956E-01	3.609E-01	2.088E-01	9.585E-02	2.955E-02	9.084E-03

Table 9.3: Critical volumes calculated at different z parameters using the MMK criterion.

9.4.2 Notch fatigue strength vs. critical volume regressions (MMK)

Regression parameters of the preliminary notch fatigue strength vs. critical volume dependencies evaluated with the MMK criterion are reported hereafter. Concerning the axial loading case, parameters of both power law and K-V regressions are reported in Table 9.4 and Table 9.5, respectively, with reference to the best-fit condition ($z = 0.56$). While power law regression parameters found for the torsion case are collected in Table 9.6, again with reference to the best condition ($z = 0.70$).

Axial load case – power law model (MMK)					
$\boldsymbol{N_f}$	$\boldsymbol{z}$	$\boldsymbol{C_B}$	$\boldsymbol{w}$	$\boldsymbol{R^2}$	$\boldsymbol{RMSE}$ **[MPa]**
500000	0.56	9.35E+28	10.943	0.7495	39.16

Table 9.4: Power law regression parameters for axial load dependencies evaluated with MMK.

Axial load case – K-V model (MMK)							
$\boldsymbol{N_f}$	z	A	B	C_{K-V}	β	R^2	$\boldsymbol{RMSE}$ **[MPa]**
500000	0.56	1082.82	1.64	2.64	-1.343	0.8889	28.83

Table 9.5: K-V regression parameters for axial load dependencies evaluated with MMK.

Torsion load case – power law model (MMK)					
$\boldsymbol{N_f}$	$\boldsymbol{z}$	$\boldsymbol{C_B}$	$\boldsymbol{w}$	$\boldsymbol{R^2}$	$\boldsymbol{RMSE}$ **[MPa]**
500000	0.70	1.27E+25	9.901	0.9975	2.71

Table 9.6: Power law regression parameters for torsion dependencies evaluated with MMK.

9.4.3 Critical volumes evaluated with Dang Van criterion

Specimen	Load	Mark	Critical volume [mm^3] according to z parameter (Dang Van)										
			0.5	0.55	0.6	0.65	0.7	0.75	0.8	0.85	0.9	0.95	0.99
Unnotched	**push-pull**	**FF2030**	2.031E+03	1.852E+03	1.701E+03	1.571E+03	1.446E+03	1.336E+03	1.230E+03	1.119E+03	1.009E+03	8.773E+02	3.588E+01
	plane bending	**FF2035**	5.655E+02	4.644E+02	3.620E+02	2.665E+02	1.824E+02	1.169E+02	6.680E+01	3.231E+01	1.250E+01	2.953E+00	2.558E-01
V-notch	**push-pull**	**FF2040**	4.942E+01	3.325E+01	2.353E+01	1.667E+01	1.139E+01	7.860E+00	4.797E+00	3.128E+00	1.394E+00	6.960E-01	3.039E-01
	plane bending	**FF2045**	1.379E+01	9.483E+00	6.535E+00	4.449E+00	2.914E+00	1.852E+00	1.118E+00	5.918E-01	2.861E-01	1.187E-01	2.335E-02
U-notch R1.5	**push-pull**	**FF2050**	6.542E+01	4.408E+01	3.043E+01	2.131E+01	1.469E+01	9.806E+00	6.671E+00	3.972E+00	1.664E+00	7.840E-01	3.221E-01
	plane bending	**FF2055**	1.719E+01	1.191E+01	8.187E+00	5.637E+00	3.757E+00	2.312E+00	1.445E+00	7.277E-01	3.945E-01	1.691E-01	3.281E-02
Fillet R0.7	**push-pull**	**FF2060**	2.035E+01	1.127E+01	6.020E+00	3.998E+00	2.745E+00	1.783E+00	9.212E-01	7.851E-01	4.595E-01	2.971E-01	1.350E-01
	plane bending	**FF2065**	5.963E+00	3.271E+00	1.923E+00	1.168E+00	7.130E-01	4.374E-01	2.467E-01	1.312E-01	6.357E-02	2.585E-02	7.425E-03
U-notch R5	**push-pull**	**FF2070**	5.128E+02	3.965E+02	2.732E+02	1.897E+02	1.306E+02	8.865E+01	5.676E+01	3.386E+01	1.695E+01	6.031E+00	1.051E+00
	plane bending	**FF2075**	7.474E+01	5.495E+01	3.966E+01	2.795E+01	1.890E+01	1.219E+01	7.309E+00	3.886E+00	1.668E+00	4.342E-01	7.053E-02
Fillet R0.2	**push-pull**	**FF2080**	1.609E+00	9.689E-01	6.179E-01	4.066E-01	2.724E-01	1.814E-01	1.153E-01	6.913E-02	2.774E-02	1.286E-02	5.797E-03
	plane bending	**FF2085**	5.210E-01	3.074E-01	1.899E-01	1.219E-01	7.454E-02	4.828E-02	2.694E-02	1.674E-02	9.344E-03	4.492E-03	8.676E-04

Specimen	Load	Mark	Critical volume [mm^3] according to z parameter (Dang Van)										
			0.5	0.55	0.6	0.65	0.7	0.75	0.8	0.85	0.9	0.95	0.99
Unnotched	**torsion**	**FF2032**	1.623E+03	1.489E+03	1.368E+03	1.254E+03	1.140E+03	9.648E+02	7.332E+02	5.420E+02	3.370E+02	1.489E+02	2.171E+01
V-notch	**torsion**	**FF2042**	6.381E+01	4.831E+01	3.517E+01	2.577E+01	1.850E+01	1.285E+01	8.503E+00	4.841E+00	2.770E+00	1.044E+00	3.473E-01
U-notch R1.5	**torsion**	**FF2052**	7.751E+01	5.670E+01	4.299E+01	3.065E+01	2.250E+01	1.563E+01	9.945E+00	5.789E+00	3.262E+00	1.246E+00	3.681E-01
Fillet R0.7	**torsion**	**FF2062**	1.670E+02	1.272E+02	8.622E+01	4.429E+01	1.233E+01	6.035E+00	3.156E+00	1.771E+00	8.387E-01	4.595E-01	2.155E-01
U-notch R5	**torsion**	**FF2072**	2.334E+02	1.837E+02	1.447E+02	1.107E+02	8.294E+01	5.961E+01	4.012E+01	2.488E+01	1.304E+01	4.593E+00	9.755E-01
Fillet R0.2	**torsion**	**FF2082**	1.399E+01	5.558E+00	2.845E+00	1.620E+00	9.702E-01	5.956E-01	3.609E-01	2.088E-01	9.585E-02	2.955E-02	9.084E-03

Table 9.7: Critical volumes calculated at different z parameters using the Dang Van criterion adapted to the critical volume approach.

9.4.4 Notch fatigue strength vs. critical volume regressions (Dang Van)

Regression parameters of the notch fatigue strength vs. critical volume dependencies evaluated with the Dang Van criterion adapted to the critical volume approach are reported hereafter. Power law regression parameters for axial load case are reported in Table 9.8 with respect to the best-fit condition ($z = 0.56$). While, power law regression parameters found for the torsion load case are collected in Table 9.9, again with reference to the best condition ($z = 0.70$). It is important to note that here the power law was written as in equation 1.6

Axial load case – power law model (Dang Van)					
N_f	z	a	b	R^2	$RMSE$ [MPa]
500000	0.60	565.35	-0.107	0.8615	46.24

Table 9.8: Power law regression parameters for axial load dependencies evaluated with Dang Van.

Torsion load case – power law model (Dang Van)					
N_f	z	C_B	w	R^2	$RMSE$ [MPa]
500000	0.70	295.84	-0.085	0.9858	4.75

Table 9.9: Power law regression parameters for torsion load dependencies evaluated with Dang Van.

9.5 POINT METHOD DATA

9.5.1 Critical distance vs. fatigue life

The dependency between critical distance (evaluated according the Point Method) and fatigue life was fitted with the power law model presented in equation 2.35 (where D_{PM} is considered instead of L): the regression parameters are presented in Table 9.10.

Axial load case – power law model (Dang Van)				
N_f	z	C_1	C_2	R^2
500000	0.60	565.35	-0.107	0.8615

Table 9.10: Power law regression parameters for fitting the critical distance vs. fatigue life dependency.